

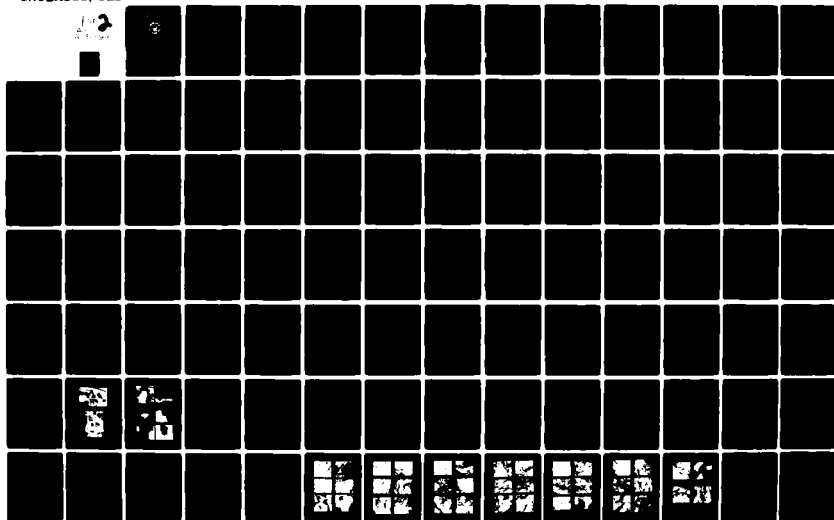
AD-A115 199

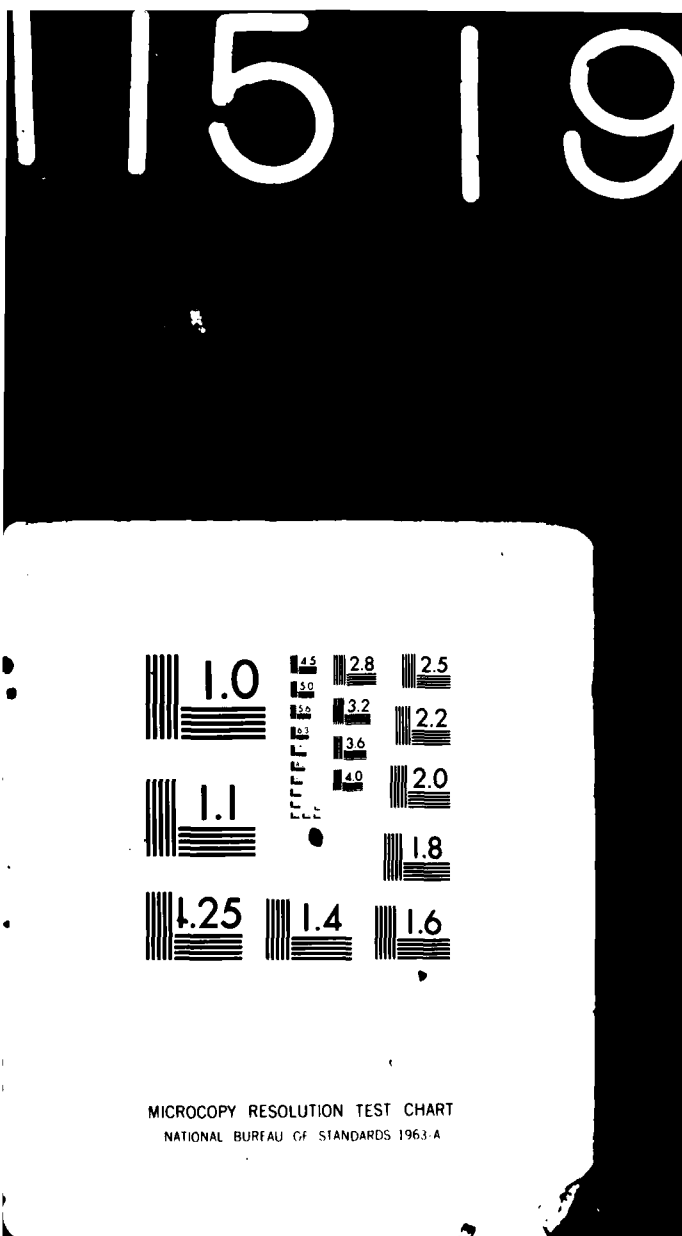
NAVAL POSTGRADUATE SCHOOL MONTEREY CA  
USE OF IMPLANT TESTING TO EVALUATE THE SUSCEPTIBILITY OF HY-130--ETC(U)  
DEC 81 B J MASON

F/8 11/8

UNCLASSIFIED

NL





MICROCOPY RESOLUTION TEST CHART  
NATIONAL BUREAU OF STANDARDS 1963-A

2

# NAVAL POSTGRADUATE SCHOOL

Monterey, California



## THESIS

USE OF IMPLANT TESTING TO EVALUATE  
THE SUSCEPTIBILITY OF HY-130 STEEL  
WELDMENTS TO HYDROGEN EMBRITTLEMENT

by

Bradley J. Mason

December 1981

Thesis Advisor:

K. D. Challenger

Approved for public release; distribution unlimited.

DTIC  
ELECTE  
JUN 8 1982

B

82 06 07 007

AD A115199

DTIC FILE COPY

UNCLASSIFIED

SECURITY CLASSIFICATION OF THIS PAGE (When Data Entered)

REPORT DOCUMENTATION PAGE		READ INSTRUCTIONS BEFORE COMPLETING FORM
1. REPORT NUMBER	2. GOVT ACCESSION NO. <b>AD-A115199</b>	3. RECIPIENT'S CATALOG NUMBER
4. TITLE (and Subtitle) Use of Implant Testing to Evaluate the Susceptibility of HY-130 Steel Weldments to Hydrogen Embrittlement		5. TYPE OF REPORT & PERIOD COVERED Master's Thesis; December 1981
7. AUTHOR(s)  Bradley J. Mason		6. PERFORMING ORG. REPORT NUMBER
9. PERFORMING ORGANIZATION NAME AND ADDRESS Naval Postgraduate School Monterey, California 93940		8. CONTRACT OR GRANT NUMBER(s)
11. CONTROLLING OFFICE NAME AND ADDRESS Naval Postgraduate School Monterey, California 93940		10. PROGRAM ELEMENT, PROJECT, TASK AREA & WORK UNIT NUMBERS
14. MONITORING AGENCY NAME & ADDRESS (if different from Controlling Office)		12. REPORT DATE December 1981
		13. NUMBER OF PAGES 107
		15. SECURITY CLASS. (of this report) Unclassified
		16a. DECLASSIFICATION/DOWNGRADING SCHEDULE
16. DISTRIBUTION STATEMENT (of this Report)  Approved for public release; distribution unlimited.		
17. DISTRIBUTION STATEMENT (of the abstract entered in Block 20, if different from Report)		
18. SUPPLEMENTARY NOTES		
19. KEY WORDS (Continue on reverse side if necessary and identify by block number) Implant Testing Hydrogen Embrittlement HY-130 Steel		
20. ABSTRACT (Continue on reverse side if necessary and identify by block number)  The cracking that may occur near the fusion zone of a steel weldment can often be attributed to the embrittlement of the microstructure by hydrogen induced during the welding process. The modified implant test was used in this case to evaluate the hydrogen-assisted cracking susceptibility of three separate heats of HY-130 steel, which included both cast and wrought plate. Welding was accomplished by the gas metal-arc spray		

DD FORM 1473  
1 JAN 73EDITION OF 1 NOV 65 IS OBSOLETE  
S/N 0102-014-6601

UNCLASSIFIED

SECURITY CLASSIFICATION OF THIS PAGE (When Data Entered)

UNCLASSIFIED

SECURITY CLASSIFICATION OF THIS PAGE (When Data Entered)

#20 - ABSTRACT - (CONTINUED)

transfer process. Cracking in all plates was observed to initiate and propagate in an area near the weld interface. The exact location of the fractures varied according to the amounts of diffusible hydrogen present and the type of material being tested. The effect of stress intensity together with hydrogen content on the mode of fracture present is also addressed in detail.

Accession For	
NTIS GRA&I	<input checked="checked" type="checkbox"/>
DTIC TAB	<input type="checkbox"/>
Unannounced	<input type="checkbox"/>
Justification	
By	
Distribution/	
Availability Codes	
Dist	Avail and/or Special
A	



UNCLASSIFIED

SECURITY CLASSIFICATION OF THIS PAGE (When Data Entered)

Approved for public release, distribution unlimited.

Use of Implant Testing to Evaluate the  
Susceptibility of HY-130 Steel Weldments  
to Hydrogen Embrittlement

by

Bradley J. Mason  
Lieutenant, United States Navy  
B.S.M.E., United States Naval Academy, 1976

Submitted in partial fulfillment of the  
requirements for the degree of

MASTER OF SCIENCE IN MECHANICAL ENGINEERING

from the

NAVAL POSTGRADUATE SCHOOL  
December 1981

Author

Bradley J. Mason

Approved by:

Lennard D. Challen Thesis Advisor

Henry R. McNelly Second Reader


Paul J. Martz  
Chairman, Department of Mechanical Engineering

William M. Loller  
Dean of Science and Engineering



## ABSTRACT

The cracking that may occur near the fusion zone of a steel weldment can often be attributed to the embrittlement of the microstructure by hydrogen induced during the welding process. The modified implant test was used in this case to evaluate the hydrogen-assisted cracking susceptibility of three separate heats of HY-130 steel, which included both cast and wrought plate. Welding was accomplished by the gas metal-arc spray transfer process. Cracking in all plates was observed to initiate and propagate in an area near the weld interface. The exact location of the fractures varied according to the amounts of diffusible hydrogen present and the type of material being tested. The effect of stress intensity together with hydrogen content on the mode of fracture present is also addressed in detail.



## TABLE OF CONTENTS

I.	INTRODUCTION -----	11
II.	BACKGROUND INFORMATION -----	14
	A. HYDROGEN EMBRITTLEMENT -----	14
	B. IMPLANT TESTING -----	17
	C. HYDROGEN ANALYSIS -----	20
	D. PREVIOUS WORK -----	21
III.	EXPERIMENTAL PROCEDURE -----	25
	A. MATERIAL DESCRIPTION -----	25
	B. IMPLANT TESTING -----	25
	C. HYDROGEN ANALYSIS -----	29
	D. FRACTOGRAPHY -----	33
	E. METALLOGRAPHY -----	33
	F. MICROHARDNESS -----	34
IV.	RESULTS -----	35
	A. IMPLANT TESTING -----	35
	B. FRACTOGRAPHY -----	37
	C. HARDNESS STUDIES -----	39
	D. METALLOGRAPHY -----	39
V.	DISCUSSION -----	42
VI.	CONCLUSIONS -----	51
VII.	RECOMMENDATIONS -----	53
	TABLES -----	54
	FIGURES -----	65
	LIST OF REFERENCES -----	105
	INITIAL DISTRIBUTION LIST -----	107



## LIST OF TABLES

<u>Table</u>		
I.	Chemical Composition of Plates 2, 4, and 6 (Weight Percent) -----	54
II.	Mechanical Properties of Plates 2, 4, and 6 ---	55
III.	Heat Treatments of Plates 2, 4, and 6 -----	56
IV.	Composition and Properties of HY-130 Weld Wire (MIL 140S-1) -----	57
V.	Comparison of Welding Parameters for Implant Testing and Operational Welding of HY-130 Steels -----	58
VI.	Implant Testing Data and Results -----	59
VII.	Statistical Data on Hydrogen Content of Implant Test Weldments -----	62
VIII.	Summary of Implant Test Results -----	63
IX.	Specimens Examined for S.E.M. Fractography ----	64

## LIST OF FIGURES

### Figure

1.	Solubility of Hydrogen in Iron -----	65
2.	Comparison of the Notch Configuration in Granjon's Implant Test and Sawhill's Modified Implant Test -----	66
3.	Orientation of Implant Test Specimens -----	67
4.	Details of Implant Test Assembly -----	68
5.	Implant Welding Equipment and Hydrogen Analysis Apparatus -----	69
6.	Procedures Involved in Implant Testing -----	70
7.	Schematic of Hydrogen Analysis Apparatus -----	71
8.	Orientation of Hydrogen Analysis Specimen During Implant Test Welding -----	72
9.	Stress vs. Time-to-Rupture for Plate 2, Short Transverse Direction, Normal Welding Conditions -----	73
10.	Stress vs. Time-to-Rupture for Plate 2, Short Transverse Direction, Enhanced Hydrogen Welding Conditions -----	74
11.	Stress vs. Time-to-Rupture for Plate 2, Longitudinal Direction, Normal Welding Conditions -----	75
12.	Stress vs. Time-to-Rupture for Plate 2, Longitudinal Direction, Enhanced Hydrogen Welding Conditions -----	76
13.	Stress vs. Time-to-Rupture for Plate 4, Short Transverse Direction, Normal Welding Conditions -----	77
14.	Stress vs. Time-to-Rupture for Plate 4, Short Transverse Direction, Enhanced Hydrogen Welding Conditions -----	78
15.	Stress vs. Time-to-Rupture for Plate 4, Longitudinal Direction, Normal Welding Conditions -----	79

16.	Stress vs. Time-to-Rupture for Plate 4, Longitudinal Direction, Enhanced Hydrogen Welding Conditions -----	80
17.	Stress vs. Time-to-Rupture for Plate 6, Short Transverse Direction, Normal Welding Conditions -----	81
18.	Stress vs. Time-to-Rupture for Plate 6, Short Transverse Direction, Enhanced Hydrogen Welding Conditions -----	82
19.	Stress vs. Time-to-Rupture for Plate 6, Longitudinal Direction, Normal Welding Conditions -----	83
20.	Stress vs. Time-to-Rupture for Plate 6, Longitudinal Direction, Enhanced Hydrogen Welding Conditions -----	84
21.	Comparison of the Lower Critical Stress for Normal and Enhanced Hydrogen Welding Conditions -----	85
22.	Comparison of the Embrittlement Index for Normal and Enhanced Hydrogen Welding Conditions -----	86
23.	Scanning Electron Fractographs of Implant Specimen Fracture Surfaces from Plate 2, Short Transverse Direction, for Normal and Enhanced Hydrogen Welding Conditions -----	87
24.	Scanning Electron Fractographs of Implant Specimen Fracture Surfaces from Plate 2, Longitudinal Direction, for Normal and Enhanced Hydrogen Welding Conditions -----	88
25.	Scanning Electron Fractographs of Implant Specimen Fracture Surfaces from Plate 4, Short Transverse Direction, for Normal and Enhanced Hydrogen Welding Conditions -----	89
26.	Scanning Electron Fractographs of Implant Specimen Fracture Surfaces from Plate 4, Longitudinal Direction, for Normal and Enhanced Hydrogen Welding Conditions -----	90
27.	Scanning Electron Fractographs of Implant Specimen Fracture Surfaces from Plate 6, Short Transverse Direction, for Normal and Enhanced Hydrogen Welding Conditions -----	91

28.	Scanning Electron Fractographs of Implant Specimen Fracture Surfaces from Plate 6, Longitudinal Direction, for Normal and Enhanced Hydrogen Welding Conditions -----	92
29.	Scanning Electron Fractographs of Implant Specimen Fracture Surfaces, NTS from Plates 2 and 6, Short Transverse Direction, Enhanced Hydrogen Welding Conditions -----	93
30.	Percent Intergranular Fracture vs. Stress Intensity for Plate 6, Short Transverse Direction, Enhanced Hydrogen Welding Conditions -----	94
31.	Microhardness Transverse of Plate 2 -----	95
32.	Microhardness Transverse of Plate 4 -----	96
33.	Microhardness Transverse of Plate 6 -----	97
34.	Orientation of Microhardness Transverse -----	98
35.	Microstructure of Wrought Plate Weldment (Plate 2) -----	99
36.	Microstructure of Cast Plate Weldment (Plate 6) -----	100
37.	Crack Initiation Site and Alloy Banding of Plate 2 -----	101
38.	Microstructure of Fractured Implant Specimens from Plate 2, Normal and Enhanced Hydrogen Welding Conditions -----	102
39.	Microstructure of Fractured Implant Specimens from Plate 4, Normal and Enhanced Hydrogen Welding Conditions -----	103
40.	Microstructure of Fractured Implant Specimens from Plate 6, Normal and Enhanced Hydrogen Welding Conditions -----	104

### ACKNOWLEDGMENTS

I wish to express my deep gratitude to Professor Ken Challenger for his guidance and enthusiasm, and especially for his words of encouragement when they were so badly needed. I would also like to thank Petty Office First Class Caceres, without whose help with equipment and specimen preparation this work would not have been completed. In addition I want to express my deep gratitude and love to my father who has instilled the importance of education in me, and to Mr. Rick Clothier for teaching me the meaning of persistence. I would also like to acknowledge the continual financial support of the U.S. Naval Sea System Command (NAVSEA), and the helpful comments of Dr. Charlie Zanis at NSRDC. Finally I would like to express a special thought of love and thanks to my wife-to-be Pamela, without whose patience and support this work would not have been possible.

## I. INTRODUCTION

HY-130 steel is an alloy steel containing less than 0.12 percent carbon and having a tempered martensite structure in the as-delivered state. It is not only characterized by its high yield strength, 130-145 ksi, but also by its high levels of fracture toughness. U.S. Navy interest in HY-130 steel stems from the need to provide reliable hull materials for deep submersibles and combatant submarines, as replacements for lower strength HY-80 steel systems. Advantages to the use of a higher strength alloy include deeper operating depths and an increased strength-to-weight ratio.

Although available in either cast or wrought forms, only the supplies and manufacturing processes for wrought plate have been certified. A few failures of explosion bulge tests by cast HY-130 steel weldment systems is the reason why the cast form has yet to achieve certification. In addition to concern over explosion bulge test failures in cast weldment systems, their susceptibility to hydrogen induced cracking has not been determined.

It has been recognized for some years that higher strength quenched and tempered alloy steels have a tendency to fracture under conditions of hydrogen embrittlement. Normal production-type welding procedures can often lead to hydrogen absorption in the weldment system and eventual cracking problems related to hydrogen embrittlement. Previous studies conducted by

Sawhill, Dix and Savage [Refs. 1,2] have evaluated and compared the differences between hydrogen embrittlement of HY-80 and HY-130 steels. However, no work has been conducted to determine if significant differences to hydrogen embrittlement exist between cast and wrought HY-130 steel weldments.

It was the purpose of this thesis to investigate the effect of hydrogen embrittlement on HY-130 steel weldments and in particular to determine if any distinct differences exist between the embrittlement susceptibility of HY-130 cast and wrought plates.

By using a technique known as an implant test a study was made to evaluate the effect of weld metal hydrogen content on the degree of embrittlement for three separate heats of HY-130 steel. The method employed was developed by Granjon [Ref. 3] and further refined by Savage and Sawhill [Ref. 1]. All weldments evaluated were made using the gas metal-arc (GMA) process.

Because a critical amount of diffusible hydrogen must be present for hydrogen induced cracking, it was necessary to determine the amount of hydrogen introduced by the GMA welding process. A silicone oil extraction method developed by Savage and Nippes [Ref. 4] was used to determine amounts of diffusible hydrogen present in each weldment system that was evaluated.

Fracture surfaces of implant specimens were examined using metallographic techniques and scanning electron

microscopy, in order to evaluate the type of microstructure present and the mode of fracture. In addition, microhardness traverses were conducted in an attempt to correlate hardness variations between the weld metal, composite zone, heat-affected zone, and base metal; and the actual location of fracture in the implant specimen.

This thesis presents the data obtained from the implant testing of both cast and wrought HY-130 steel. Microstructural evidence of the diffuse fracture modes and microstructures observed is included as a means of evaluating the degree of hydrogen embrittlement encountered for each heat of steel and the position of crack propagation in the weldments for each steel.



## II. BACKGROUND INFORMATION

### A. HYDROGEN EMBRITTLEMENT

The development of HY-130 steel with its improved strength, fracture toughness and weldability has brought with it additional hydrogen induced cracking problems not previously experienced in HY-series steel weldments. This is in line with the accepted theory that as the yield strength is increased in steels, they become increasingly sensitive to hydrogen-induced cracking.

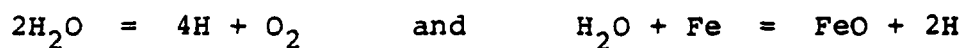
The weldability of high strength steels is generally accepted to depend to a large extent on the susceptibility of the steel to hydrogen-induced cracking in the heat-affected zone of the base metal. Low alloy, high strength steels, which depend upon the properties of the transformation products for their strength, exhibit high susceptibility to hydrogen cracking. Hydrogen cracking may occur in either the heat-affected zone or weld metal if four conditions are present simultaneously. These conditions have been defined by Savage [Ref. 1] as:

1. A critical concentration of hydrogen at the crack tip,
2. a stress intensity of sufficient magnitude,
3. a susceptible microstructure, and
4. temperature in the range of -100 to 200 degrees centigrade.

In U.S. Navy applications of HY-130 steel, the combination of

service stresses, temperatures, and susceptible microstructures is unavoidably present.

Hydrogen is introduced into weldments because the extremely high temperatures present in a welding arc are capable of dissociating hydrogen gas, water vapor, and hydrogen bearing compounds to produce atomic hydrogen. Some major sources of this hydrogen during welding are moisture in covered electrodes, contaminated filler wire, and moisture in shielding gases and the atmosphere. When moisture is present, hydrogen is the product of the following reactions:



which can also occur with any of the alloying elements present in steel. Other factors which increase the susceptibility of HY-130 weldments to hydrogen embrittlement are the presence of residual stresses due to welding equal to about the yield strength, due to HY-130 steel's high hardenability, and the as-welded microstructure is martensitic/bainitic.

Although the conditions for hydrogen-induced cracking are well known, the mechanism of hydrogen cracking is somewhat disputed. There are four basic theories which try to explain hydrogen embrittlement. Tettleman [Ref. 5] proposed the planar-pressure theory which postulates that atomic hydrogen diffuses through the iron lattice and collects in voids or other defects. Inside these voids atomic hydrogen reassociates

to form molecular hydrogen and creates high internal pressure. The interaction of the high internal pressure with applied and residual stresses is postulated to result in crack initiation and propagation.

A second theory proposed by Williams and Nelson [Ref. 6] states that absorbed hydrogen reduces the critical fracture stress. Initial cracks are formed and the presence of hydrogen increases the ease of crack propagation.

The third theory, known as the triaxial stress theory was proposed by Troiano [Ref. 7]. This theory assumes that hydrogen in solution near a void causes embrittlement. The concentration of hydrogen in the region of maximum triaxial stress near a void exceeds that in the lattice. When the hydrogen reaches a critical concentration in the location of the maximum triaxial stress, initiation of a crack occurs. The crack is propagated by the same mechanism after hydrogen diffuses to the triaxial stress region ahead of the newly located crack tip.

Finally, Beachem [Ref. 8] emphasizes the interaction of hydrogen with moving dislocations. In this model, the pressure of hydrogen dissolved in the lattice ahead of the crack tip assists microscopic deformation. In effect, this lowers the level of stress necessary to cause fracture by a dislocation-multiplication mechanism.

Although differing in principle, all four of these theories depend on the fact that hydrogen is soluble and can

readily diffuse in iron base alloys. This is in fact the case, and is a highly temperature dependent process. Figure 1 shows the variation of hydrogen solubility with temperature. The highest levels of solubility occur at or near the liquid iron region in the temperature range of 1450-1550 degrees centigrade. This correlates with temperatures and conditions present at the arc tip of a GMA weld used in producing HY-130 weldments.

#### B. IMPLANT TESTING

Since hydrogen induced cracking is so important in determining the weldability of high strength steels, many tests have been proposed to evaluate this tendency. These tests are classified as either direct or indirect tests.

The direct tests consists of actual welds of varying joint geometries simulating in-service welds. Tests in this category include the Lehigh test, Tekken test, and controlled thermal severity test. A major drawback to these tests is their complex nature and lack of reproducibility.

Indirect tests include constant load rupture tests of hydrogen-charged specimens and the charged notched tensile test. While these tests better control stress levels, they do not evaluate the true heat-affected zone region. Additionally, because no actual welding occurs, it is uncertain if hydrogen distributions approach those found with actual welding conditions.

Recently, Granjon [Ref. 3] developed the implant test which enables examination of the true, not simulated, weld

heat-affected zone structure. Here, the hydrogen distribution is determined by actual welding conditions.

The implant test has been shown to be a suitable means for grading steels according to their propensity towards hydrogen embrittlement in the weld heat-affected zone. It allows microstructural changes by variation of the weld thermal cycle through manipulation of arc energy, plate-thickness, and changes in pre-heat and post-heat weld treatments. The potential hydrogen can be varied by altering the moisture in the welding fluxes, or the hydrogen content in the gas-shielded arc atmosphere. Consequently hydrogen induced during testing is through an actual welding process. Independent and close control of stress level is also allowed by this test.

In implant testing, a cylindrical test specimen with a single circumferential notch is inserted into a test plate and affixed by a single weld bead, known as the test weld (figure 2a). The notch provides a state of triaxial stress which can act as a crack initiation site. Hydrogen can be induced or restrained from the test weld by controlling the arc atmosphere. Because the cylindrical specimen experiences the exact heat-affected zone thermal cycle, it represents a typical weld.

A series of specimens is welded under uniform conditions and loaded under various stress levels below the notch tensile stress of the subject metal. Normally an incubation time is observed before the implant specimen fractures.

Below certain stress levels failure does not occur, this level is referred to as the lower critical stress.

Time to failure at higher stress levels and the lower critical stress are used as a measure of hydrogen-cracking susceptibility of a given material. Any material having a high lower critical stress reasonably close to its notch tensile stress, and long incubation times before failure at stresses above the lower critical stress, is generally considered less susceptible to hydrogen embrittlement than materials exhibiting opposite characteristics.

Granjon's proposal of a single circumferential notch in the test specimen results in an uncertainty in the exact location of the notch relative to the most susceptible region of the heat-affected zone. This occurs because it is not always possible to predict the depth of weld penetration throughout an entire weld due to welding arc fluctuations. To overcome this problem, Sawhill [Ref. 1] proposed the use of a modified implant test specimen, which uses a helical notch in place of the single circumferential notch (figure 2b). With this modified specimen, the helical notch provides a stress raiser throughout the entire heat-affected zone from the fusion line well into the base metal. In this manner failure is sure to initiate and propagate in the most crack susceptible microstructure and eliminates the uncertainty involved with the original specimen configuration.

Use of the modified implant test is clearly advantageous to other cracking susceptibility tests. These advantages are

summarized [Ref. 1] as follows:

1. amounts of induced hydrogen can be easily controlled,
2. test specimens are small and easy to machine,
3. the composition of the implant specimen may be different than that of the base plate, the latter acting merely as a support and heat sink, and
4. imposed stress is independent of the welding procedure used.

### C. HYDRGOEN ANALYSIS

Because a critical amount of diffusible hydrogen must be present to initiate hydrogen-induced cracking, it is necessary to determine the amount of hydrogen introduced into weldments by various welding procedures. Many techniques have been employed to measure hydrogen concentration in steel weldments. Most of these methods require elaborate and expensive equipment and test times of up to three days.

The silicone-oil extraction method developed by Savage and Nippes [Ref. 4] is a reliable and rapid technique for the determination of diffusible-hydrogen content in weldments. Its relative simplicity and inexpensive nature make it an attractive method for use in hydrogen analysis of steel weldments.

In the silicone oil extraction method, diffusible hydrogen is extracted from a weld sample in hydrogen-saturated silicone oil at elevated temperatures. As the hydrogen is extracted it collects in a burette located above the weld sample. Results from this method have been shown to correlate

well with those obtained by use of the British Welding Research Association mercury extraction technique [Ref. 4].

#### D. PREVIOUS WORK

Savage, Sawhill and Nippes [Refs. 1,2] initiated work on hydrogen induced cracking of HY-130 steel weldments. Their initial study used the modified implant test to evaluate HY-80 and HY-130 wrought plate for susceptibility to delayed cracking. In addition, acoustic-emission and metallographic techniques were used to study the microstructural features which influence the initiation and propagation of hydrogen induced cracking in implant test specimens. The implant specimens were welded using an AX-140 electrode and a moisture enriched shielding gas to introduce hydrogen into the weldments.

The cracking susceptibility was rated by defining an embrittlement index,  $I$ , which was calculated from the relationship:

$$I = \frac{NTS - LCS}{NTS}$$

where NTS is defined as the notch tensile stress and LCS is the lower critical stress. This nondimensional parameter increases in value as susceptibility to hydrogen embrittlement increases. In this study HY-130 was found to have a similar value for the embrittlement index as the heat of HY-80 that they studied. This particular heat of HY-80 was known to be extremely crack sensitive.



Microhardness traverses showed large variations in heat-affected zone hardness in the HY-130 steel. In particular a large increase in hardness near the weld interface occurred in the implant specimens. It was also concluded that higher heat-affected zone hardness indicated a higher susceptibility to hydrogen-embrittlement and delayed cracking.

Crack initiation was observed to occur at the weld metal interface in HY-130 specimens. The interface between the fusion zone and the partially melted zone served as the area for crack propagation. This agrees with work done by Rathbone and Conners [Ref. 9] in developing procedures for welding HY-130 steel. Additionally, a higher concentration of hydrogen present at the weld interface was concluded as being the major contributing factor for increased tendency to crack at that location.

The higher levels of hydrogen present at the weld interface were postulated to exist since hydrogen initially enters the system via the molten weld pool and then reaches the heat-affected zone by diffusion. For this reason Savage and Nippes felt it reasonable to expect the weld metal always to be richer in hydrogen.

Orientation of the implant specimens within the rolled plate was found to play a role in the susceptibility to hydrogen-induced cracking. Those specimens machined from the longitudinal direction (parallel to the rolling direction), were less susceptible to hydrogen-induced cracking than specimens from the short transverse (through-thickness), direction.

Fractography work indicated the presence of intergranular, dimpled and quasi-cleavage type fracture surfaces. Savage and Nippes reasoned that levels of stress intensity and hydrogen concentrations at the crack tip directly effect the mode of fracture present. Conclusions reached in their study would indicate that hydrogen induced cracking of HY-130 steels occurs primarily by microvoid coalescence.

A subsequent study by Savage, Nippes and Silvia [Ref. 10] used the augmented strain cracking test to evaluate hydrogen-induced cracking in HY-130 steels. Although directed towards determining the effects of preheat and postheat on hydrogen content and propagation of hydrogen induced cracks, the results were generally supportive of those from the previous study.

The mode of fracture in these tests was determined to be intergranular in the weld metal and a mix of intergranular and transgranular in the heat-affected zone. These results differ from the previous study which determined the primary mode of failure to be microvoid coalescence. Two factors found to be important in determining crack initiation sites were the presence of sulfide inclusions and banding due to alloy segregation. Hydrogen-induced cracking was found to be associated with non-metallic inclusions in the heat-affected zone and partially melted zone. The orientation of bands of alloying elements in the steel had considerable effect on the degree of hydrogen-induced cracking

in the heat-affected zone. The banding effect was caused by higher hardness levels being present in the alloy rich bands.

### III. EXPERIMENTAL PROCEDURES

#### A. MATERIAL DESCRIPTION

The material selected for evaluation was three separate heats of HY-130 steel. One heat, no. 5P4184, was rolled and is referred to as plate 2. It was produced by United States Steel Corporation. The remaining two heats, nos. 21327 and 36615 were cast and are referred to as plates 4 and 6. They were produced by the ESCO corporation. Plate 4 had previously been subjected to explosive bulge testing by Mare Island Naval Shipyard. The sample from plate 6 was a prelongation on the casting and was not explosion bulge tested.

Tables I and II summarize the chemical composition and mechanical properties of each plate. Included in these tables are target specifications as presented by Palko, Byrne, and Zanis [Ref. 11]. The heat treatment schemes for each plate appear in table III.

Welding was done using HY-130 weld wire manufactured by the Linde Corporation. Heat number 951140 was used for this research. The composition and properties of this electrode are given in table IV.

#### B. IMPLANT TESTING

As stated earlier, implant testing allows evaluation of a material's true heat-affected zone susceptibility to hydrogen-induced cracking. A small cylindrical specimen is

machined with a helical notch at one end and fit into a hole drilled in a base metal specimen plate. A test weld is then deposited on the surface to fuse the top of the specimen. This creates a heat-affected zone which contains the notch as indicated in figure 2b. Varying amounts of hydrogen can be introduced into the weldment as desired. After welding, the specimen is loaded in tension and the time to failure is noted for a series of tests performed at different stress levels.

Implant specimens were machined with their axis parallel to both the short transverse direction and the longitudinal direction for each plate, as shown in figure 3. Starting with a blank 50.8 mm in length and 9.5 mm in diameter the end to be notched was machined to a diameter of 6.3 mm for a distance of 41.2 mm. The helical notch was then machined in a lathe for a distance of 9.5 mm from the specimen end. The pitch of the notch was 0.9 mm with a notch angle of 60 degrees. Figure 4 shows the implant specimen and helical notch in detail.

Test blocks to hold the implant specimens were cut from a 1020 cold rolled steel plate. These blocks were 66.6 mm x 50.8 mm and 9.5 mm thick. At the center of each test block a hole 6.3 mm in diameter was drilled and reamed on a lathe. Each implant specimen was then press fit into a test block to complete the test assembly. The test block and implant test assembly are shown in figure 4.

The implant test weld was deposited using 1.6 mm diameter weld wire and the gas metal-arc process. Welding conditions are summarized in table V. These welding parameters were chosen to simulate as closely as possible the normal operational welding procedures which would be utilized in a production operation.

The entire welding apparatus consisted of an Airco miget power supply with the welding gun mounted on the radial arm of a Cincinnati vertical milling machine. A support unit was attached to the table of the milling machine to hold the implant test assembly during welding. Figures 5a and 6a show the details of the apparatus. The welding gun was mounted in a stationary position to give the desired arc length, as the milling table moved the implant assembly at a uniform speed beneath the weld arc. This process assured reproducibility of welding conditions for each test. When increased levels of hydrogen were required to be introduced, the argon shielding gas was bubbled through a sealed beaker containing 2000 ml of water. The height of water in the beaker was kept constant for each weld made under enhanced hydrogen conditions. This apparatus is shown in figure 6a.

Tests were conducted on all three heats of HY-130 steel using implant specimens machined from both the short transverse and longitudinal directions. Additionally, each sample orientation was welded using normal and enhanced hydrogen conditions. All welding under normal conditions was completed

first in order to avoid contaminating the shielding gas hoses with water vapor before it was required for the enhanced hydrogen welding tests. After depositing the test weld, the implant specimens were loaded in an Instron Universal Testing Machine which was configured for constant load testing. In this manner the full specimen test load could be attained within five seconds after the loading cycle was begun. The load was then held until fracture occurred or for a period of twenty-four hours.

In order to assure that the specimens were all subjected to the same testing conditions, the following standardized procedures were used:

1. the implant specimen was assembled in the test block and degreased with acetone,
2. the entire test assembly was preheated in an oven at 100 degrees centigrade for a minimum of four hours,
3. the implant test assembly was placed in the support unit and the GMA test weld was deposited as specified in table V,
4. immediately after welding, the implant test assembly was removed from the support unit and allowed to air cool for two minutes,
5. upon completion of the air cool, the entire implant test assembly was quenched in an alcohol ice bath at zero degrees centigrade, letting it remain there until loading,
6. within ten minutes after quenching the assembly was placed in the Instron Universal Testing Machine and the desired test load was applied,
7. after the specimen fractured, the load and time to rupture was recorded (the maximum time any specimen remained loaded was twenty-four hours),

8. the maximum stress level that could be sustained for a period of twenty-four hours was used as the lower critical stress (LCS),
9. the notch tensile stress (NTS) was taken as the stress level required to cause failure while conducting a normal tensile test, and
10. an embrittlement index was calculated for each heat and each orientation under normal and enhanced hydrogen welding conditions as follows:

$$I = \frac{NTS - LCS}{NTS} .$$

Figures 6a through 6f shows the steps involved in implant testing.

#### C. HYDROGEN ANALYSIS

Determination of the amount of diffusible hydrogen present in each test weld made was essential for both normal and enhanced hydrogen welding procedures. In this investigation the RPI silicone-oil extraction method was used for measuring amounts of diffusible hydrogen present. This method was developed and qualified by Savage and Nippes [Ref. 4]. It involves extraction of diffusible hydrogen from a weld sample placed in hydrogen saturated silicone oil at 100 degrees centigrade. The total time required for this procedure is approximately ninety minutes.

Figure 7 is a schematic of the apparatus developed by Savage and Nippes. The equipment consists of a 4000 ml and a 2000 ml pyrex beaker set up in a "double-boiler" configuration and heated by an electric hot plate. The inner and



outer baths are both high grade, high temperature silicone oil with a viscosity of fifty centistokes and stable to a temperature of 200 degrees centigrade. The inner bath was maintained at a temperature of 100 degrees centigrade, plus or minus five degrees.

The inner bath was maintained saturated with hydrogen by bubbling hydrogen gas directly into it through a fritted-disc of pore size EC, at a flow rate of one liter per hour. To ensure saturation, hydrogen gas was bubbled through the inner bath at the test flow rate for one hour prior to conducting analysis. Maintaining the inner bath saturated with hydrogen gas ensured that all hydrogen evolved from the weld specimen was collected, and not lost in solution to the silicone oil.

Collection of the hydrogen gas from the weld specimen was accomplished through a pyrex collection funnel attached to a five-milliliter calibrated burette. Silicone oil was drawn up the column to place the meniscus in the calibrated portion of the burette. The weld specimen was placed under the collection funnel and the evolved hydrogen gas rose to the top of the silicone-oil meniscus, and was trapped in the burette. Figure 5b shows the entire apparatus.

Before hydrogen analysis could be accomplished an initial calibration procedure needed to be conducted. After the silicone oil bath reached an equilibrium temperature of 100 degrees centigrade, and the silicone oil had been saturated with hydrogen, an initial hydrogen volume was established.

To do this, silicone oil was first drawn up the entire length of the burette. Then by placing the fritted-disc bubbler under the funnel, and allowing hydrogen gas to bubble into the collection funnel, the silicone-oil meniscus was lowered to the calibrated portion of the burette.

Hydrogen analysis specimens were machined from HY-130 steel with the dimensions 15.8 x 15.8 mm, and 9.53 mm in thickness. All surfaces were ground flat and the surface to be welded was polished using 320 grit SiC paper. Each polished specimen was numbered and initial weights were recorded.

A polished specimen was placed in front of and behind each implant test assembly, and welded at the same time each implant test weld was made. Orientation of the hydrogen analysis specimens is shown in figure 8. The following standardized procedures were used to ensure uniform test results:

1. a polished hydrogen-analysis specimen was placed at either end of each implant test assembly prior to laying the test weld head,
2. the test weld bead was laid,
3. within fifteen seconds of completing the test weld the hydrogen-analysis specimens were mechanically separated from the implant test assembly and placed in liquid nitrogen at minus 190 degrees centigrade,
4. the initial position of the silicone-oil meniscus in the burette was recorded,
5. the test specimen was removed from the liquid nitrogen bath and rinsed first in pure ethyl alcohol for five seconds, next it was rinsed in anhydrous ethyl ether for five seconds, and then dried with a blast of argon gas,

6. the total time of the rinse was never to exceed sixty seconds,
7. after ninety minutes the new silicone-oil meniscus level was recorded,
8. the specimen was then removed from the silicone-oil bath, rinsed in acetone to remove residual oil, and reweighed to determine the amount of deposited weld metal.

The purpose of the rinsing procedures outlined in step five was to remove any surface contaminants which may have led to an erroneous determination of the amount of diffusible hydrogen present in the test weld.

The amount of evolved hydrogen from the test weld was calculated by subtracting initial and final levels of the silicone-oil meniscus. Next, by using the following equation developed by Savage and Nippes, the volume of hydrogen present was converted into parts-per-million (ppm) of diffusible hydrogen present in the implant test weld:

$$\text{PPM} = (V_2 - V_1) (273/T) (P/29.92) (90/W)$$

where:

$(V_2 - V_1)$  = volume of evolved hydrogen (ml),

T = absolute temperature of silicone-oil at the collection point,

P = atmospheric pressure at the time of the analysis (inches Hg),

W = weight of deposited weld metal (grams),

90 = a conversion factor to convert the results from ml per gram to ppm of deposited weld metal.

In tests conducted by Savage and Nippes the RPI silicone-oil extraction method was found to be a reliable technique, with results consistent with standard British Welding Research Association methods.

#### D. FRACTOGRAPHY

Fractured implant specimens from each heat and sample orientation which had been loaded near the lower critical stress and welded using enhanced hydrogen and normal welding conditions were sectioned and mounted to permit examination of the fracture surfaces. A Cambridge 54-10 scanning electron microscope was utilized to observe these fracture surfaces. An additional series of fractured specimens from the same heat and sample orientation, and welded with enhanced hydrogen conditions, was also viewed. For this latter series all stress levels were examined between the lowest stress above the lower critical stress, and up to and including the notch tensile stress. The entire fracture surface of each specimen was examined to determine the various modes of fracture present and the relative amounts of each fracture mode observed.

#### E. METALLOGRAPHY

Fractured and unfractured implant specimens were sectioned and mounted from each heat of HY-130 steel to examine the microstructures and crack initiation sites.

Metallographic samples were mounted in bakelite and polished using wet sand papers through 600 grit. The final

finish was obtained using 1.0 micron and 0.5 micron aluminum oxide slurries. The polished specimens were then etched with a one percent nital solution for fifty to sixty seconds and examined using a Zeiss optical microscope.

#### F. MICROHARDNESS

One implant test assembly from each heat of HY-130 steel was welded using enhanced hydrogen welding conditions, quenched in the alcohol-ice bath, and then sectioned longitudinally. Each of these sectioned assemblies was polished using the same procedures as for the metallographic samples. After achieving the desired surface finish the specimens were etched to more closely reveal the fusion line and visible heat-affected zone. An ammonium persulphate etchant was used for this purpose.

In an effort to determine hardness variations between weld metal, heat-affected zone, and base metal, a microhardness traverse was made on each sample. An eight millimeter traverse was made, beginning in the weld metal and proceeding perpendicular to the fusion line, through the heat-affected zone, and finishing in the base metal. The distance between each hardness penetration was 0.15 mm.

#### IV. RESULTS

##### A. IMPLANT TESTING

The data obtained from the implant testing of all three heats of HY-130 steel is summarized in tables VI and VII. A plot of applied stress versus time to rupture for each orientation and welding condition was made for each plate. These plots are presented in figures 9 through 20. Adjacent to each data point displayed on these graphs is a number representing the amount of diffusible hydrogen present, in ppm, for that implant test weldment.

From the data, an embrittlement index was calculated using the notch tensile stress and lower critical stress for each plate orientation and welding condition. These results are presented in table VIII. It should be noted that for each specimen orientation the embrittlement index increased when enhanced hydrogen welding conditions were used. It should also be recalled that a higher value for the embrittlement index in a particular material indicates increased susceptibility to hydrogen embrittlement. The percent increase in the embrittlement index for enhanced hydrogen welding conditions is also presented in table VIII.

A more vivid comparison of the differences in values of lower critical stress and embrittlement indices, and how they are affected by increased levels of diffusible hydrogen is seen in the histograms shown in figures 21 and 22. As

presented, the data indicates a wide range of values for the lower critical stress under normal welding conditions. In this case plate 6 had the highest value of lower critical stress in the short transverse direction, while plate 2 had the lowest value of lower critical stress in the short transverse direction. These two values differed by almost 28,000 psi. When making the same comparison with enhanced hydrogen welding conditions, plate 2 in the longitudinal direction had the highest value of lower critical stress while plate 6 had the lowest value in this direction. These values were much closer, differing by only 8,000 psi. Having made this comparison it becomes evident that plate 6 experienced the greatest degradation in lower critical stress due to the presence of increased amounts of diffusible hydrogen. This reduction in the values of lower critical stress is easily seen in figure 21.

Specimen orientation also had a noticeable effect on the lower critical stress. Specimens machined with their axis parallel to the short transverse direction in plate 2 indicated a lower resistance to hydrogen embrittlement. Plate 6 also exhibited an orientation effect. Here the specimens machined parallel to the longitudinal direction exhibited a lower resistance to hydrogen embrittlement. No appreciable orientation effect was noticeable in plate 4.

Examination of figure 22 indicates similar trends occurred in the values of the embrittlement indices as was seen for

the lower critical stress. A specimen orientation effect was again noticed in plates 2 and 6. For plate 2, those specimens machined in the short transverse direction had the highest embrittlement index, indicating lower resistance to hydrogen embrittlement. The longitudinal direction for plate 6 showed the highest embrittlement index and increased susceptibility to hydrogen embrittlement. Again no appreciable difference due to specimen orientation was noticed in plate 4.

Final analysis of all the data indicates that plate 6 underwent the most adverse change in susceptibility to hydrogen embrittlement when enhanced hydrogen welding conditions were used. Specimens machined in the longitudinal direction exhibited a 31 percent increase in the embrittlement index, while those machined in the short transverse direction experienced a 40 percent increase in the embrittlement index. Increases noted in the other plates were not nearly as great.

A final observation regarding times for specimen failure can also be made. Those specimens welded with enhanced hydrogen conditions consistently failed more rapidly than those welded using normal conditions and loaded at similar stress levels.

#### B. FRACTOGRAPHY

Data on the specimens whose fracture surfaces were chosen to be viewed with the scanning electron microscope is presented in table IX. These surfaces all contained dimpled



(microvoid coalescence), quasi-cleavage and intergranular type fractures. Specific areas of the fracture surfaces for each specimen orientation and welding condition are shown in figures 23 through 29. Each figure contains a low magnification view (50x) of the majority of the fracture surface, and higher magnification views (500x) of dimpled and intergranular fracture areas which were seen on each specimen. The relative amounts of each fracture mode observed on the specimens examined are also summarized in table IX.

From the data collected during SEM fractography, microvoid coalescence appears to be the primary fracture mode for specimens welded using normal conditions. However, those specimens welded with enhanced hydrogen conditions were observed as having an intergranular fracture mechanism as the primary fracture mode. Both intergranular and dimpled fractures were observed in various amounts on each fracture surface examined.

In order to determine the effect of stress level on fracture mode, a series of fractured specimens was examined from the same plate and axis orientation, welded using enhanced hydrogen conditions. Figure 30 presents the results utilizing a graph of percent intergranular fracture versus stress. It can be seen that as stress levels are decreased and time to fracture increases, the percent of brittle intergranular fracture present increases.

### C. HARDNESS STUDIES

Microhardness traverses of implant test weldments from each plate showed a large hardness variation between the weld metal, heat-affected zone and base metal of the HY-130 steel. The microhardness traverses for each plate were plotted as microhardness ( $HV_{200}$ ) versus distance from the implant specimen end. These plots appear in figures 31 through 33. The orientation of the hardness readings taken on the implant test weldment is shown in figure 34.

Each traverse indicated a sharp increase in hardness near the weld interface. The maximum values of hardness observed were 421  $HV_{200}$  for plate 2, 429  $HV_{200}$  for plate 4, and 412  $HV_{200}$  for plate 6. In each case the hardness decreased rapidly shortly after reaching the maximum value. This would indicate the presence of a sharp metallurgical notch in this region of the weldment. The distances over which this occurred were 1.5 mm in plate 2, 0.75 mm in plate 4 and 1.6 mm in plate 6.

### D. METALLOGRAPHY

Crack initiation and propagation was studied using metallographically prepared samples from fractured and unfractured implant test specimens. After etching, a hardness traverse was performed across each of three unfractured specimens from the different heats of HY-130. Each traverse was oriented as shown in figure 34, with indentations spaced 0.2 mm apart. These indentations were used as reference

marks in locating microstructural variations in the weld metal, fusion zone and heat-affected zone.

The microstructure observed in plates 4 and 6 were essentially identical throughout. Four distinct regions were observed, namely the weld metal, fusion zone, coarse-grained heat-affected zone and the fine-grained heat-affected zone. The combined area of the visible heat-affected zone appeared as a narrow band between the weld metal and base metal. Immediately adjacent and below the fusion zone was a coarse structure. At a distance of 1 mm below the fusion line the grain size rapidly decreased, forming a region of fine martensite.

The same regions observed in the cast plates were also found in the wrought plate, plate 2. However, the characteristic alloy banding formed in wrought materials was clearly visible in plate 2. This banding was not observed in plates 4 and 6, however the original dendritic structure of the cast material was obvious in the heat-affected zone. Micrographs showing the structures just discussed are presented in figures 35 and 36. They clearly show the weld metal interface and area of weld penetration, in addition to the fine-grained and coarse-grained heat-affected zone.

A crack initiation site was observed in an unfractured specimen from plate 2, and is shown in figure 37. The crack had initiated at the root of the helical notch, an area of high triaxial stress. Also shown in figure 37 are the solute-rich bands characteristic of wrought plate.

Examination of fractured specimens from all three heats of HY-130 revealed that crack initiation and propagation occurred at or near the area of the weld metal interface. However, major differences were observed in the exact location of the specimen fracture. Plates 2 and 4 cracked almost entirely through the area of weld metal penetration when enhanced hydrogen welding conditions were utilized. When welded using normal conditions, plate 2 cracked almost entirely through the base metal heat-affected zone. At the same time specimens from plate 4 were observed to crack in a very ill-defined region combining the weld metal penetration and base metal heat-affected zone when welded with normal conditions. These fractures in plate 4 appeared to closely follow the weld fusion line. Fractured specimens examined from plate 6 were clearly observed to crack in the base metal heat-affected zone for both enhanced hydrogen and normal welding conditions. Representative micrographs of the fracture areas are shown in figures 38 through 40.

## V. DISCUSSION

In welding, the amount of hydrogen available for assisting the cracking process is determined by three factors. These are: (1) the amount of hydrogen introduced during welding; (2) the amount of hydrogen that escapes to the atmosphere and adjacent base metal; and (3) the diffusion of hydrogen to regions of high triaxial stress.

Initially the weld bead and heat-affected zone immediately adjacent to the fusion line have a similar and uniform hydrogen concentration [Ref. 15]. The hydrogen, being an interstitial atom is attracted to any region of high triaxial stress, such as ahead of a crack or notch. Thus, the hydrogen concentrations in these regions becomes greater than in the surrounding matrix. When the hydrogen concentration in the regions of high triaxial stress reaches some critical value, which is dependent upon the magnitude of the local stress, initiation or extension of a crack occurs. Note that the higher the level of stress present, the lower is the critical concentration of hydrogen necessary. As the hydrogen concentration at the crack tip falls below the critical level due to diffusion of hydrogen with the passage of time, crack growth will cease [Ref. 2].

Implant specimens loaded above the lower critical stress failed because the increase in stress intensity at the crack tip was sufficient to keep pace with the decreasing concentration

of hydrogen. However, for those specimens loaded below or at the lower critical stress, cracking either never initiated on loading, or, if cracking is initiated, the crack growth rate was slow enough so that the increase in stress intensity as the crack advanced could not keep pace with the decreasing concentration of hydrogen. Therefore crack propagation ceased, and specimen failure never occurred. Evidence of cracks initiating but never propagating to failure is shown in figures 37a and 37b. The same result was reported by Savage and Nippes [Ref. 2].

The purpose of the helical notch in the implant test specimen was to provide an area of high triaxial stress in all regions of the weldment ranging from the weld metal through the heat-affected zone and into the base metal. This notch, being helical in nature, provides a site for crack initiation around the entire circumference of the specimen and throughout the specimen thickness. Once the crack propagates to failure, it is very difficult to determine its exact origin. Thus the micrographs of figures 38 through 40, which show fracture regions of implant specimens, indicate the general location of the crack propagation, but most likely do not reveal the exact location of crack initiation. Keeping in mind the helical nature of the notch, all three plates when welded with normal welding conditions exhibited cracking in the base metal heat-affected zone, indicating that this is the most susceptible region of the weldment to

hydrogen-induced cracking when a low hydrogen concentration is present. However, when enhanced hydrogen welding conditions were used, plates 2 and 4 cracked in the weld metal, but plate 6 continued to crack in the base metal heat-affected zone. This appears to indicate a much higher susceptibility to hydrogen embrittlement in plate 6. It would appear that when the low levels of diffusible hydrogen are present, the base metal heat-affected zone is more susceptible to hydrogen-assisted cracking than the weld metal. This is probably due to the much higher yield strength of the HY-130 steel in the heat-affected zone. Elger [Ref. 16] reported that the microstructure of HY-130 wrought plate weldments consisted of lower bainite in the weld metal and a region of a mixture of upper bainite (containing a small amount of twinned martensite) and fine lath martensite between the fusion line and approximately 2.5 mm into the heat-affected zone. From 2.5 mm away from the fusion line and into the base metal only fine lath martensite was present. The highly dislocated lower bainite is very susceptible to hydrogen embrittlement [Ref. 17]. This would explain fracture of plates 2 and 4 in the weld metal when enhanced hydrogen welding conditions were used. The amount of upper bainite present in the heat-affected zone increases as more carbides are dissolved in the matrix. Twinned martensite is highly susceptible to hydrogen embrittlement and probably occurs in this region due to carbon segregation [Ref. 18]. It is possible then that plate

6 with its higher percentage of carbon and still segregated microstructure after welding (figure 40), would have a large amount of twinned martensite in the heat-affected zone. As a result, the heat-affected zone microstructure of plate 6 would be highly susceptible to hydrogen embrittlement. This would explain the location of fracture in specimens machined from plate 6.

Another possible explanation for heat-affected zone cracking in specimens from plate 6 is the presence of untempered martensite. Higher carbon contents in steels generally means lower martensite start temperatures. This would imply that martensite formed during welding would not auto-temper during cooling and very high internal stresses could be present, leading to a situation where lower critical concentrations of hydrogen would be necessary for crack initiation and propagation. This implies that plate 6 was highly susceptible to hydrogen embrittlement. Plates 2 and 4 however, with their lower carbon content would tend to have higher martensite start temperatures. This would allow auto-tempering to occur after martensite was formed in the weld zone. Auto-tempering would reduce the internal stresses present within the microstructure and consequently higher external stresses and higher hydrogen concentrations would be necessary for crack initiation and growth [Ref. 15].

Close examination of the scanning electron microscope fractographs shows a correlation between these fractographs and the optical microscopy work. The coarse granular



appearance of fracture surfaces in plate 6 (both normal and enhanced hydrogen welding conditions), would indicate the occurrence of base metal heat-affected zone fracture (figures 27b, 28a, 28b). An area of dimpled fracture surface showing non-metallic inclusions at low magnification is also visible in plate 6 (figure 27a). The fractographs are similar in appearance to those of plates 2 and 4 which were welded using normal conditions (figures 23a, 24a, 25a, 26a). Micrographs 38a and 39a show that cracking occurs in the weld-metal for plates 2 and 4 when welded using enhanced hydrogen welding conditions. The corresponding fractographs (figures 23b, 24b, 25b, and 26b) all differ from those of normal welding conditions for the same plates, supporting the results of the optical microscopy work.

When viewed in a scanning electron microscope, the HY-130 fracture surfaces contained regions of microvoid coalescence, intergranular, and quasi-cleavage fracture. Regions of quasi-cleavage were always associated with the intergranular regions. In each plate the fracture areas appeared to be similar in nature whether enhanced hydrogen or normal welding conditions were used. In other words, dimpled or intergranular areas on fracture surfaces from a specific plate not only were alike for that specimen but were the same as like regions found in the same plate with the enhanced hydrogen welding conditions. However, the amount of each fracture mode observed changed significantly depending on the amounts of diffusible hydrogen present and the stress level. Data from table IX

indicates that for specimens loaded at similar stress levels, those welded with enhanced hydrogen conditions showed a greater percentage of intergranular fracture surface. A similar effect occurs for specimens welded with enhanced hydrogen conditions but loaded under varying stress levels. Increased stress levels caused a lower percentage of intergranular fracture in this case (figure 30). From these results it would appear that differences in the lower critical stress can be explained by the amount of intergranular fracture present. Those specimens that fractured at the lowest stress levels would have the greatest amount of intergranular fracture.

Areas of quasi-cleavage indicate a certain amount of local plastic deformation is occurring during fracture. All three heats of HY-130 were observed to exhibit varying amounts of quasi-cleavage in the regions of intergranular fracture. The intergranular fractures occurring in plate 6 were observed to have the least amount of quasi-cleavage associated with them. Small areas of quasi-cleavage were noted in specimens from plate 6 welded using normal welding conditions (figures 27e and 28e). The ridges present on the fracture surface in these fractographs indicate plastic deformation or tearing, i.e., quasi-cleavage fracture, occurred after the initial intergranular fracture mode. However, these ridges or indications of tearing disappeared almost entirely for the enhanced hydrogen weldments (note the flat smooth grains in figures 27f and 28f).

Plates 2 and 4 exhibited more areas of the quasi-cleavage fracture mode than plate 6, as indicated by the increase in the amounts of tearing visible in the fractographs from those plates (figures 23 e,f; 24 e,f; 25 e,f; and 26 e,f). These plates do not exhibit a decrease in the amounts of quasi-cleavage present for enhanced hydrogen welding conditions as does plate 6. This would indicate that the amount of quasi-cleavage present is not a function of hydrogen content in the weldment, but is instead dependent on the material, or heat of steel in this case.

Differences were also evident in the dimpled fracture areas depending where in the weldment the fracture occurred. Fractures in the weld metal were observed to have larger but fewer inclusions than base metal heat-affected zone fractures. Figures 24c and 24d from plate 2 and figures 25c and 25d from plate 4 clearly show this.

Porosity present in the castings was also an indication of where fractures were occurring. Micrograph 29c of a notch tensile stress specimen shows the porosity present in plate 6. This specimen was known to have fractured in the base metal outside the heat-affected zone. Comparison with micrographs 27f and 28f shows similar porosity for specimens welded with enhanced hydrogen conditions. This again would indicate fracture occurring in the base metal heat-affected zone for plate 6.

Differences in the material properties of each heat of HY-130 steel may also account for the results obtained during

implant testing. Cincotta [Ref. 12] reported that a tempering parameter  $P$ , was an excellent measure of the amount of tempering received by a material. The higher the value of  $P$  the more difficult it is to temper that material. Values of  $P$  for the heat treatments reported in table III are 29,656 for plate 2; 29,170 for plate 4; and 30,172 for plate 6. This indicates that to achieve the desired levels of hardness plates 2 and 6 required more tempering than plate 4, with plate 6 having the greatest resistance to tempering. Results reported by Cincotta support this conclusion. This may explain why auto-tempering of the microstructure of plate 6 may not occur.

One reason that plates 2 and 6 would have required higher tempering temperatures is because of secondary hardening and an inherent resistance to softening due to their increased content of certain alloying elements. The presence of increased amounts of carbide formers in a steel will cause secondary hardening to occur. Plates 2 and 6 contain greater amounts of molybdenum, vanadium and chromium than plate 4, all of which are carbide formers.

The heat-affected zone widths and hardness profiles obtained for each weldment are similar to those obtained by Brucker [Ref. 13] and Sorek [Ref. 14], in their work on HY-130 weldments. This verifies that the welding parameters used were a valid simulation of industrial gas metal-arc welding procedures.

Finally a significant orientation effect was found in plate 2, the rolled plate. Implant specimens oriented parallel to the rolling direction exhibited less susceptibility to hydrogen induced cracking than specimens oriented in the short transverse direction. This result may be attributed to the relative orientation of the alloy banding and applied stress. In the short transverse specimens, crack initiation and propagation might be assisted by the presence of banding parallel to the fracture. However, in the longitudinal specimens, the banding is parallel to the applied stress and normal to the fracture. This result agrees with work by Savage and Nippes on HY-130 rolled plate.

## VI. CONCLUSIONS

1. A lower critical stress for hydrogen-induced cracking was found for normal welding conditions (1-3 ppm hydrogen). This stress is considerably less than the yield stress of HY-130 steel and was found to vary from 76,400 psi to 104,200 psi for the three heats tested.

2. The location of the fracture for the low hydrogen content (1-3 ppm) weldments was in the base metal heat-affected zone, located, on the average about 0.25 to 1.0 mm from the fusion line. This location corresponds to a region found by Elger to consist of upper bainite (with occasional twinned martensite within the bainite laths) and fine lath martensite.

3. At high hydrogen levels (13-23 ppm) the lower critical stress is considerably lower, the lowest value measured was 68,900 psi for the longitudinal orientation of plate 6.

4. The location of the fracture for the high hydrogen welds was in the weld metal near the fusion line for plates 2 and 4 as previously reported for HY-130. However, plate 6 failed in the base metal heat-affected zone. The location of the fractures in plate 6 was at or near the location of the peak hardness in the heat-affected zone. Based on Elger's work it is presumed that plate 6 contains considerably more twinned martensite in this region of the heat-affected zone than plates 2 or 4. This is due to the higher carbon content

and the evidence of significant segregation that persisted through the processing of plate 6.

5. Plate 6 in addition to being the only heat to fail in the base metal with enhanced hydrogen welding conditions exhibited the lowest value of lower critical stress and had the highest embrittlement index of all three heats; 0.590, for enhanced hydrogen welding conditions; but the highest lower critical stress for normal welding conditions.

6. An orientation effect exists in wrought HY-130 steel. Implant specimens machined from the short transverse direction exhibited the lowest resistance to hydrogen assisted cracking.

## VII. RECOMMENDATIONS

An explanation for the behavior of plate 6 must be determined. It is strongly suggested that transmission electron microscopy be performed in the heat-affected zone of plate 6 in order to test the hypothesis of this work. Additionally, acoustical emission studies as outlined by Savage and Nippes would be beneficial in helping to determine more exactly the location of crack initiation and correlate these results with those found in a transmission electron microscopy study. An understanding of this behavior is paramount in the safe application of HY-130 cost components.



TABLES

TABLE I

CHEMICAL COMPOSITION OF PLATES 2, 4 AND 6 (WT. %)

<u>ALLOY</u>	<u>SPECIFICATION</u>		<u>PLATE 2</u>	<u>PLATE 4</u>	<u>PLATE 6</u>
	(CAST)	(WROUGHT)	(WROUGHT)	(CAST)	(CAST)
NICKEL	5.25-5.5	4.75-5.25	4.82	5.64	5.25
MOLYBDENUM	0.3-0.65	0.3-0.65	0.51	0.44	0.52
VANADIUM	0.05-0.1	0.05-0.1	0.08	0.05	0.11
CHROMIUM	0.4-0.7	0.4-0.7	0.57	0.53	0.57
ALUMINUM	0.015-0.035	-	-	0.027	0.034
TITANIUM	0.02 (max)	0.02 (max)	0.01	0.02	0.02
COPPER	0.25 (max)	0.25 (max)	0.08	0.19	0.07
MANGANESE	0.6-0.9	0.6-0.9	0.75	0.75	0.77
SULFUR	0.008 (max)	0.01 (max)	0.006	0.008	0.006
PHOSPHORUS	0.01 (max)	0.01 (max)	0.007	0.008	0.010
SILICON	0.2-0.5	0.2-0.5	0.29	0.29	0.45
CARBON	0.12 (max)	0.12 (max)	0.10	0.09	0.12
OXYGEN	100 ppm max	-	-	26	43
NITROGEN	150 ppm max	-	-	5.8	44
HYDROGEN	10 ppm max	-	-	5.1	5.5

TABLE II  
MECHANICAL PROPERTIES OF PLATES 2, 4 AND 6

<u>DATA</u>	<u>TARGET</u>		<u>PLATE 2</u>	<u>PLATE 4</u>	<u>PLATE 6</u>
	(CAST)	(WROUGHT)	(WROUGHT)	(CAST)	(CAST)
Yield Strength (ksi)	130-145	130-145	134.1	133.7	127.3
Ultimate Strength (ksi)	(1)	(1)	144.6	144.5	143.5
% Elongation	15	15	19.5	15.5	16.5
% Reduction of Area	50	50	61.8	53	49.5
Impact Energy (0°F) (Ft-lbs)	50	60	68	63.3	61
Impact Energy (Room Temp) (Ft-lbs)	(2)	(2)	73.3	72.5	67

(1) Recorded for information only

(2) Average CVN at room temperature shall not be more than 15 ft-lb above average at 0°F.

TABLE III  
HEAT TREATMENT OF PLATES 2, 4, AND 6

<u>PLATE 2</u>	<u>PLATE 4</u>	<u>PLATE 6</u>
1. Austenitize, 1525F, 3 hours, Water Quench	1. Normalize, 1900F 5 hours, Air Cool	1. Normalize, 1750F 4 hours, Air Cool
2. Temper, 1145F 3 hours, Water Quench	2. Austenitize, 1650F, 3 hours, Water Quench	2. Austenitize, 1650F, 3 hours, Water Quench
	3. Reaustenitize, 1550 F, 5.5 hours, Water Quench	3. Reaustenitize, 1550F, 3 hours, Water Quench
	4. Temper 1065F 5.5 hours, Water Quench	4. Temper, 1125F 3 hours, Water Quench
	5. Reaustenitize, 1650F, 5 hours, Water Quench	5. Retemper, 1150F, 5.5 hours, Water Quench
	6. Reaustenitize, 1550F, 5 hours, Water Quench	
	7. Retemper 1100F 5 hours, Water Quench	

TABLE IV  
COMPOSITION AND PROPERTIES OF HY-130 WELD WIRE (MIL-140S-1)

<u>ALLOY</u>	<u>WT. %</u>
NICKEL	2.6
MOLYBDENUM	0.93
VANADIUM	0.011
CHROMIUM	0.73
ALUMINUM	0.016
TITANIUM	0.021
COPPER	0.09
MANGANESE	1.63
SULFUR	0.006
PHOSPHORUS	0.007
SILICON	0.44
CARBON	0.097
ZIRCONIUM	0.01

MINIMUM YIELD STRENGTH - 135,000 PSI

TABLE V  
COMPARISON OF WELDING PARAMETERS FOR IMPLANT TESTING  
AND OPERATIONAL WELDING OF HY-130 STEELS

<u>PARAMETER</u>	<u>IMPLANT WELDING</u>	<u>OPERATIONAL WELDING</u>
AMPERAGE (I)	200	370
VOLTAGE (E)	29	27
TRAVEL SPEED (inches per minute)	6.5	11.6
HEAT INPUT (KJ/IN)	53.5	51.7
PROCESS	GMA SPRAY	GMA SPRAY
GAS/FLOW RATE (CFH)	Ar-2%O <sub>2</sub> /40	Ar-2%O <sub>2</sub> /40
PREHEAT TEMP (°C)	100	100
CURRENT	DCRP	DCRP

TABLE VI  
IMPLANT TEST DATA

PLATE 2S: NON-ENHANCED

RUN	STRESS (PSI)	TIME TO RUPTURE (MIN)	H <sub>2</sub> (PPM)
1	166,800	0.1	-
2	164,000	1.0	1.0
3	157,000	2.0	1.6
4	137,600	6.1	1.2
5	120,900	6.0	14.1
6	104,200	18.0	0.4
7	90,300	24.0	1.1
8	79,800	100	2.4
9	76,400	>1440	0.2

PLATE 2S: ENHANCED

RUN	STRESS (PSI)	TIME TO RUPTURE (MIN)	H <sub>2</sub> (PPM)
1	164,000	0.1	18.7
2	139,000	2.5	20.3
3	119,500	6.0	21.0
4	100,000	12.0	19.2
5	90,200	22	20.5
6	83,400	>1440	7.7
7	78,200	72	20.2
8	70,200	>1440	19.9

PLATE 2L: NON-ENHANCED

1	164,000	0.1	0.9
2	157,000	2.8	1.6
3	139,000	3.5	1.4
4	120,900	40	1.0
5	109,800	70	1.1
6	108,400	13	10.2
7	91,700	286	2.8
8	91,200	>1440	1.0

PLATE 2L: ENHANCED

1	168,300	0.1	18.9
2	157,000	2.5	14.0
3	139,000	5.1	14.6
4	119,500	9.5	18.5
5	104,200	15	20.6
6	86,300	66	19.4
7	80,200	250	17.6
8	77,200	>1440	20.4

TABLE VI (CONTINUED)

PLATE 4S: NON-ENHANCED

RUN	STRESS (PSI)	TIME TO RUPTURE (MIN)	H <sub>2</sub> (PPM)
1	177,900	0.1	-
2	170,900	0.9	1.5
3	163,300	5.3	2.1
4	143,100	8.5	3.7
5	119,500	22.5	0.9
6	108,400	46	0.4
7	93,100	51	12.1
8	90,000	110	1.1
9	82,000	>1440	0.5

PLATE 4S: ENHANCED

RUN	STRESS (PSI)	TIME TO RUPTURE (MIN)	H <sub>2</sub> (PPM)
1	177,900	0.1	-
2	161,200	1.5	21.6
3	159,800	2.5	20.1
4	143,800	5.2	17.3
5	123,700	12.0	20.2
6	109,800	19	20.7
7	97,300	30	20.5
8	79,200	125	18.3
9	76,400	>1440	19.5

PLATE 4L: NON-ENHANCED

1	169,500	0.1	-
2	165,400	0.8	2.1
3	158,400	1.5	3.7
4	145,900	5.3	1.0
5	137,600	25	2.7
6	119,500	36	0.2
7	102,800	135	3.0
8	90,300	360	3.2
9	82,700	>1440	0.2

PLATE 4L: ENHANCED

1	169,500	0.1	-
2	155,600	5.5	21.8
3	147,300	7.0	13.4
4	125,100	11.8	20.7
5	102,100	22	17.3
6	94,500	57	19.5
7	83,200	230	16.9
8	75,000	>1440	20.7

TABLE VI (CONTINUED)

PLATE 6S: NON-ENHANCED

RUN	STRESS (PSI)	TIME TO RUPTURE (MIN)	H <sub>2</sub> (PPM)
-----	-----------------	-----------------------------	-------------------------

1	169,800	0.1	-
2	161,200	1.7	1.1
3	150,100	9.0	2.1
4	139,010	26.5	0.9
5	132,000	38.8	3.0
6	113,900	102	0.5
7	104,200	>1440	1.8

PLATE 6S: ENHANCED

RUN	STRESS (PSI)	TIME TO RUPTURE (MIN)	H <sub>2</sub> (PPM)
-----	-----------------	-----------------------------	-------------------------

1	169,500	0.1	-
2	166,800	0.6	20.8
3	141,700	1.2	20.2
4	118,100	2.2	16.5
5	98,500	3.4	17.4
6	95,900	13.2	8.81
7	86,100	10.3	16.9
8	83,700	29	15.2
9	79,100	82	19.1
10	76,400	>1440	20.4

PLATE 6L: NON-ENHANCED

1	166,500	0.1	-
2	162,600	1.3	2.1
3	150,180	2.5	2.42
4	127,800	3.3	2.9
5	113,200	9	2.3
6	105,600	18	2.7
7	98,500	31	1.7
8	94,300	100	1.1
9	91,700	1440	2.5

PLATE 6L: ENHANCED

1	168,200	0.1	-
2	159,800	0.4	22.5
3	139,000	0.8	17.2
4	119,500	3.2	20.9
5	94,200	24.5	19.0
6	84,700	32	13.5
7	76,400	50	14.4
8	69,500	232	18.3
9	68,900	1440	19.9



TABLE VII  
STATISTICAL DATA ON HYDROGEN CONTENT  
OF IMPLANT TEST WELDMENTS

<u>ITEM</u>	<u>ENHANCED HYDROGEN</u>	<u>NORMAL CONDITIONS</u>
NO. OF DATA POINTS	46	43
HIGHEST HYDROGEN CONTENT (PPM)	22.5	3.7
LOWEST HYDROGEN CONTENT (PPM)	13.4	0.2
MEAN VALUE OF HYDROGEN (PPM)	18.79	1.65
STANDARD DEVIATION	2.29	0.975
VARIANCE	5.25	0.950

TABLE VIII  
SUMMARY OF IMPLANT TEST RESULTS

<u>PLATE</u>	<u>*NTS</u>	<u>*LCS</u>	<u>I</u>	<u>% INCREASE IN I</u>
2S (NE)	166,800	76,450	0.542	
2S (E)	164,030	70,230	0.572	5.5
2L (NE)	164,030	91,290	0.443	
2L (E)	168,360	77,250	0.541	22.1
4S (NE)	177,930	82,010	0.539	
4S (E)	177,930	76,450	0.570	5.8
4L (NE)	169,590	82,710	0.512	
4L (E)	169,590	75,000	0.558	8.9
6S (NE)	169,810	104,250	0.386	
6S (E)	169,590	76,450	0.541	40.2
6L (NE)	166,590	91,740	0.449	
6L (E)	168,200	68,900	0.590	31.0

$$\text{Embrittlement Index: } I = \frac{\text{NTS} - \text{LCS}}{\text{NTS}}$$

(NE) - non-enhanced (normal) welding conditions

(E) - enhanced hydrogen welding conditions

\* data is given in psi

TABLE IX  
SPECIMENS EXAMINED FOR S.E.M. FRACTOGRAPHY

SPECIMEN NO.	H <sub>2</sub> (ppm)	STRESS (psi)	TIME (min.)	% Ductile	% IG.
6-2S	2.4	79,800	100	70	30
12-2S	20.2	78,200	72	10	90
5-2L	1.1	109,800	70	70	30
13-2L	19.4	86,200	66	30	70
5-4S	1.1	90,000	110	80	20
10-4S	18.3	79,200	125	25	75
5-4L	4.2	102,800	135	85	15
11-4L	19.5	94,500	57	20	80
5-6S	0.7	113,900	102	80	20
11-6S	19.1	79,100	82	25	75
5-6L	1.1	94,300	100	60	40
12-6L	14.4	76,400	50	25	75
6-6S	11.9	169,500	0.1	100	0
8-6S	16.5	118,100	2.3	85	15
10-6S	17.41	95,100	10.3	70	30
7-6S	16.86	86,100	13.2	45	55
11-6S	18.81	74,500	82	25	75

FIGURES

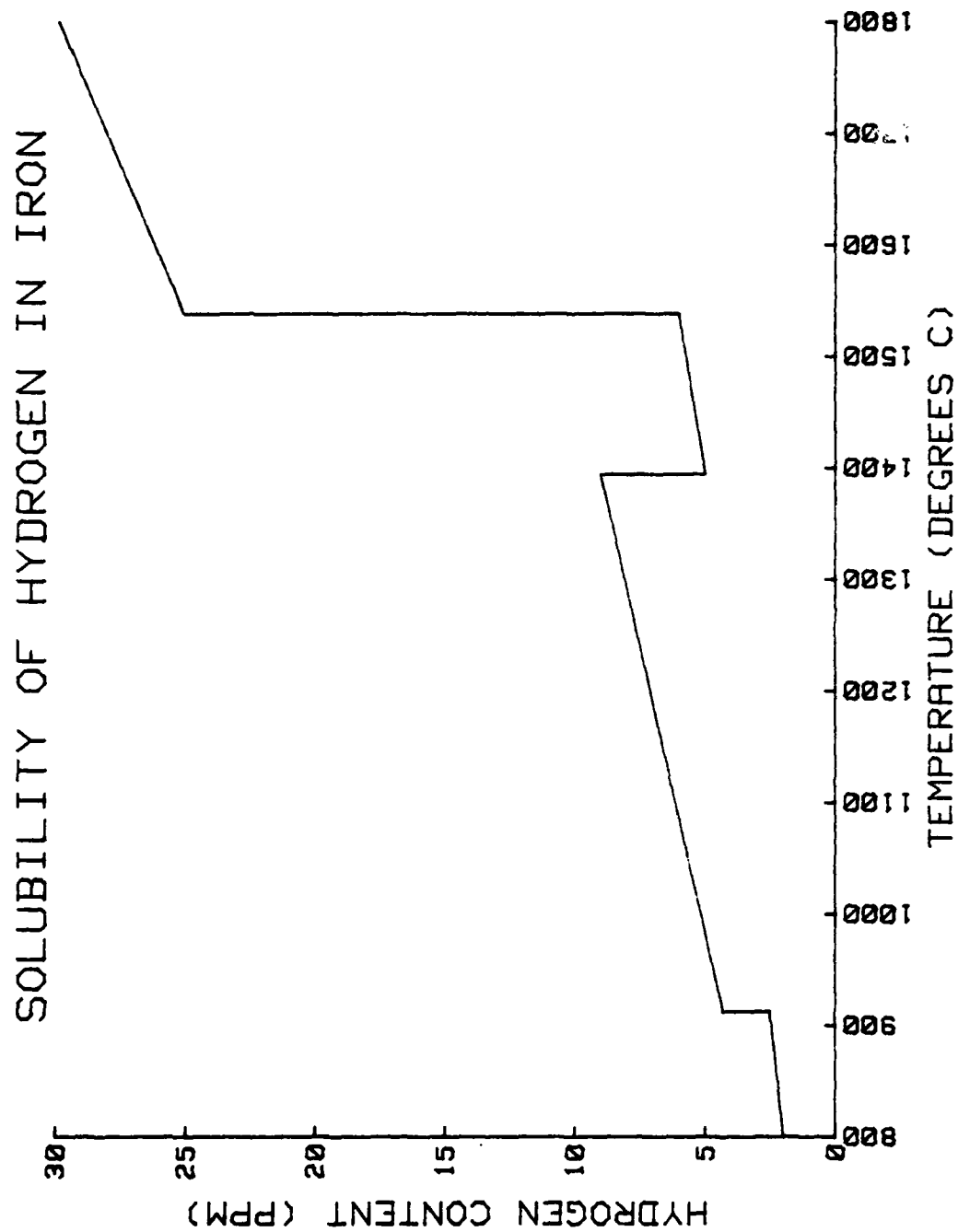


Figure 1. Solubility of Hydrogen in Iron [Ref. 10]

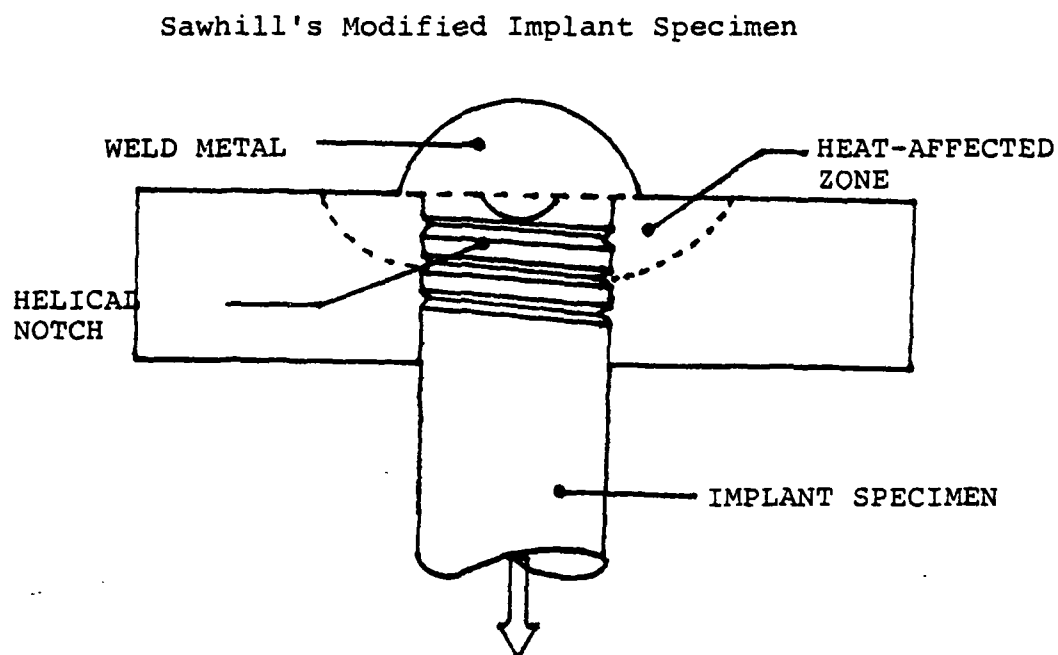
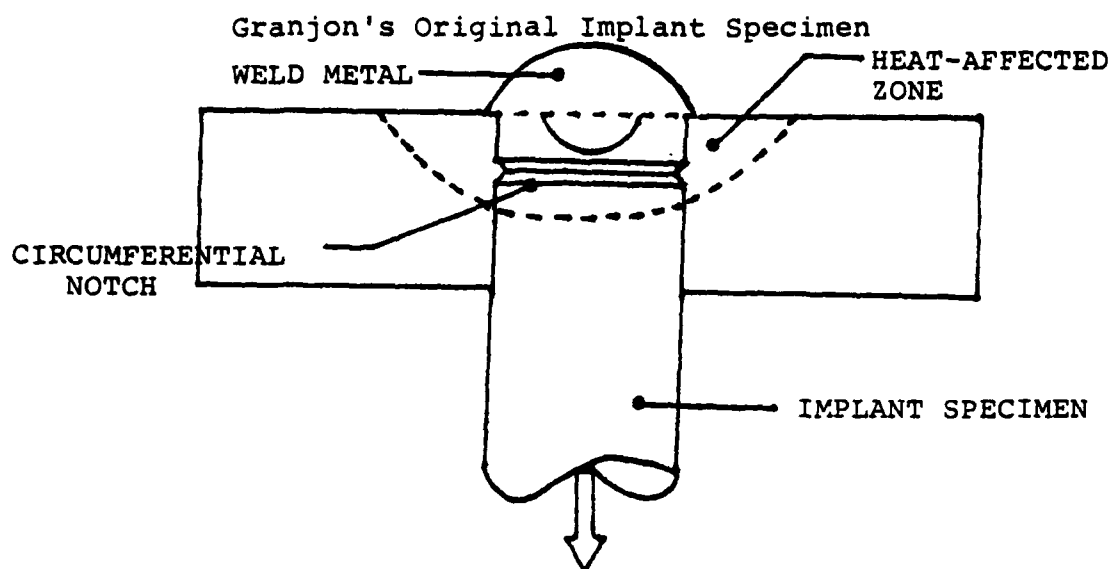


Figure 2. Comparison of Notch Configuration for Implant Test Specimens

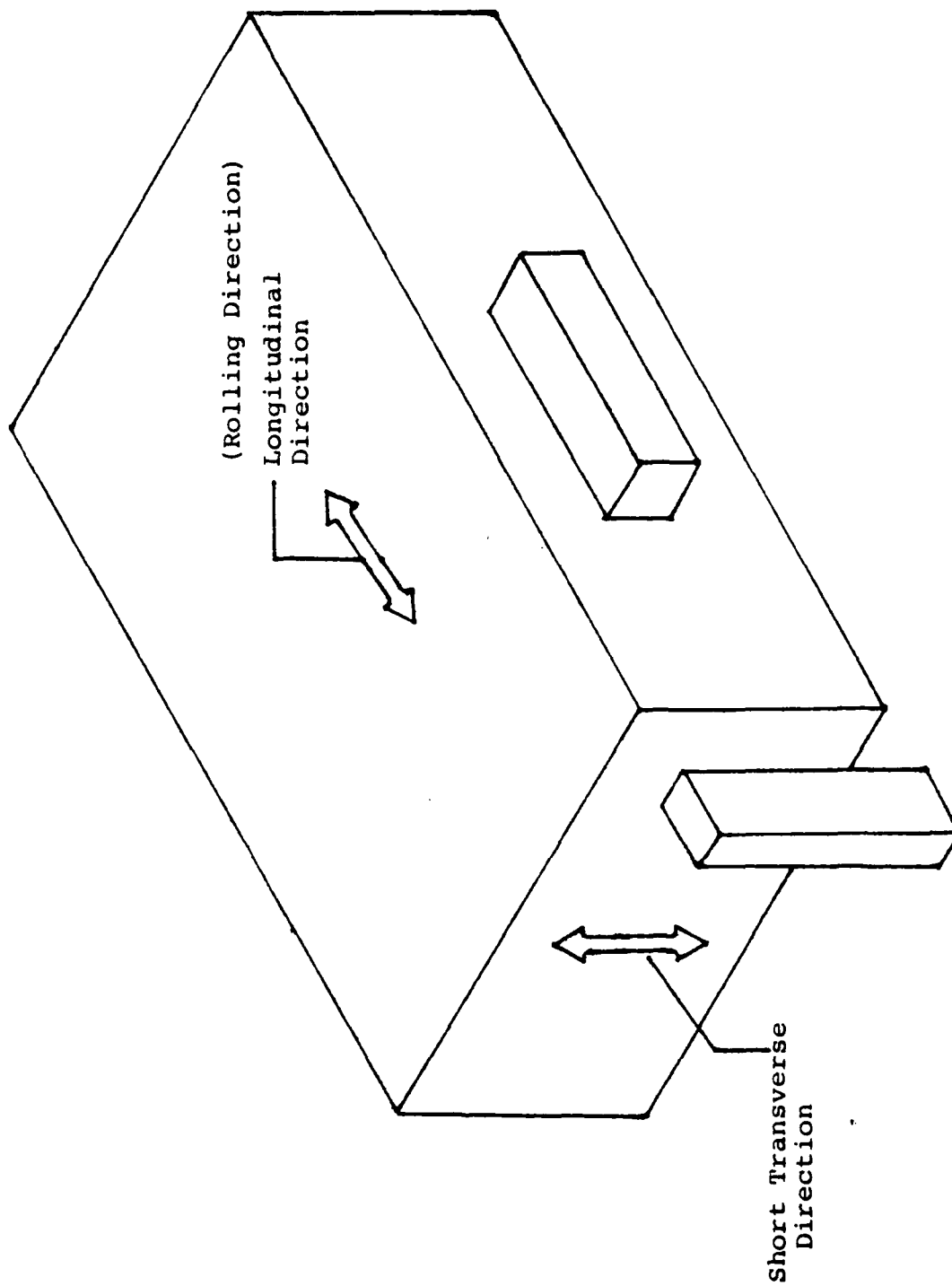


Figure 3. Orientation of Implant Test Specimens

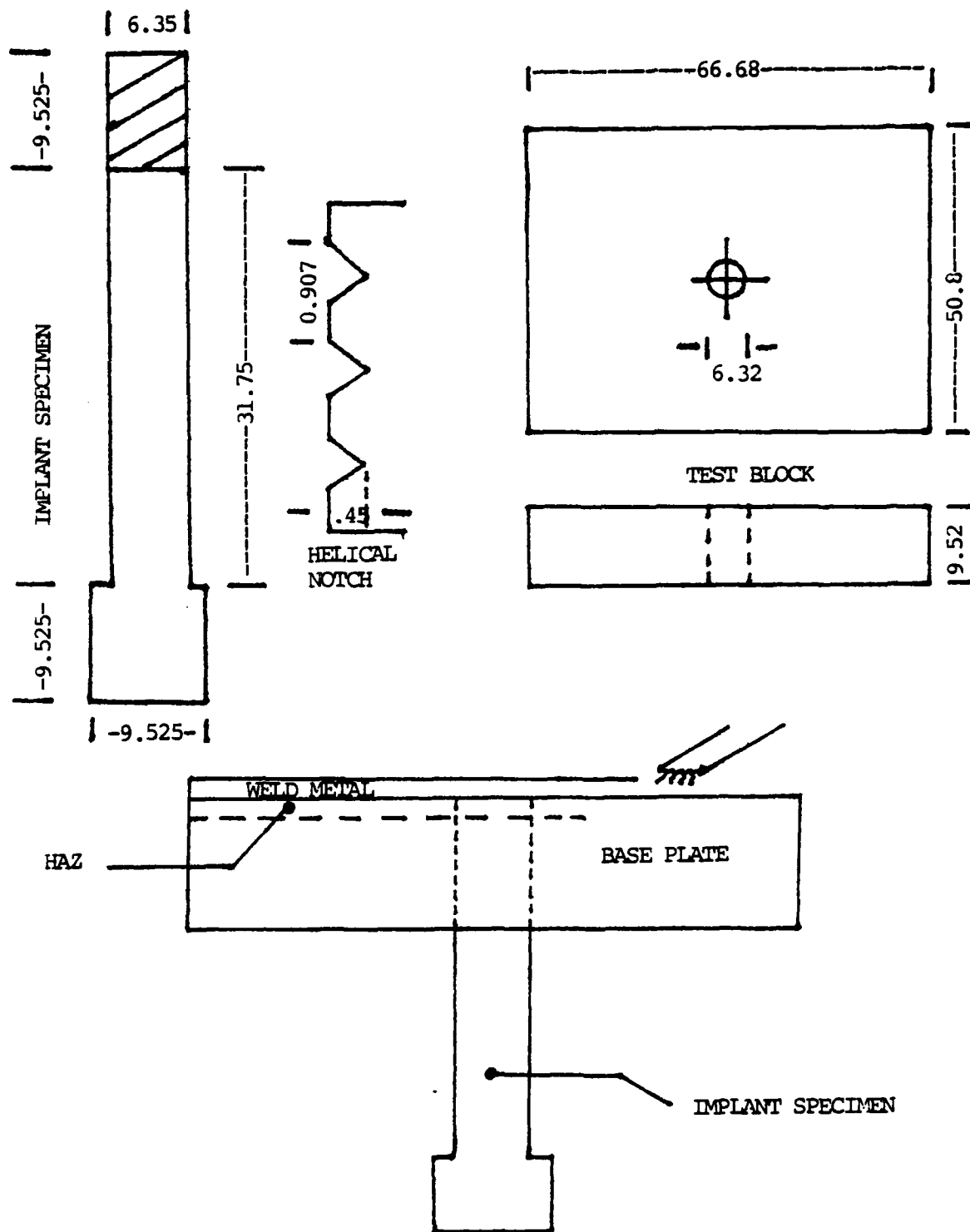
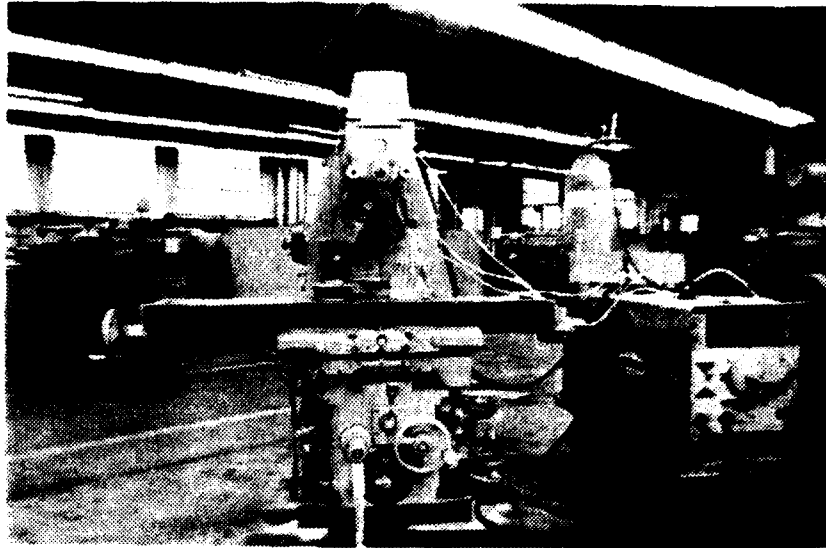


Figure 4. Details of Implant Test Assembly  
(dimensions in mm.)

5a) Implant Test Welding Equipment



5b) Hydrogen Analysis Apparatus

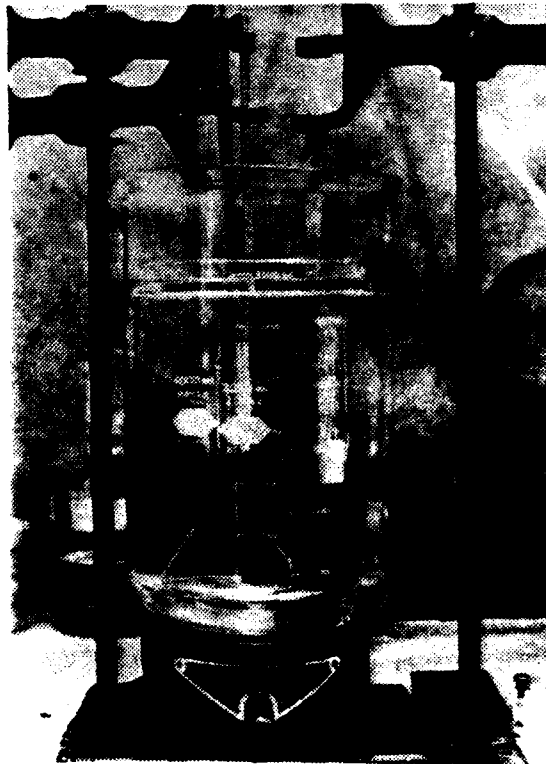
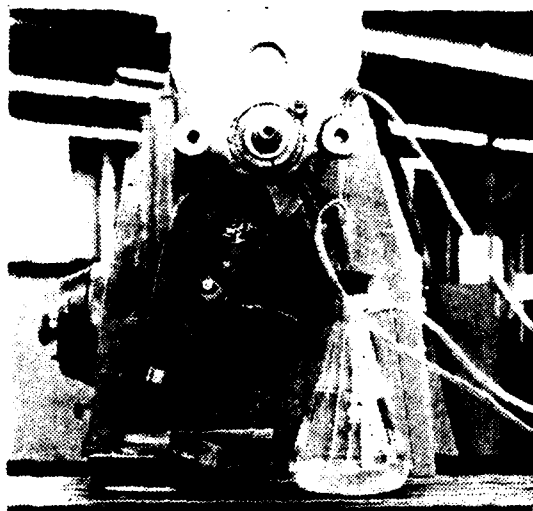


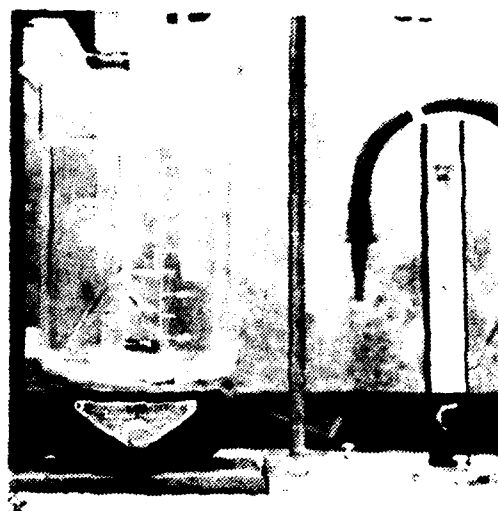
Figure 5. Implant Welding and Hydrogen Analysis Apparatus



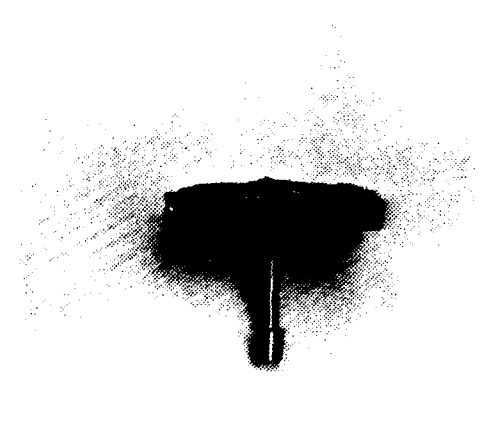
6a) Welding Apparatus



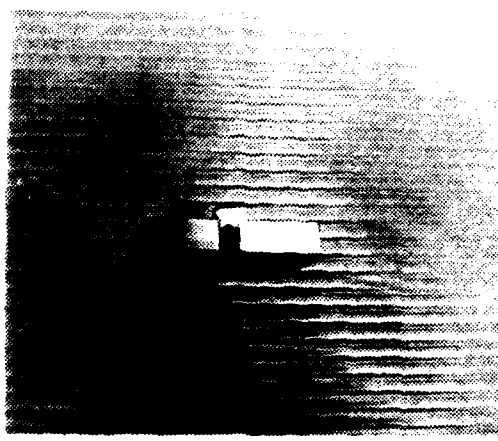
6b) Hydrogen Analysis



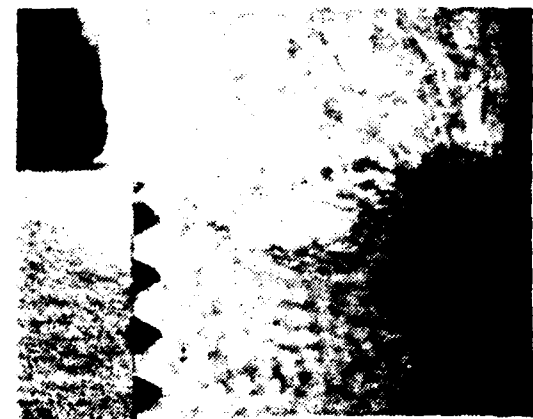
6c) Welded Implant Assembly



6d) Fractured Implant Assembly



6e) Weld Penetration HAZ



6f) Loaded Test Assembly

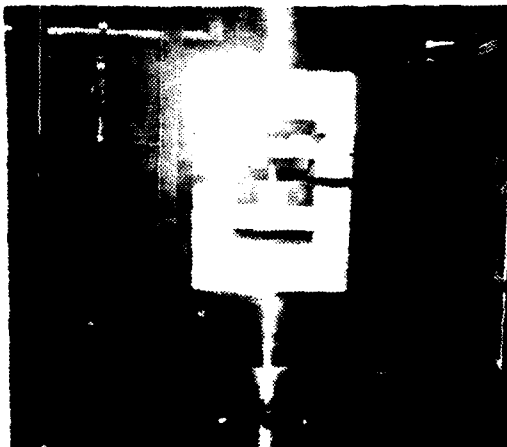


Figure 6. Procedures Involved in Implant Testing

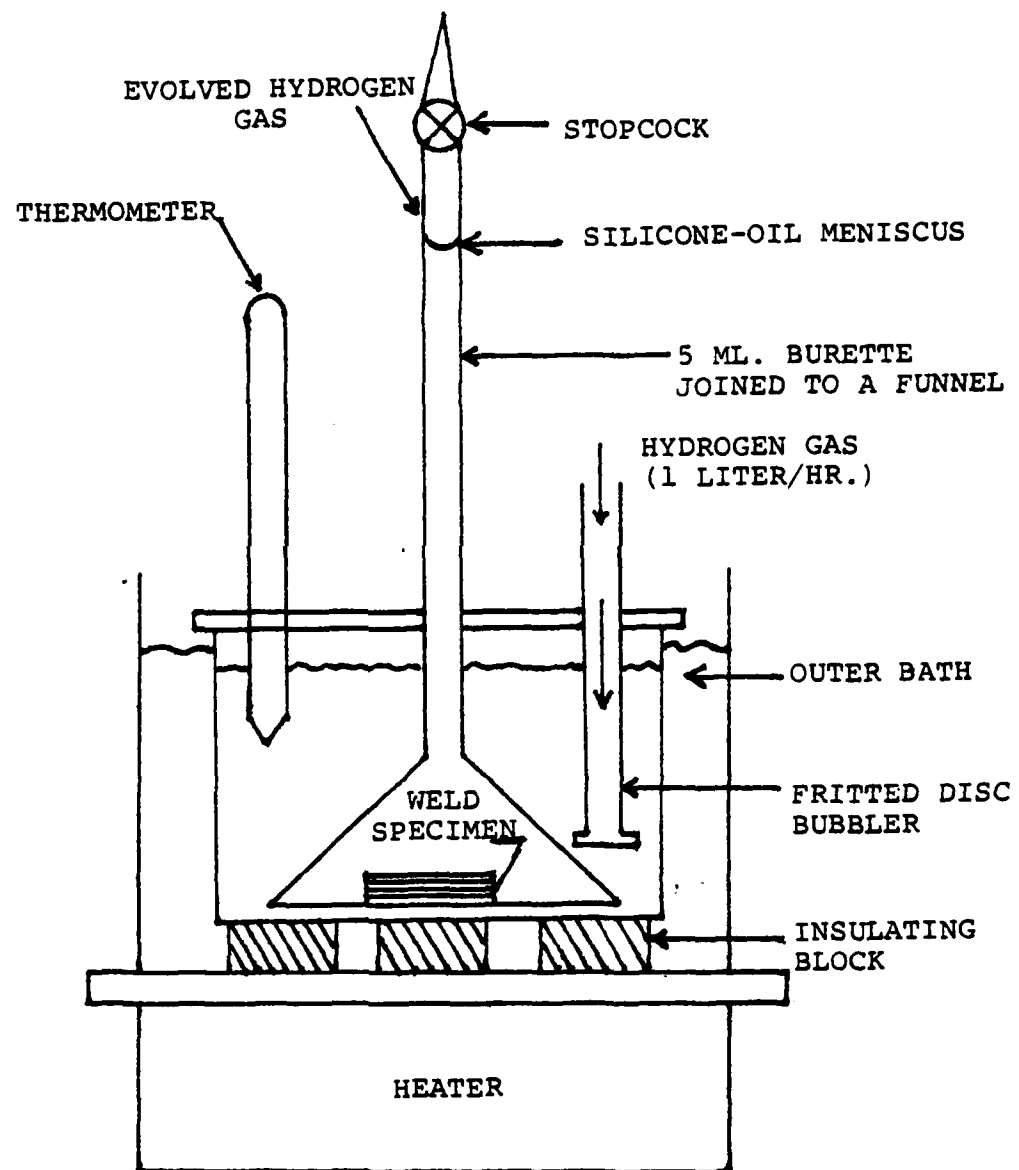


Figure 7. Schematic of Hydrogen Analysis Apparatus

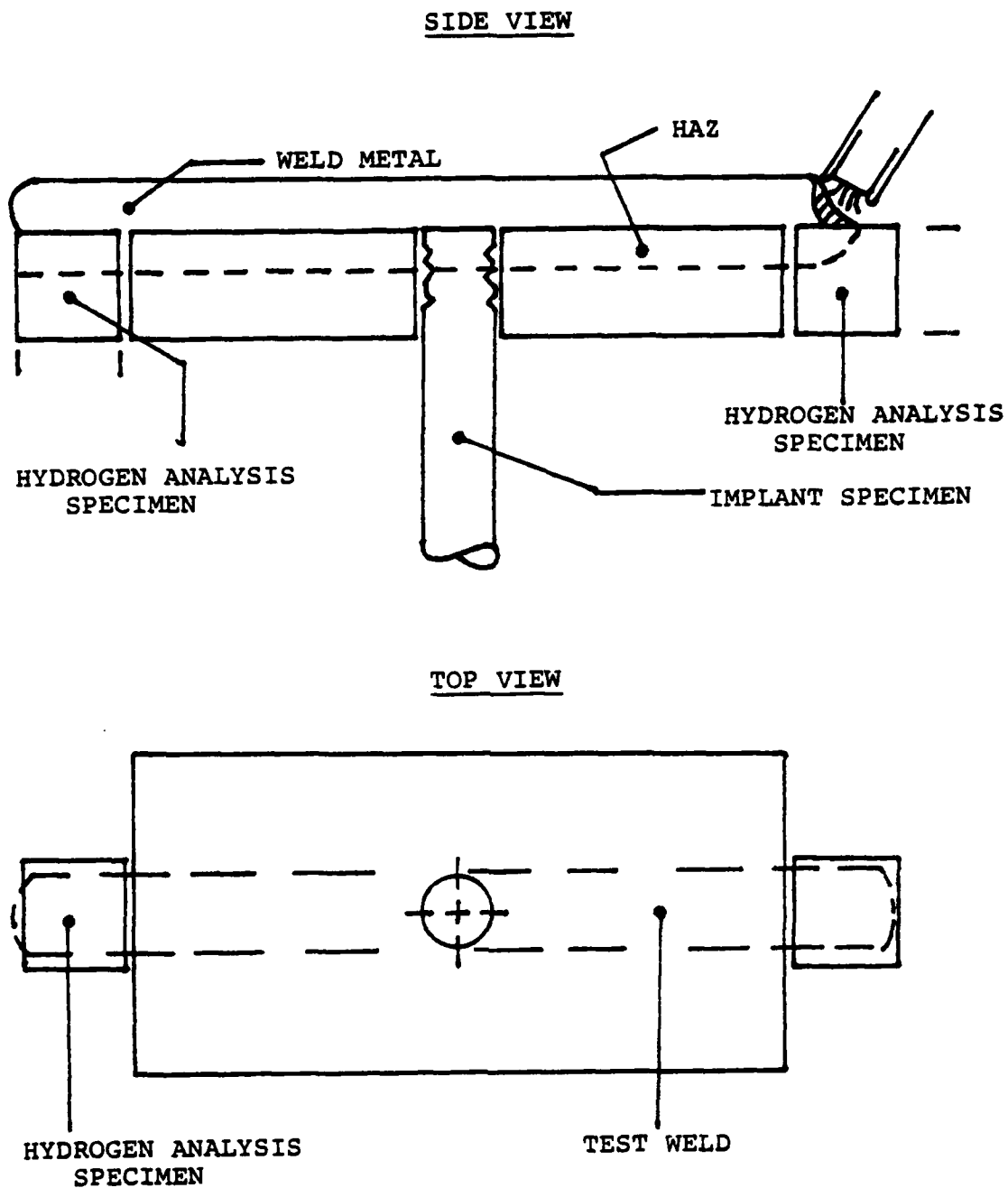


Figure 8. Orientation of Hydrogen Analysis Specimens During Implant Test Welding

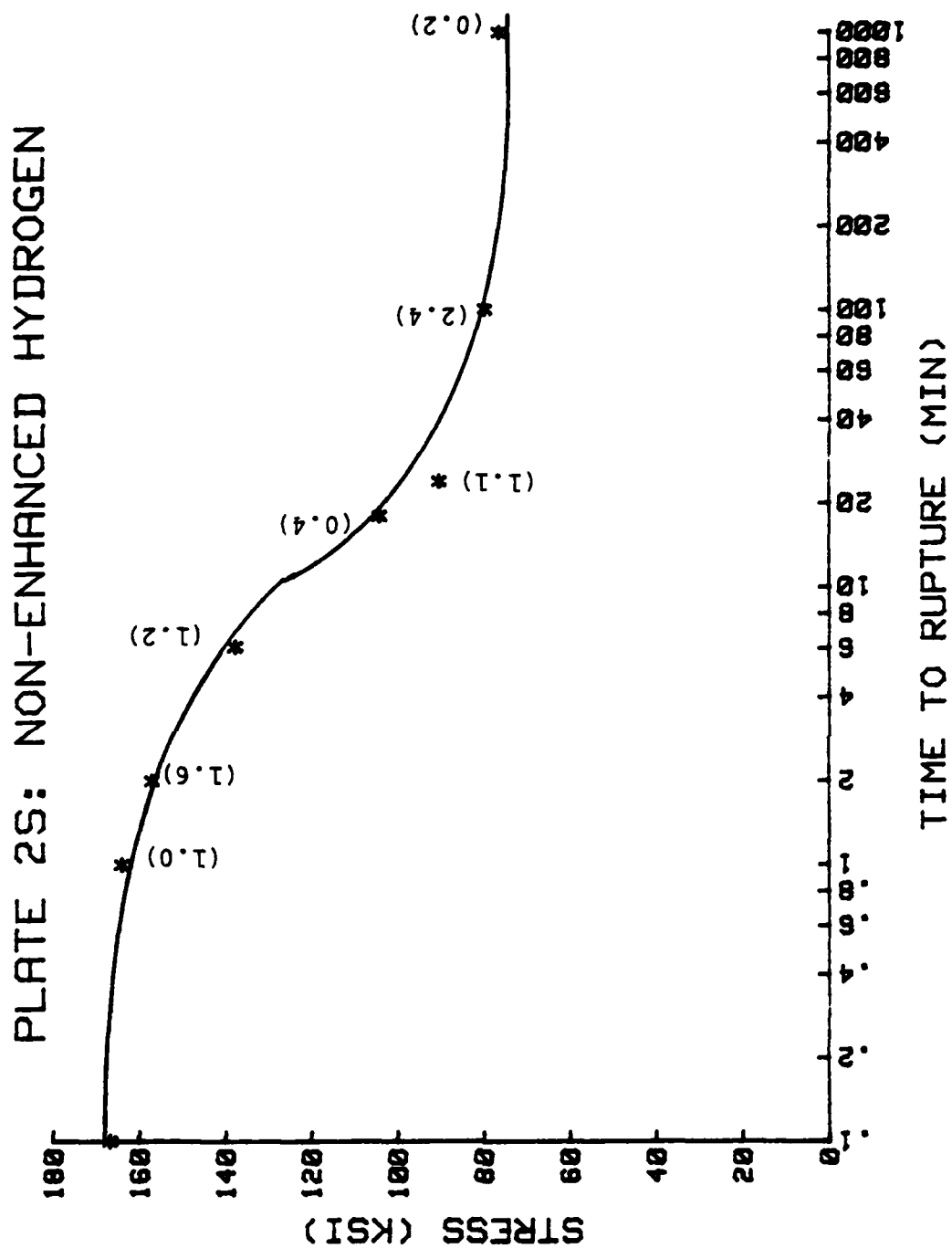


Figure 9. Stress vs. Time-to-Rupture for Plate 2 Short Transverse Direction Normal Welding Conditions

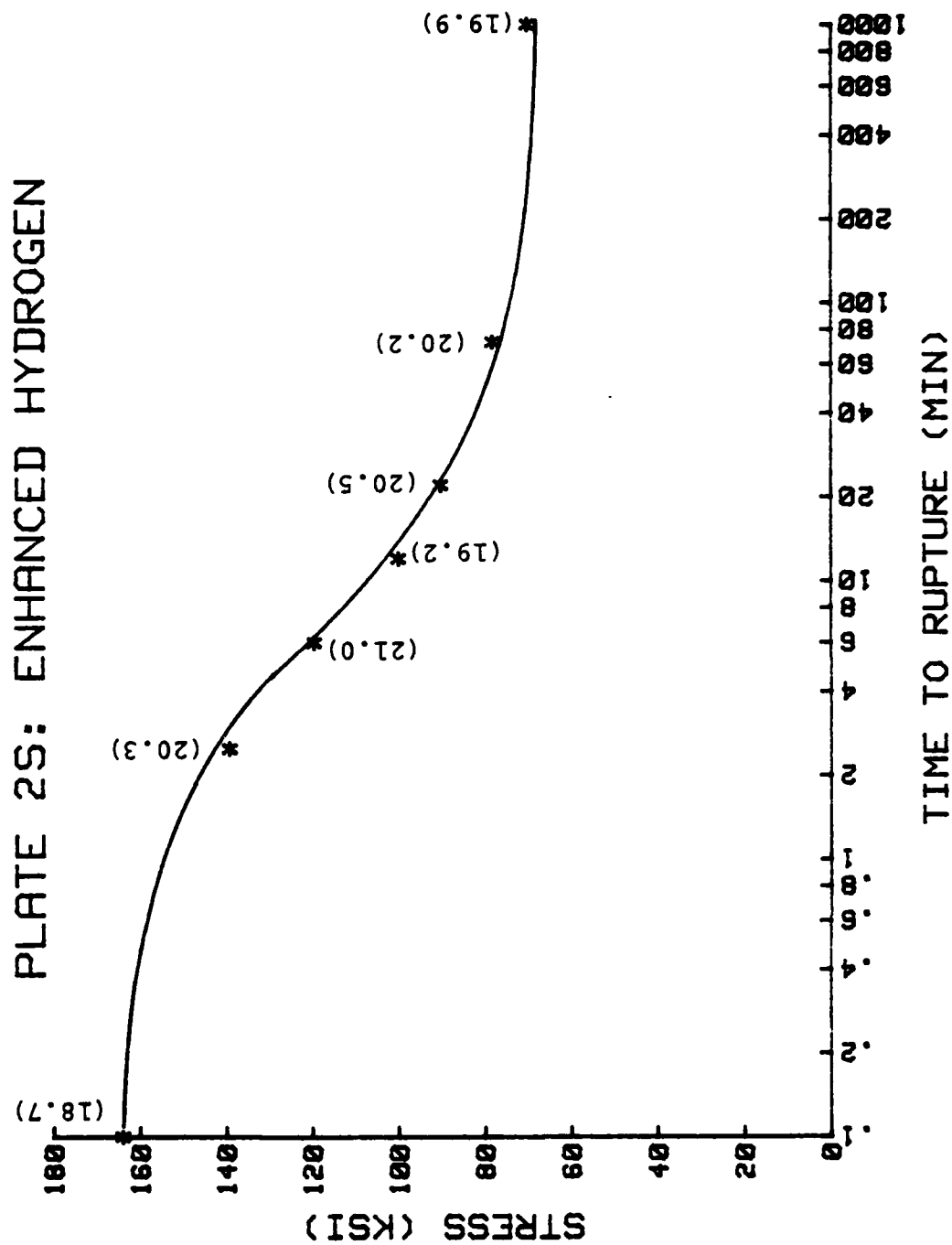


Figure 10. Stress vs. Time-to-Rupture for Plate 2 Short Transverse Direction Enhanced Hydrogen Welding Conditions

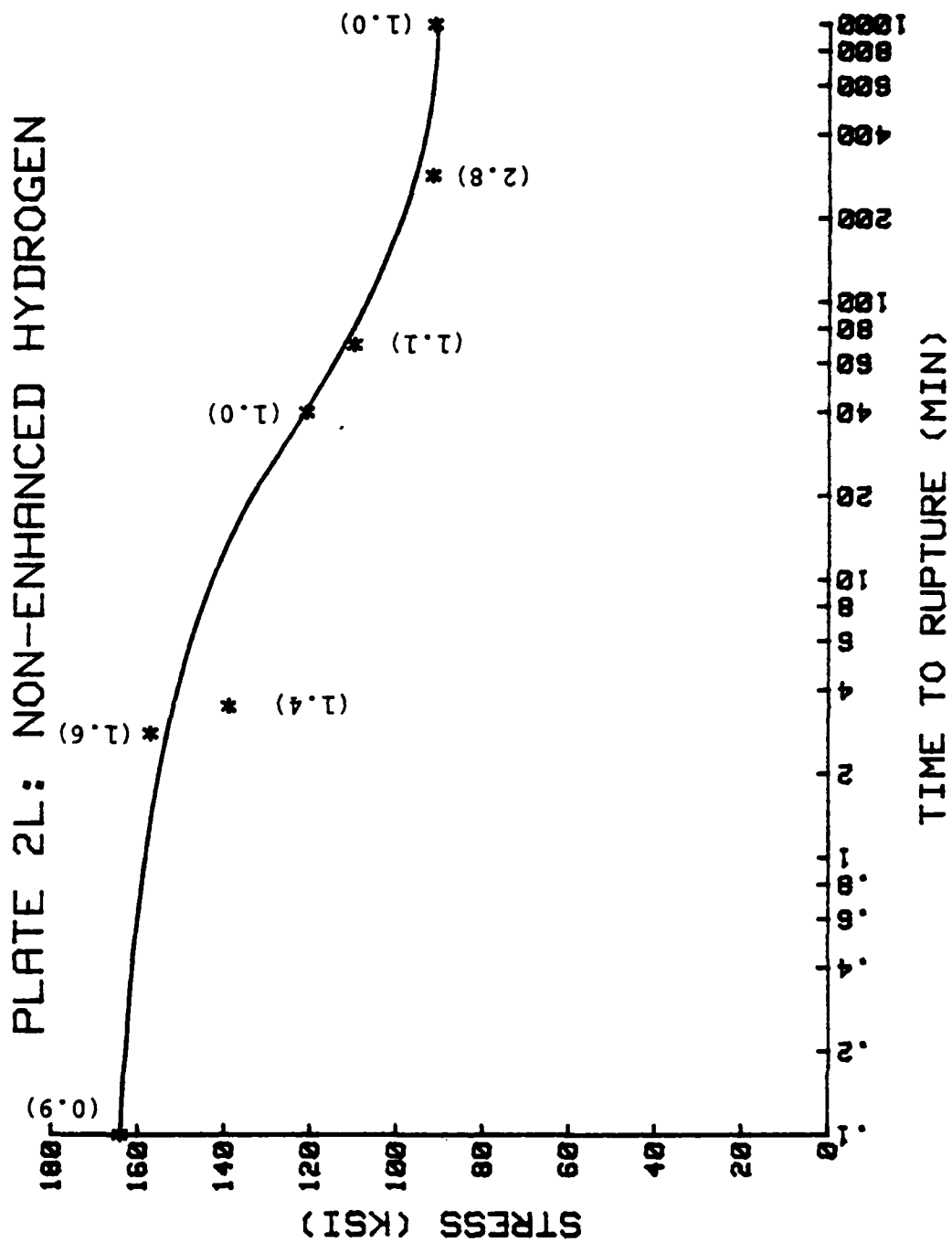


Figure 11. Stress vs. Time-to-Rupture for Plate 2 Longitudinal  
Direction Normal Welding Conditions

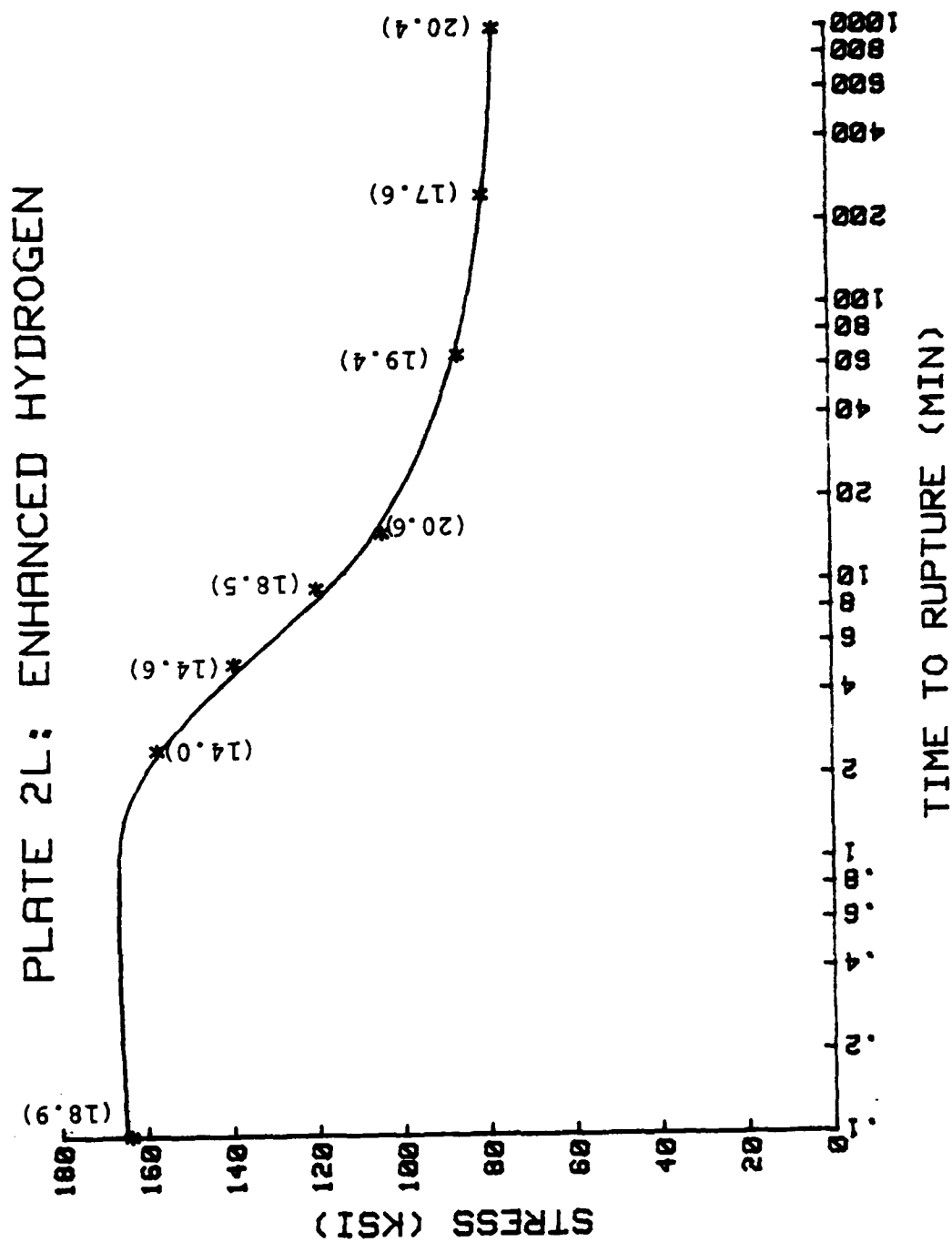


Figure 12. Stress vs. Time-to-Rupture for plate 2 Longitudinal Direction Enhanced Hydrogen Welding Conditions

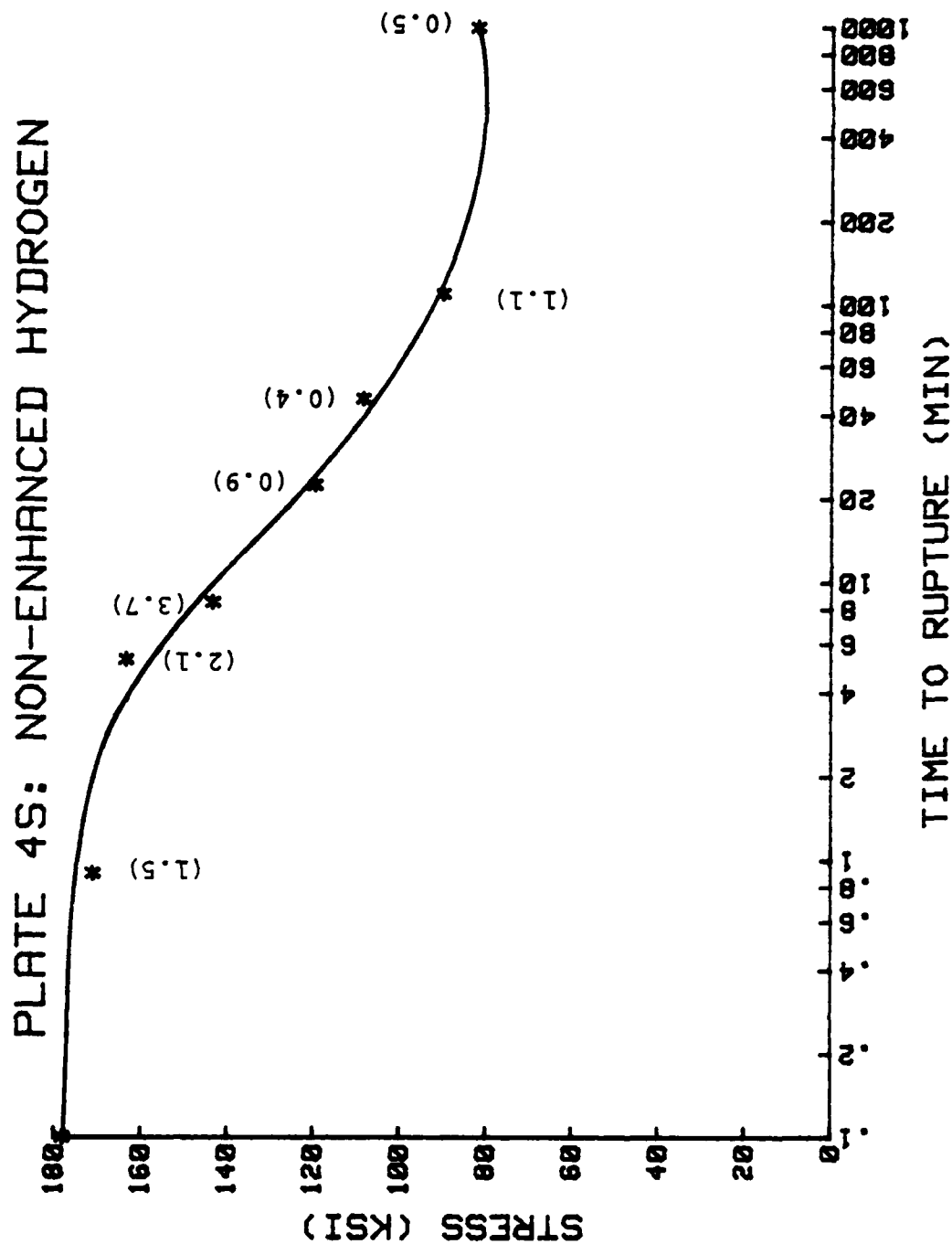


Figure 13. Stress vs. Time-to-Rupture for Plate 4 Short Transverse Direction Normal Welding Conditions



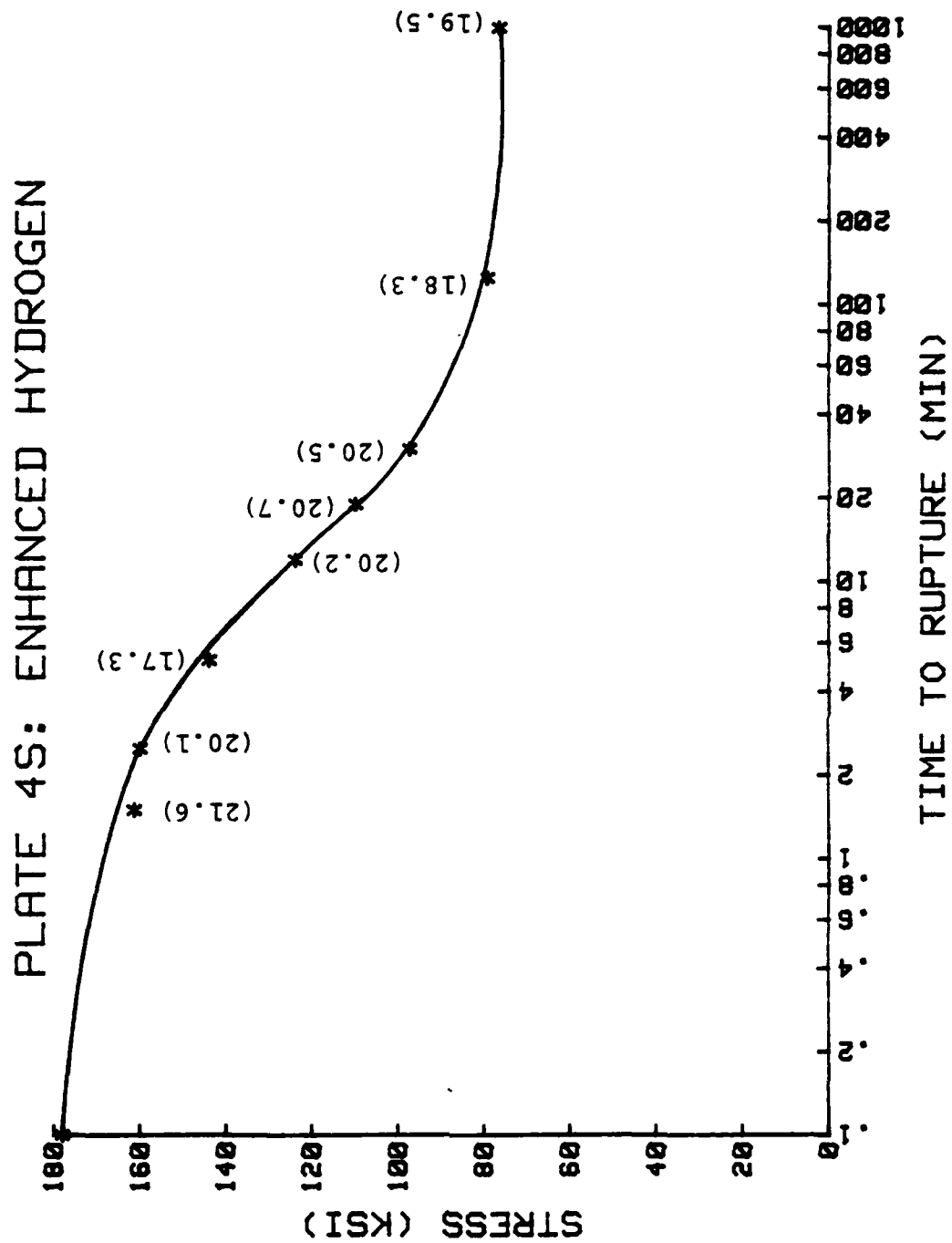


Figure 14. Stress vs. Time-to-Rupture for Plate 4 Short Transverse Direction Enhanced Hydrogen Welding Conditions

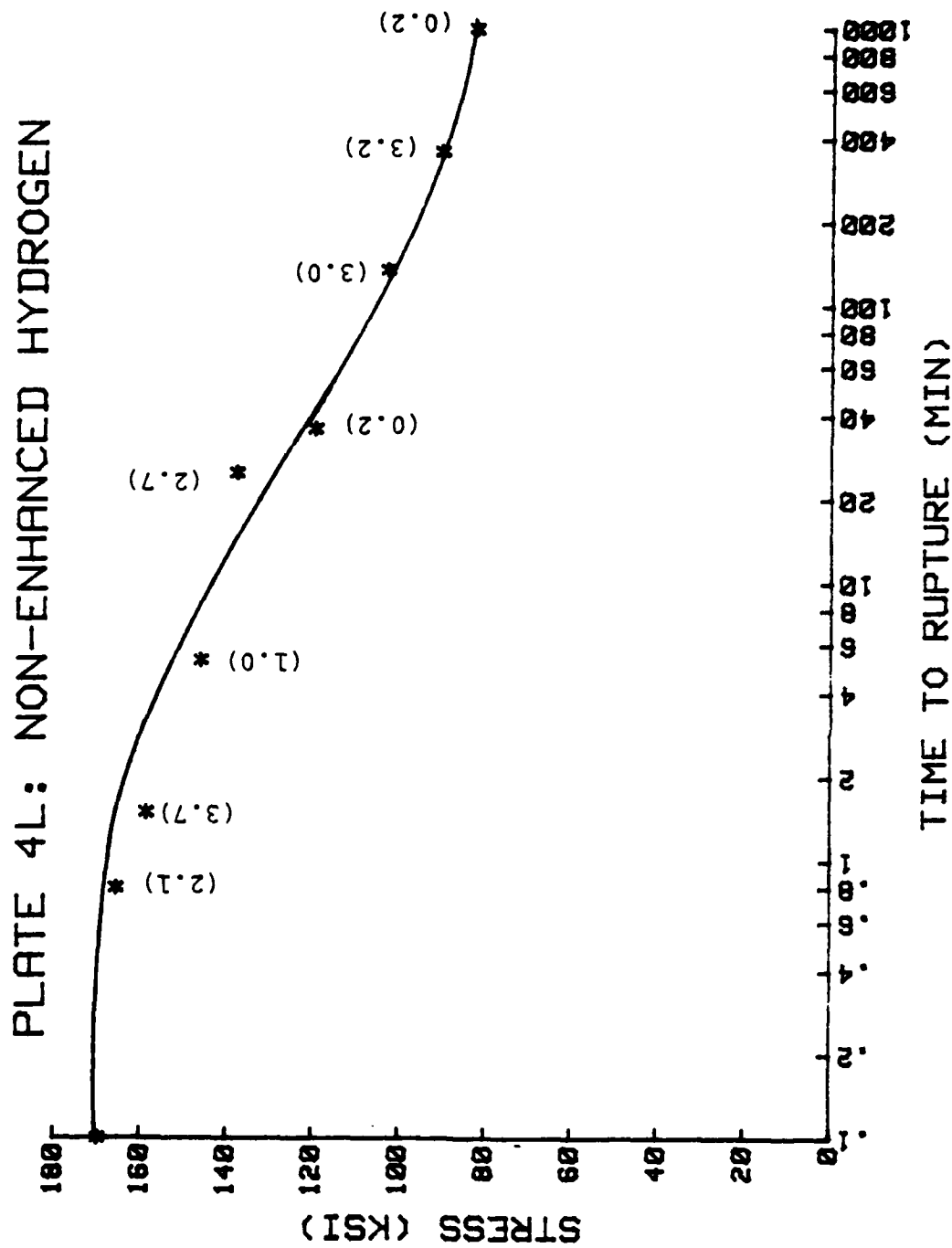


Figure 15. Stress vs. Time-to-Rupture for Plate 4 Longitudinal Direction, Normal Welding Conditions

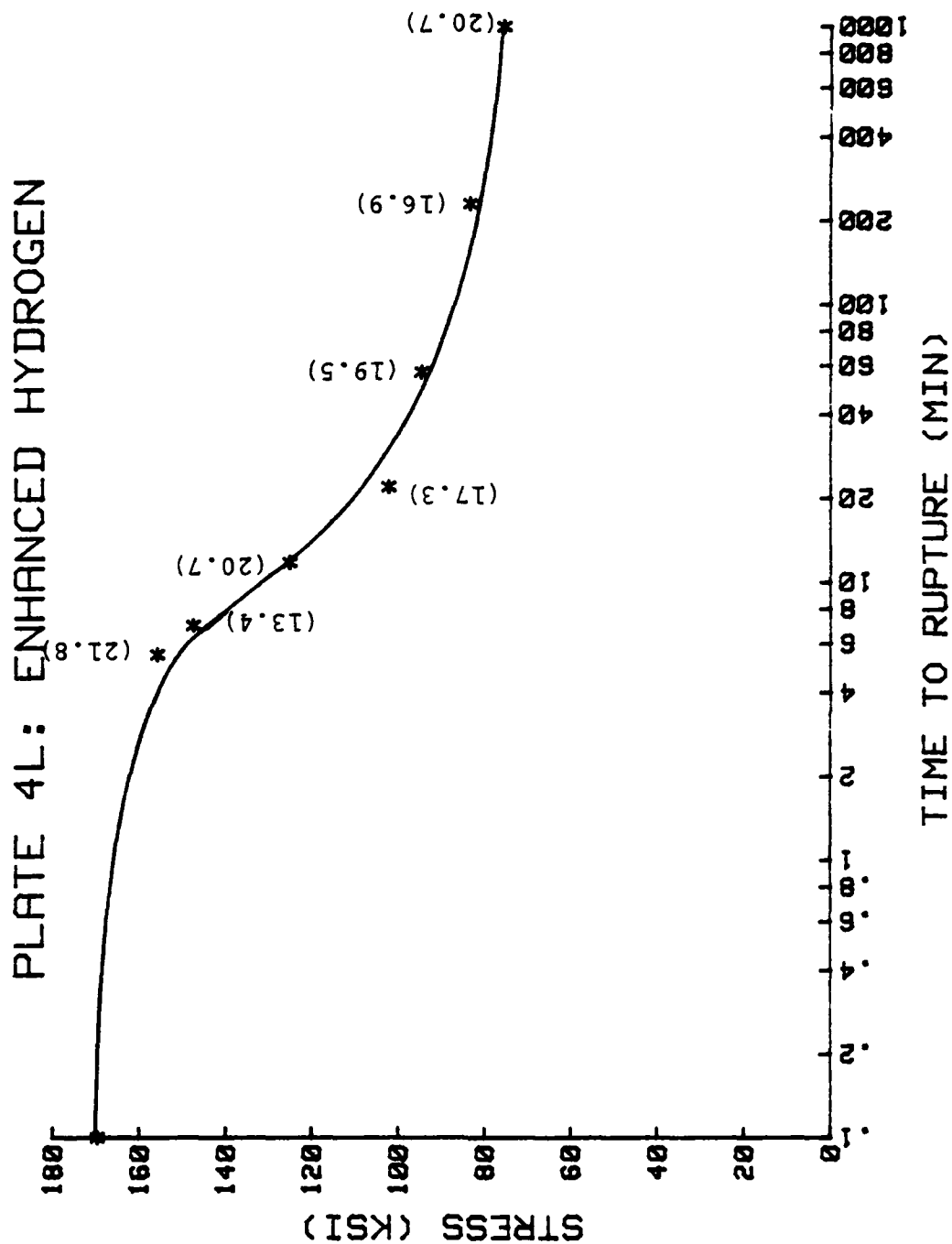


Figure 16. Stress vs. Time-to-Rupture for Plate 4 Longitudinal Direction Enhanced Hydrogen Welding Conditions

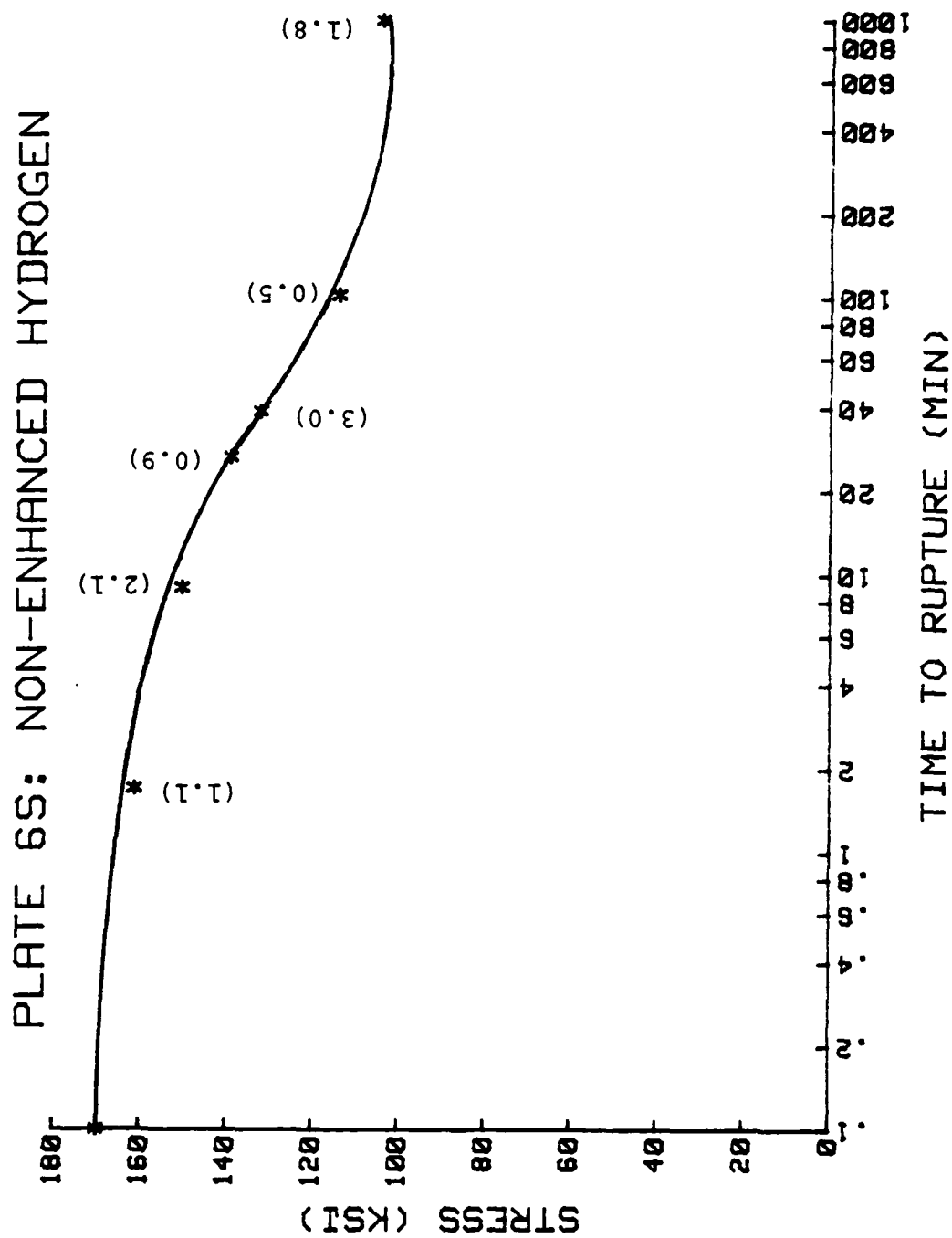


Figure 17. Stress vs. Time-to-Rupture for Plate 6 Short Transverse Direction, Normal Welding Conditions

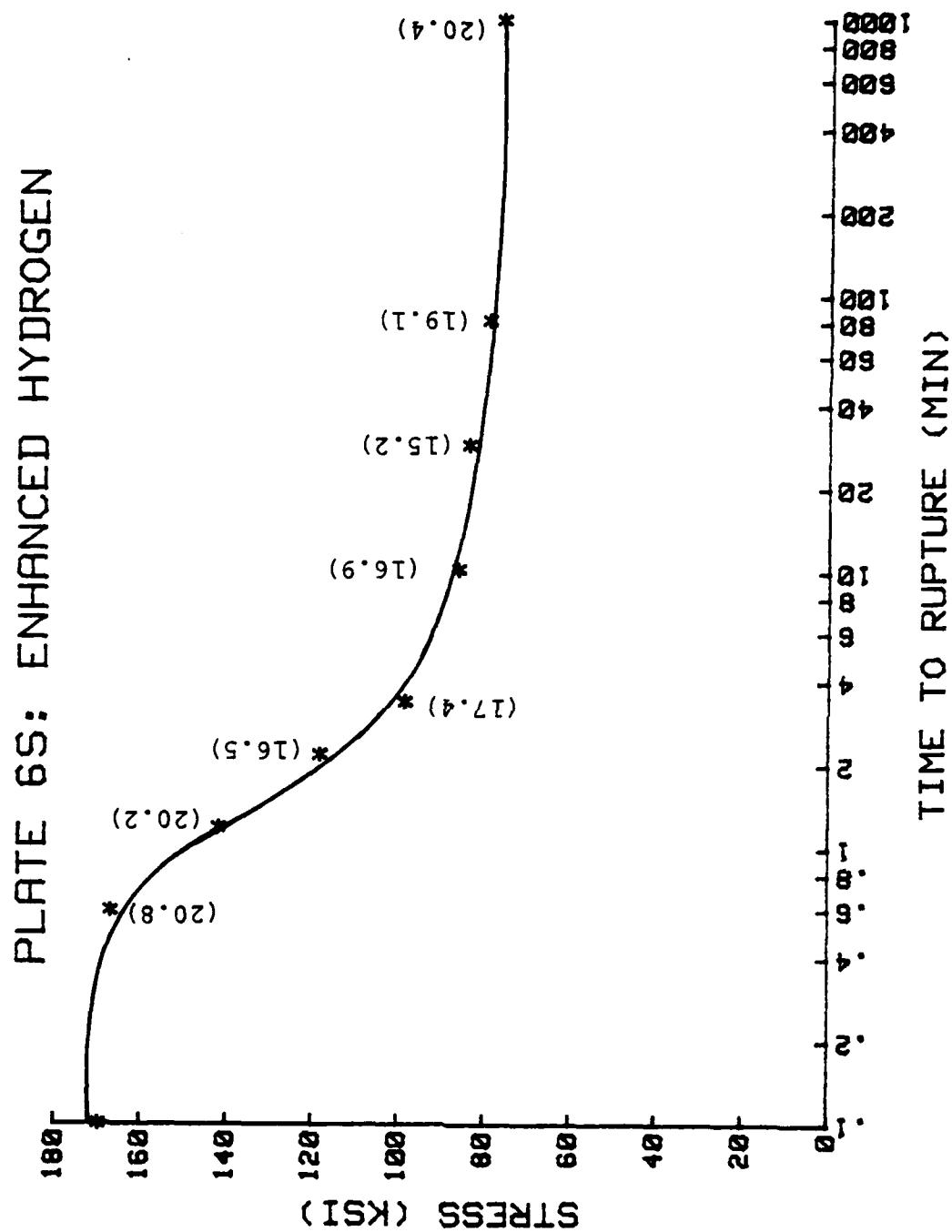


Figure 18. Stress vs. Time-to-Rupture for Plate 6 Short Transverse Direction, Enhanced Hydrogen Welding Conditions

# PLATE 6L: NON-ENHANCED HYDROGEN

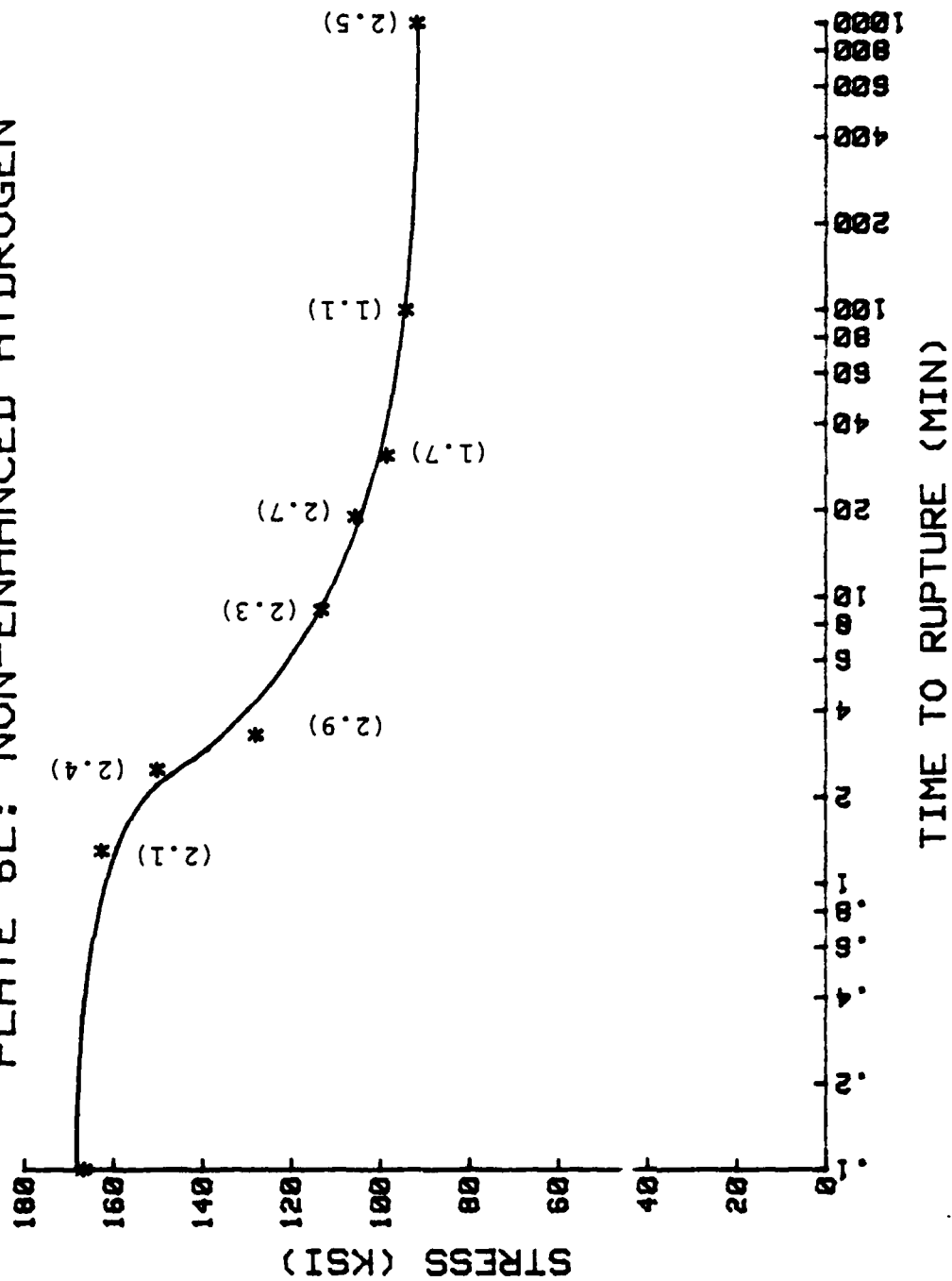


Figure 19. Stress vs. Time-to-Rupture for Plate 6 Longitudinal Direction, Normal Welding Conditions

# PLATE 6L: ENHANCED HYDROGEN

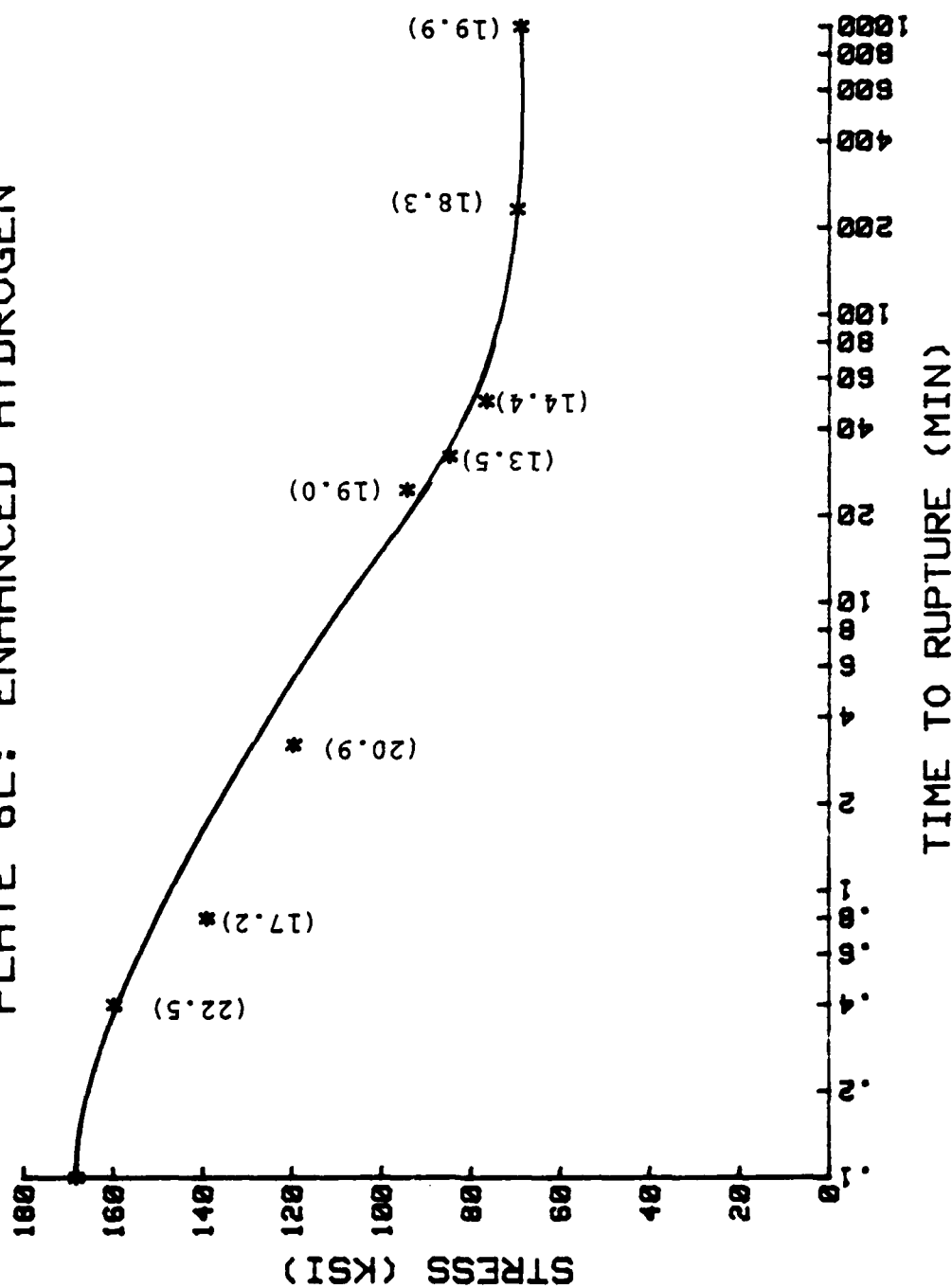


Figure 20. Stress vs. Time-to-Rupture for Plate 6 Longitudinal Direction, Enhanced Hydrogen Welding Conditions

# COMPARISON OF L.C.S.

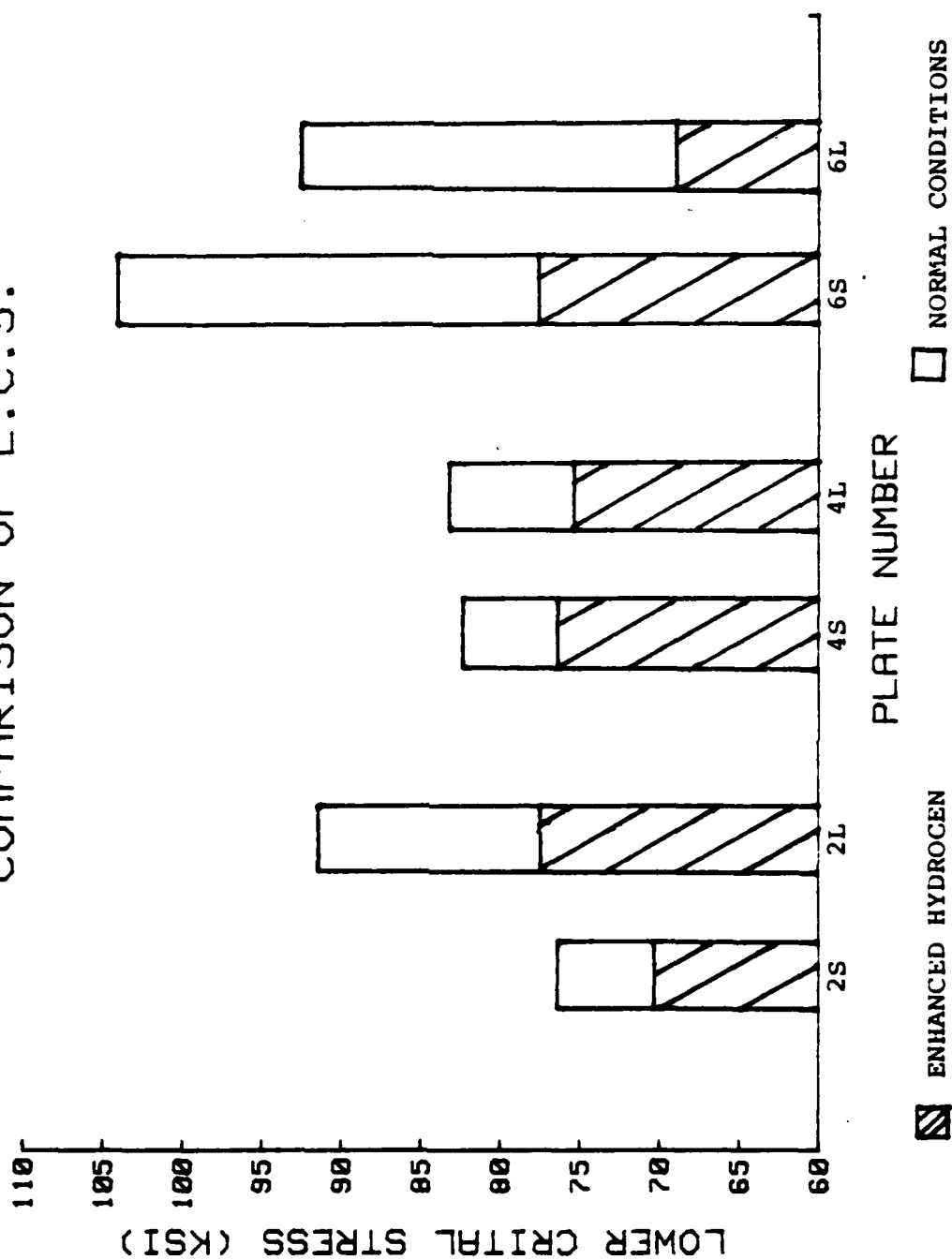


Figure 21. Comparison of the Lower Critical Stress for Normal and Enhanced Hydrogen Welding Conditions



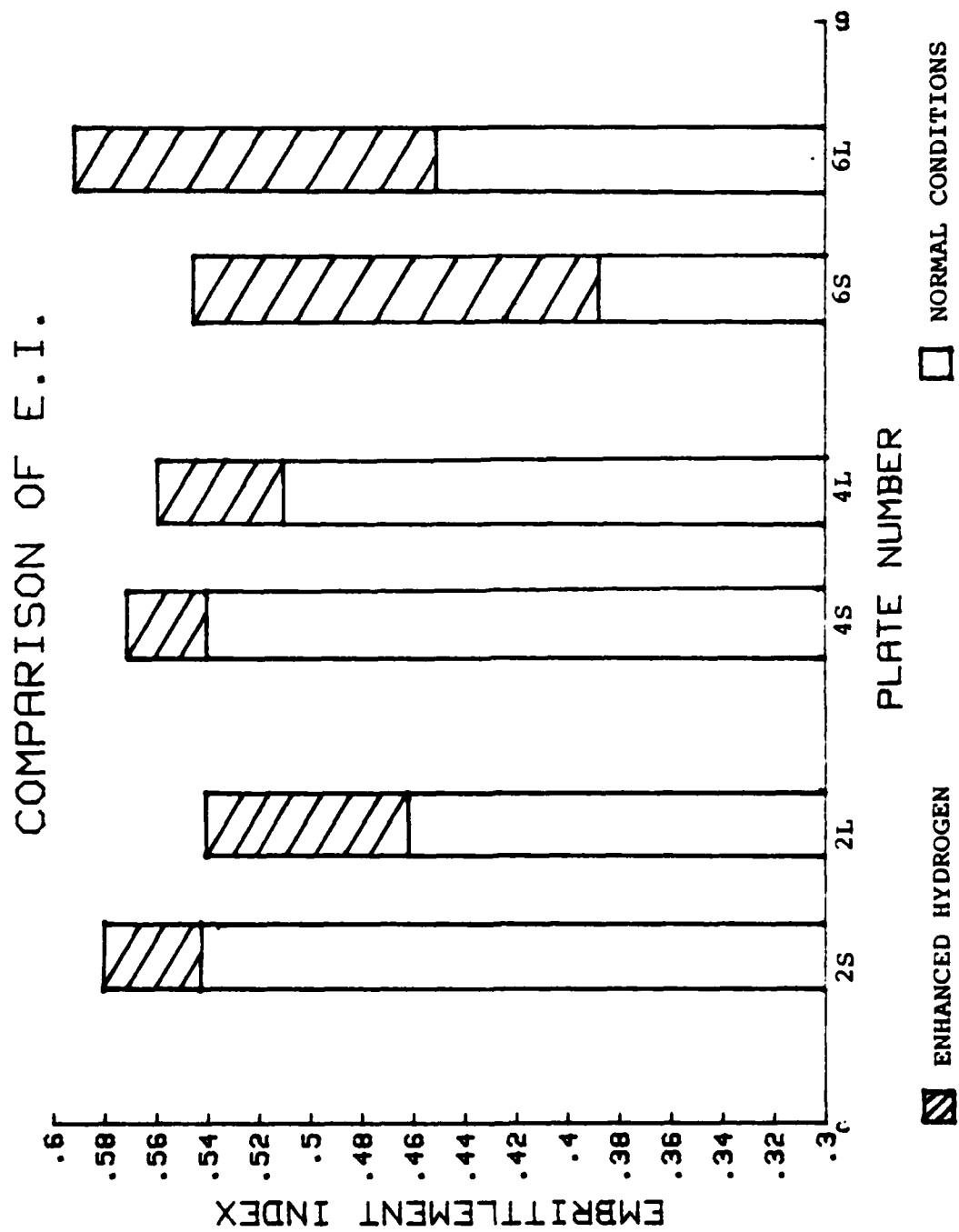
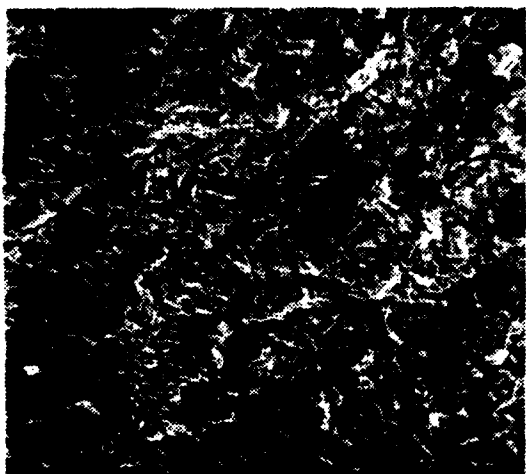
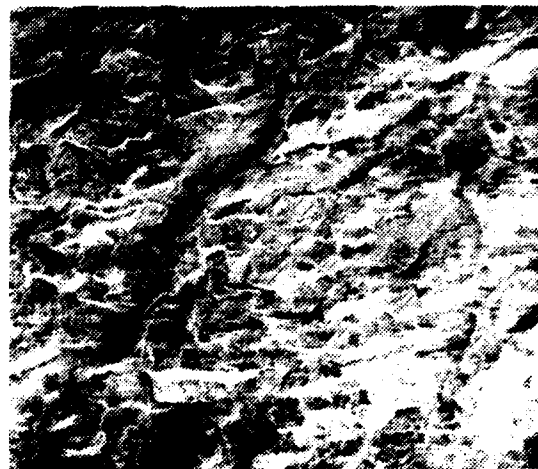


Figure 22. Comparison of the Embrittlement Index for Normal and Enhanced Hydrogen Welding Conditions

a) 50X, 2.4 ppm  $H_2$ , (70% Ductile)



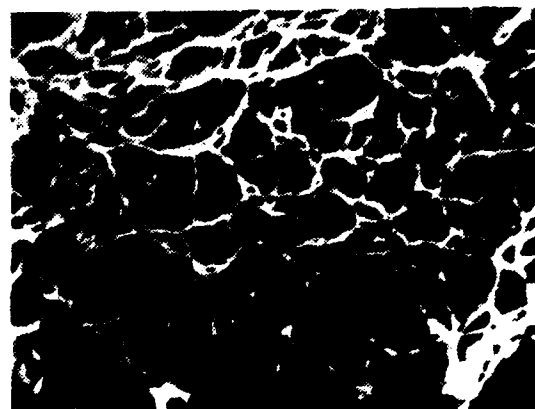
b) 50X, 20.2 ppm  $H_2$ , (10% Ductile)



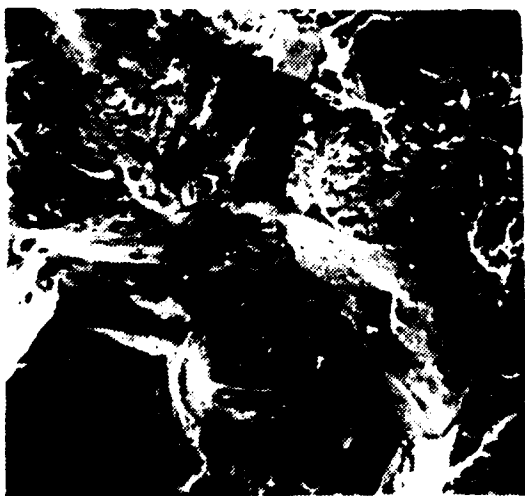
c) 500X - Dimpled Fracture



d) 500X - Dimpled Fracture



e) 500X - I.G. Fracture

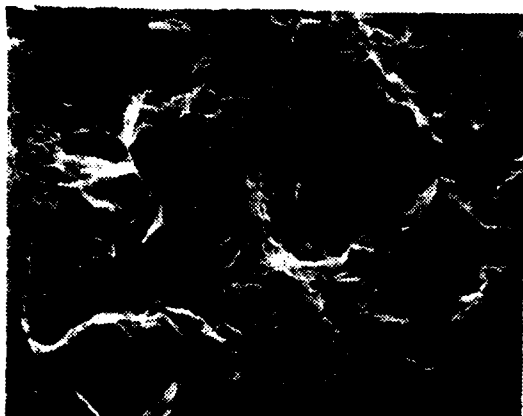


f) 500X - I.G. Fracture



Figure 23. Plate 2, Short Transverse Direction, Normal (Left) and Enhanced Hydrogen (Right) Welding Conditions

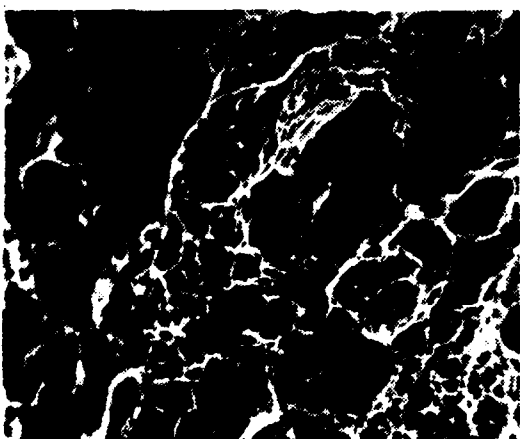
a) 50X, 1.1 ppm  $H_2$ , (70% Ductile)



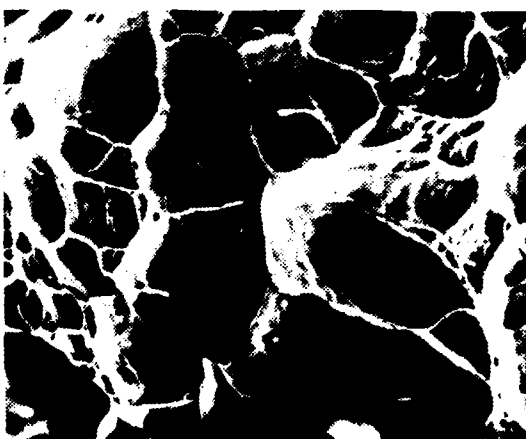
b) 50X, 19.4 ppm  $H_2$ , (30% Ductile)



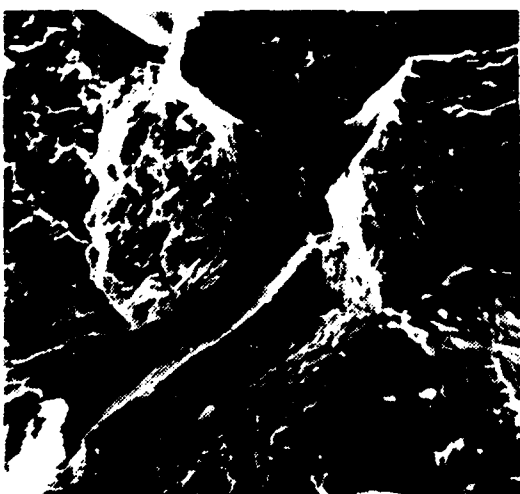
c) 500X - Dimpled Fracture



d) 500X - Dimpled Fracture



e) 500X - I.G. Fracture



f) 500X - I.G. Fracture



Figure 24. Plate 2, Longitudinal Direction, Normal (Left) and Enhanced Hydrogen (Right) Welding Conditions

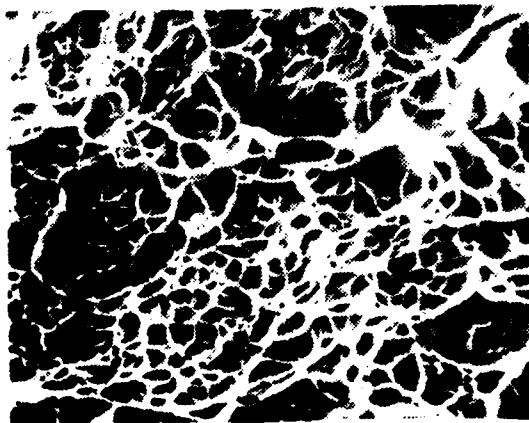
a) 50X, 1.1 ppm  $H_2$ , (80% Ductile)



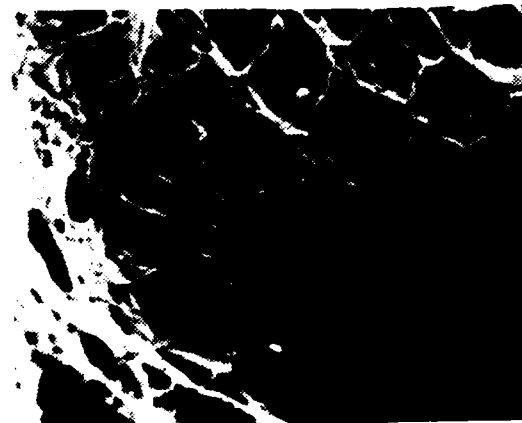
b) 50X, 18.3 ppm  $H_2$  (25% Ductile)



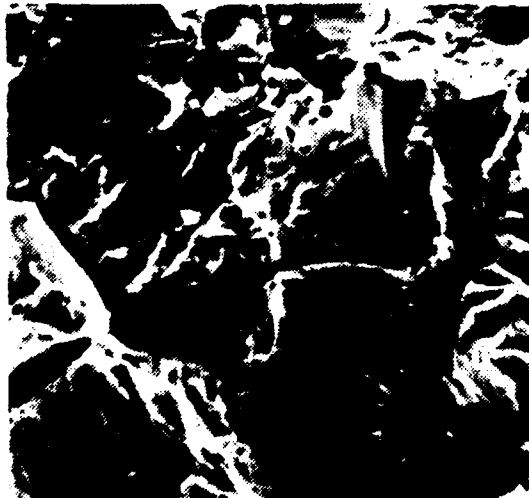
c) 500X - Dimpled Fracture



d) 500X - Dimpled Fracture



e) 500X - I.G. Fracture



f) 500X - I.G. Fracture

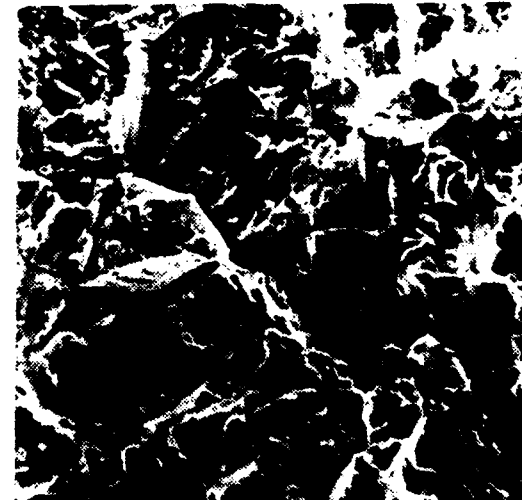
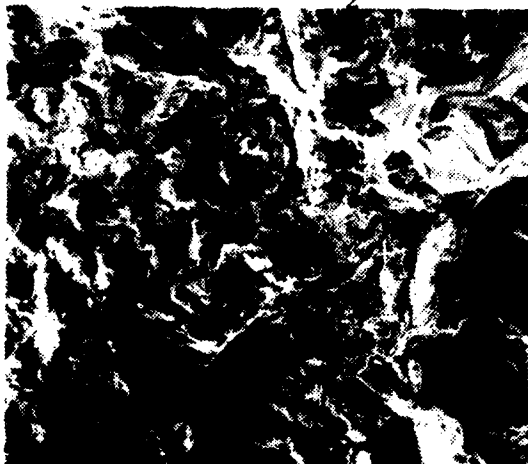
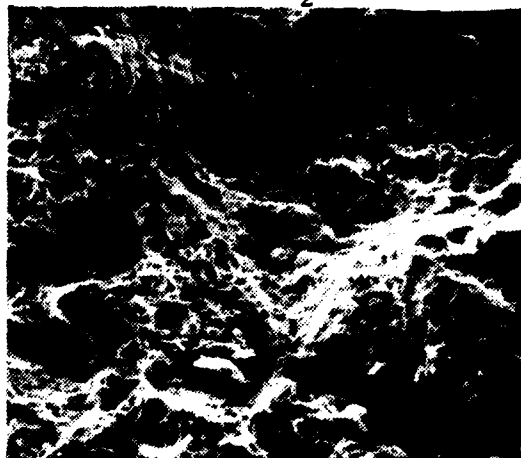


Figure 25. Plate 4, Short Transverse Direction, Normal (Left) and Enhanced Hydrogen (Right) Welding Conditions

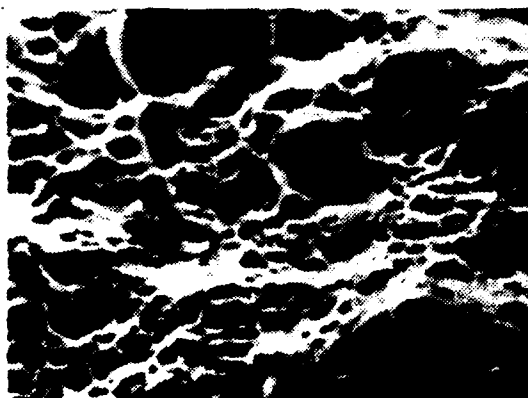
a) 50X, 4.2 ppm H<sub>2</sub> (85% Ductile)



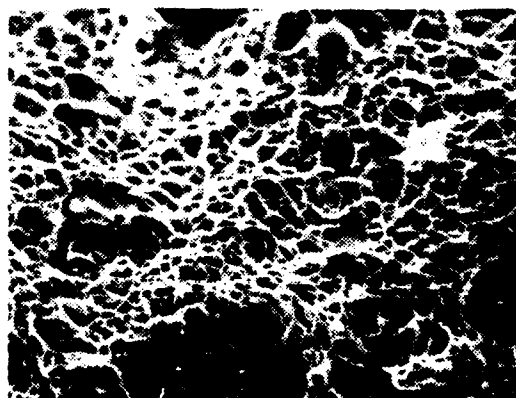
b) 50X, 19.5 ppm H<sub>2</sub> (20% Ductile)



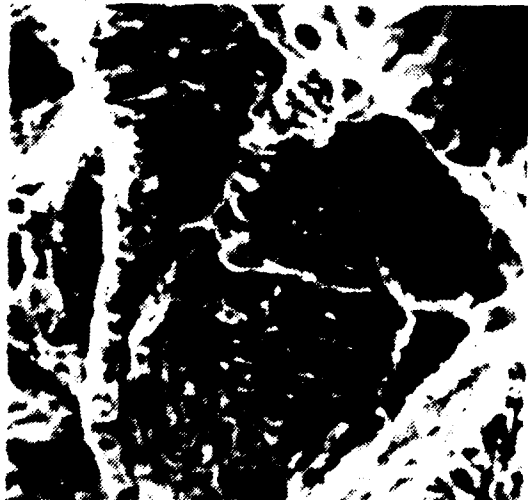
b) 500X - Dimpled Fracture



d) 500X - Dimpled Fracture



e) 500X - I.G. Fracture



f) 500X - I.G. Fracture

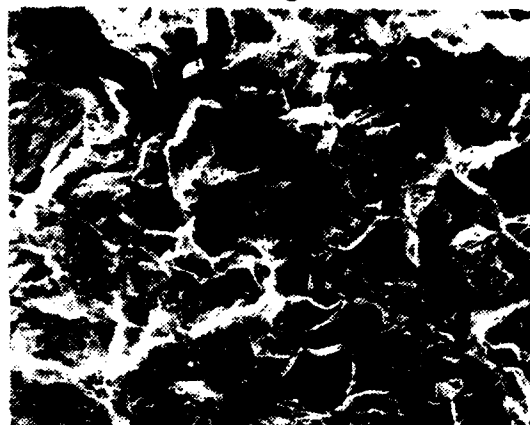


Figure 26. Plate 4 Longitudinal Direction Normal (Left) and Enhanced Hydrogen (Right) Welding Conditions

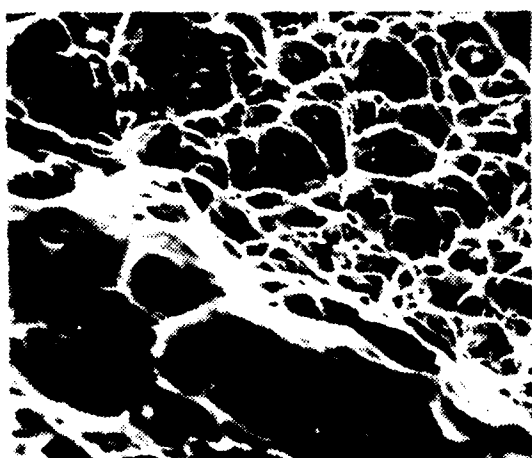
a) 50X, 0.7 ppm  $H_2$  (80% Ductile)



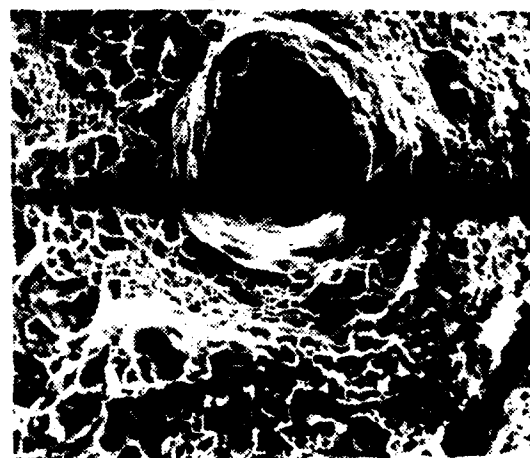
b) 50X, 19.1 ppm  $H_2$  (25% Ductile)



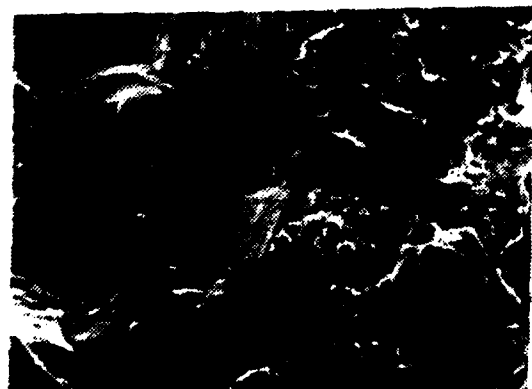
c) 500X - Dimpled Fracture



d) 500X - Dimpled Fracture



e) 500X - I.G. Fracture

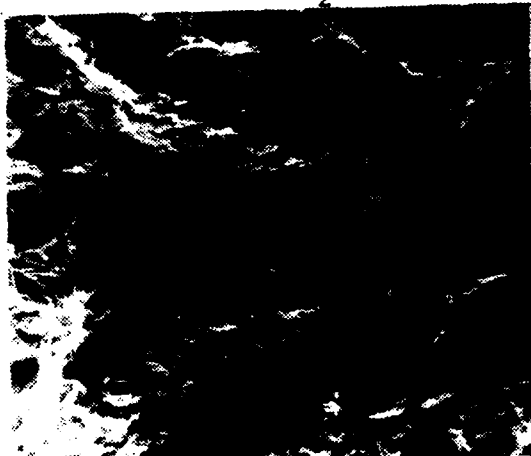


f) 500X - I.G. Fracture

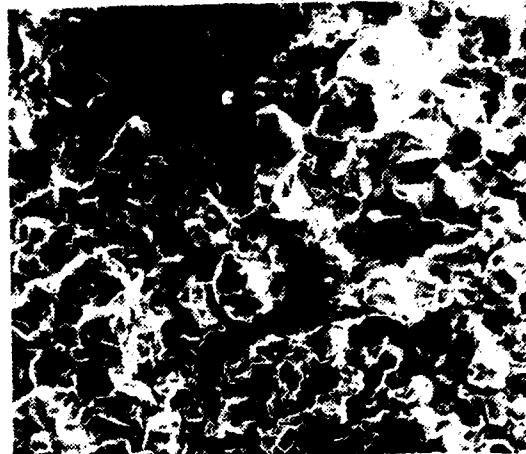


Figure 27. Plate 6, Short Transverse Direction, Normal (Left) and Enhanced Hydrogen (Right) Welding Conditions

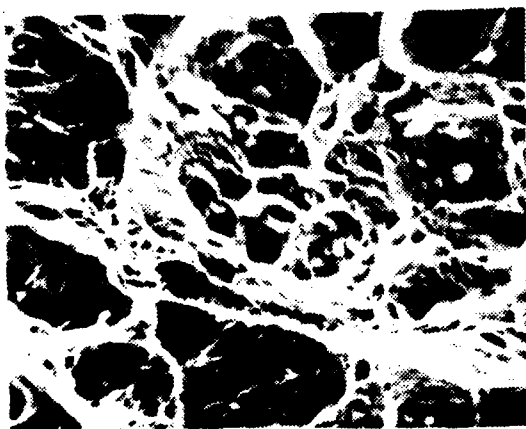
a) 50X, 1.1 ppm H<sub>2</sub> (60% Ductile)



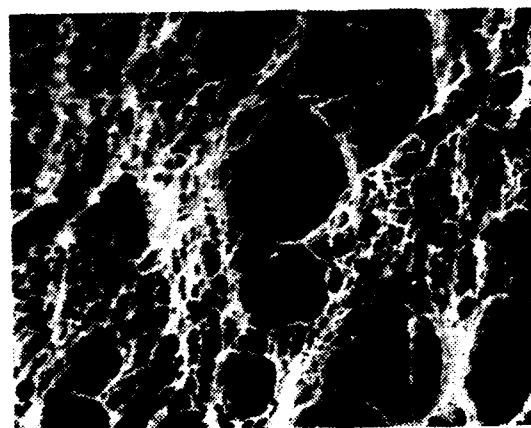
b) 50X, 14.4 ppm H<sub>2</sub> (25% Ductile)



c) 500X - Dimpled Fracture



d) 500X - Dimpled Fracture



e) 500X - I.G. Fracture

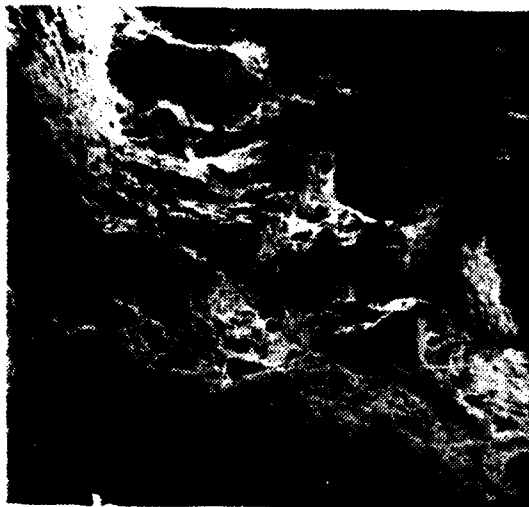


f) 500X - I.G. Fracture

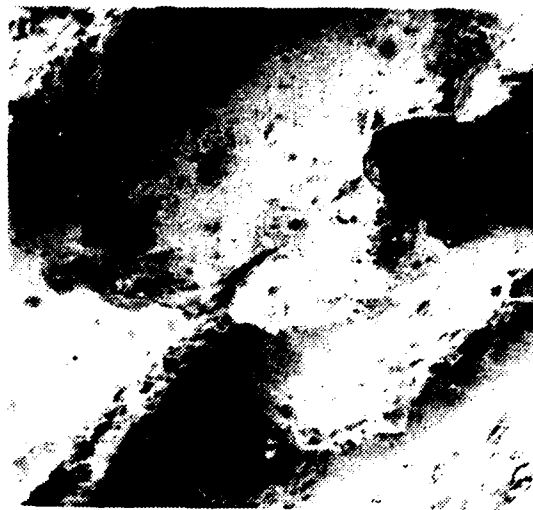


Figure 28. Plate 6, Longitudinal Direction, Normal (Left) and Enhanced Hydrogen (Right) Welding Conditions

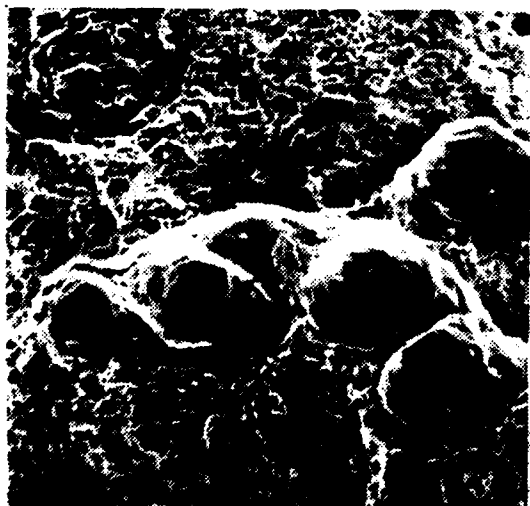
a) 50X - Plate 6



b) 50X - Plate 2



c) 500X - Plate 6



d) 500X - Plate 2

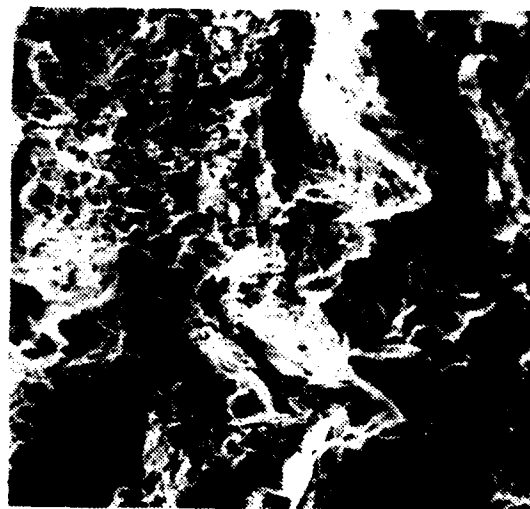


Figure 29. Notch Tensile Stress Specimens  
from Plates 2 and 6



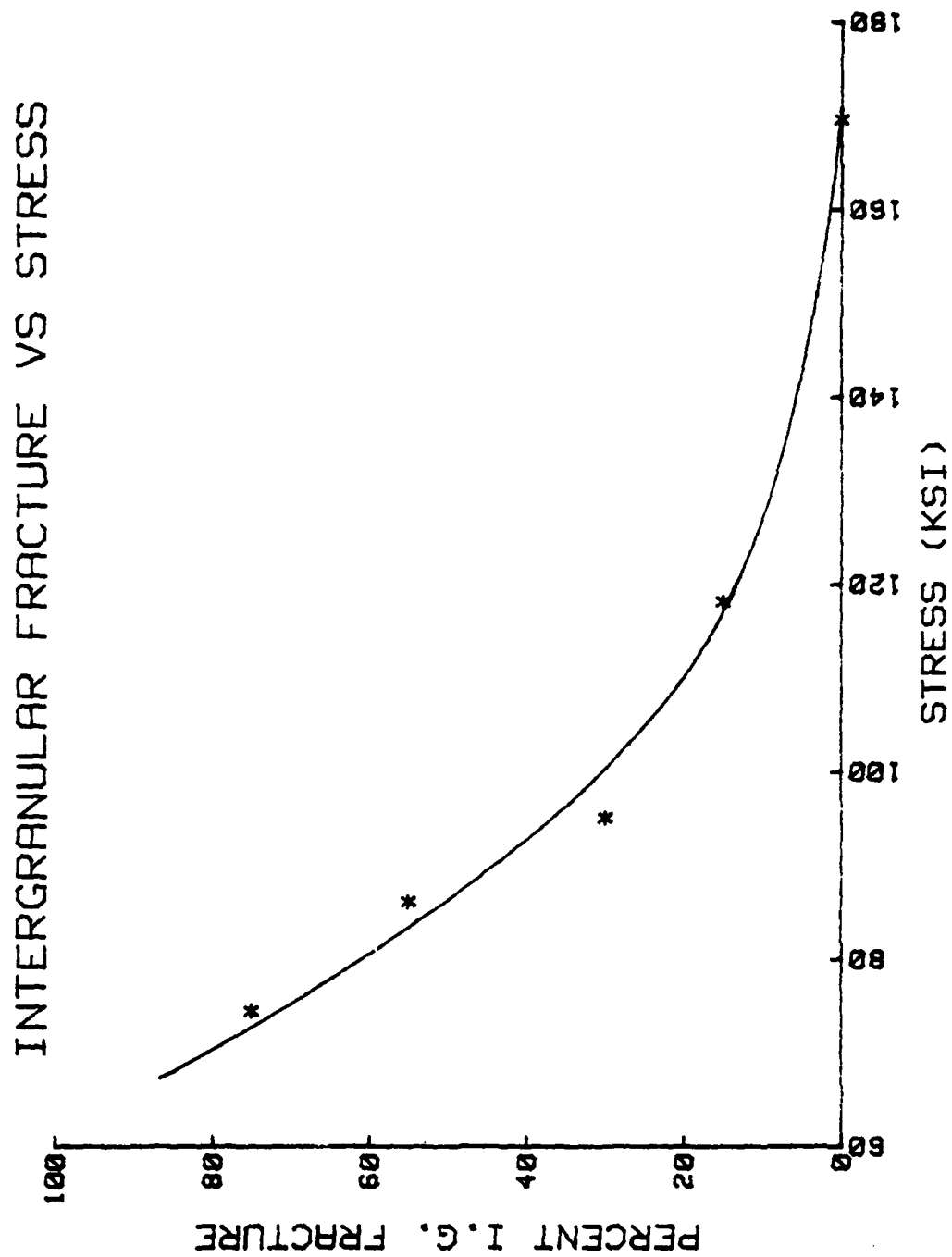


Figure 30. Percent Intergranular Fracture versus Stress  
Intensity for Enhanced Hydrogen Welding Conditions

# PLATE 2S: HARDNESS TRAVERSE

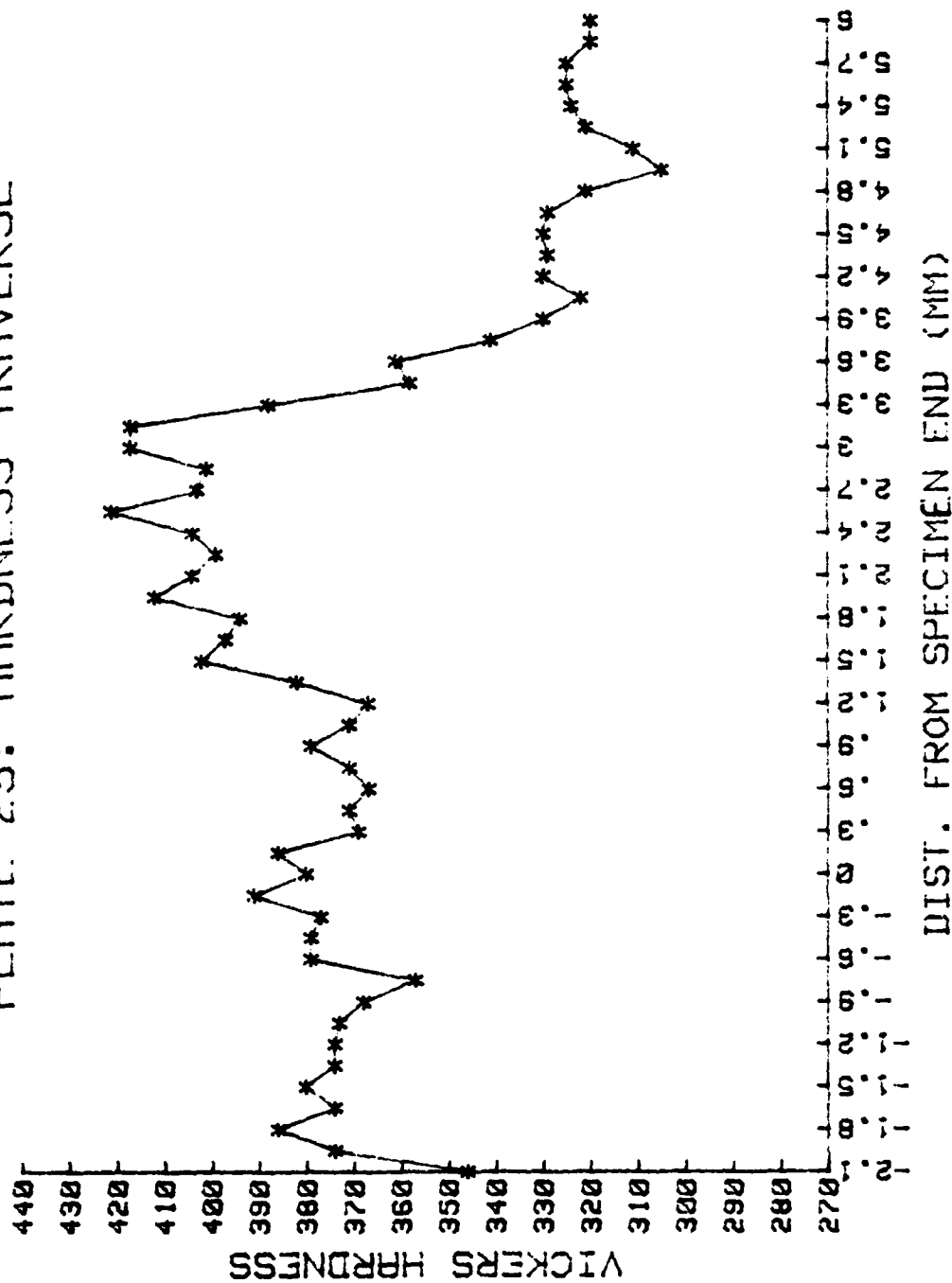


Figure 31. Microhardness Traverse of Plate 2 Short Transverse Direction

AD-A116 199

NAVAL POSTGRADUATE SCHOOL MONTEREY CA F/S 11/6  
USE OF IMPLANT TESTING TO EVALUATE THE SUSCEPTIBILITY OF HY-130--ETC(U)  
DEC 81 B J NASON

UNCLASSIFIED

NL

2 2



END  
DATE  
FILMED  
7-82  
DTIC

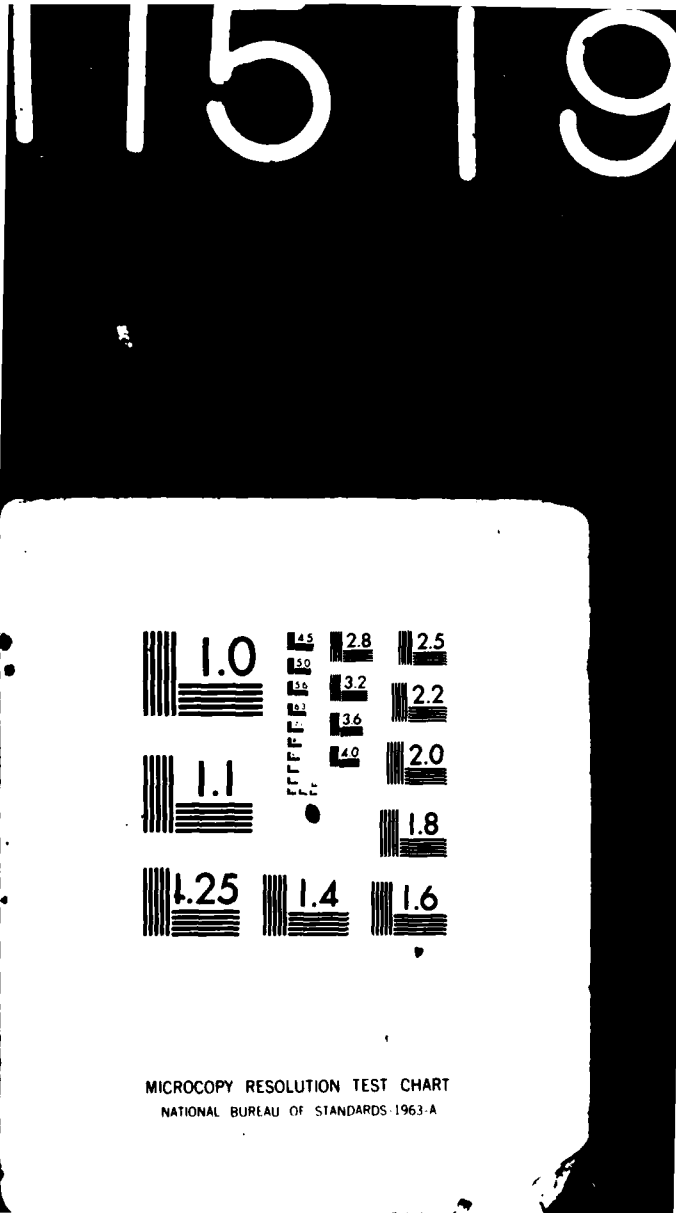


# PLATE 4S: HARDNESS TRAVERSE

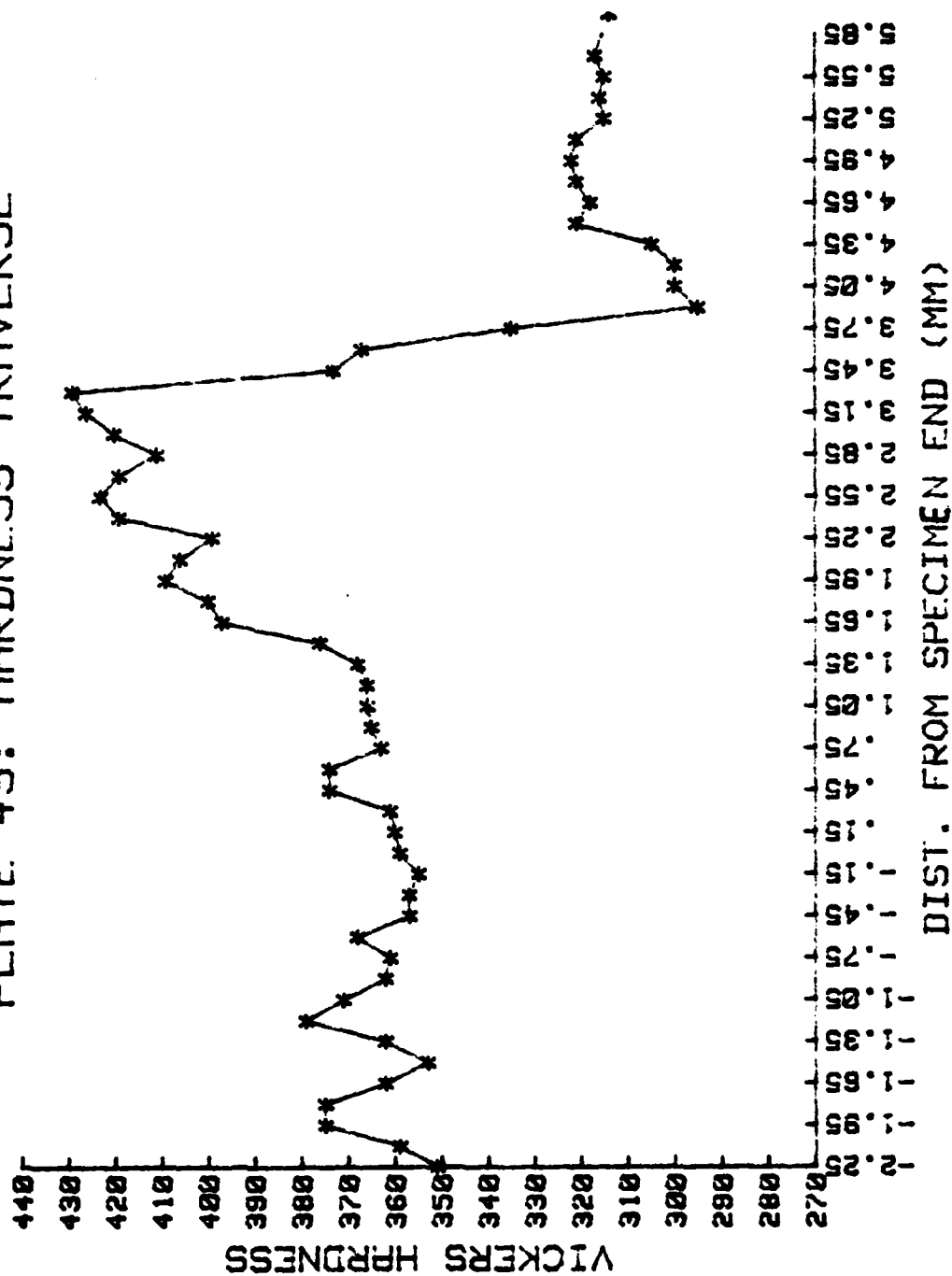


Figure 32. Microhardness Traverse of Plate 4 Short Transverse Direction

# PLATE 6S: HARDNESS TRAVERSE

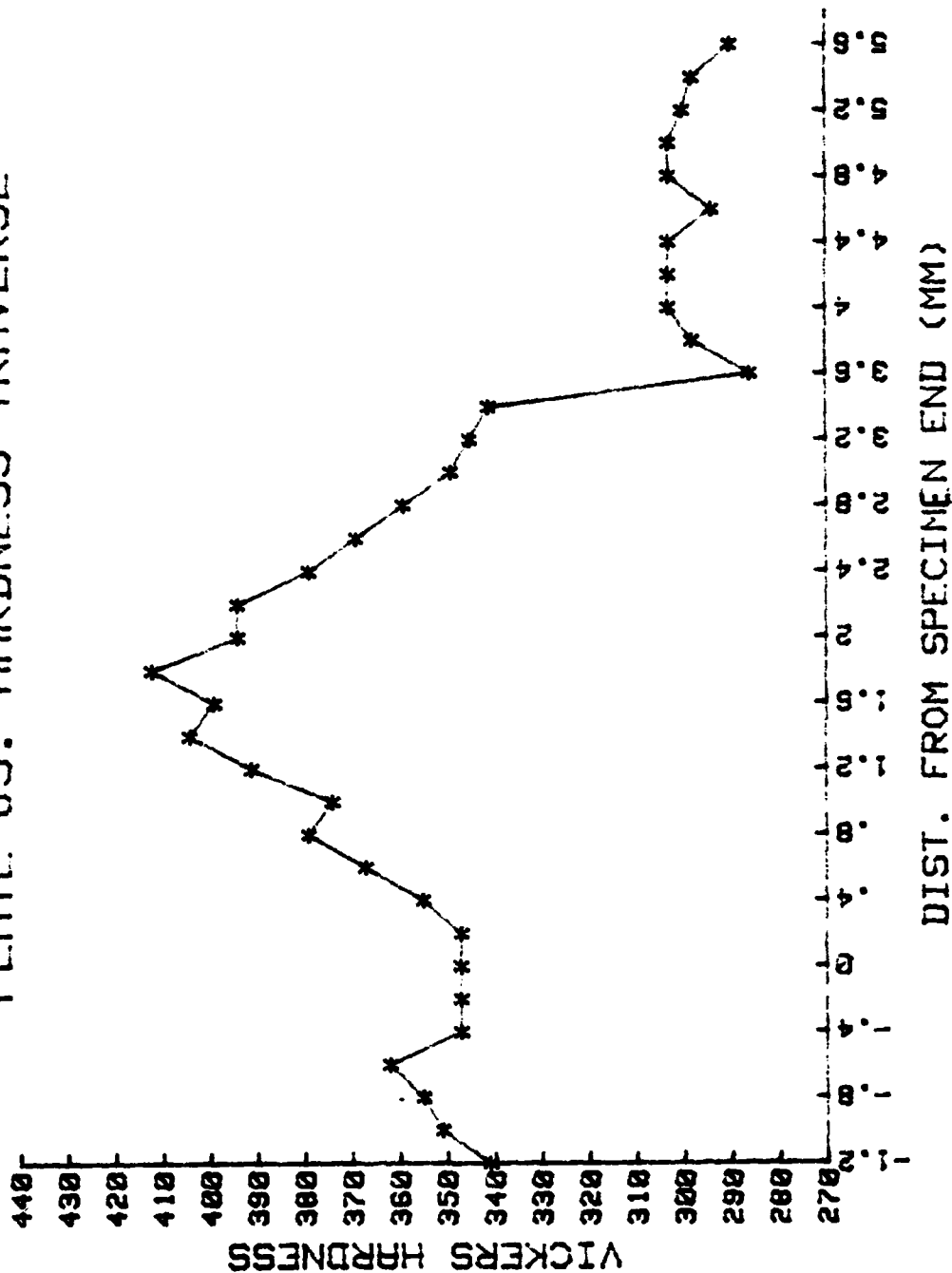
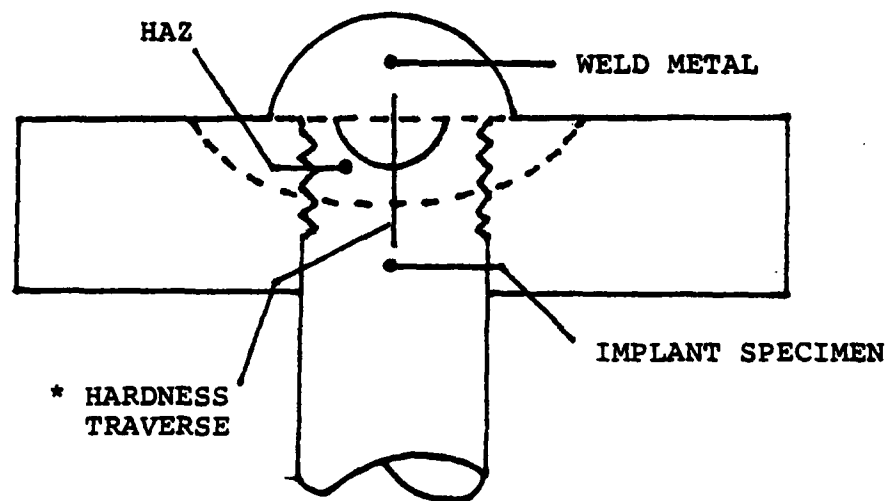


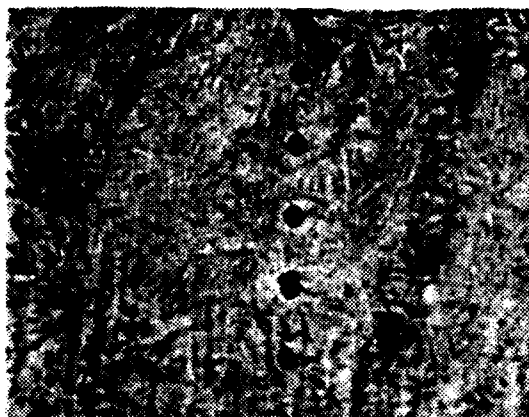
Figure 33. Microhardness Traverse of Plate 6 Short Transverse Direction



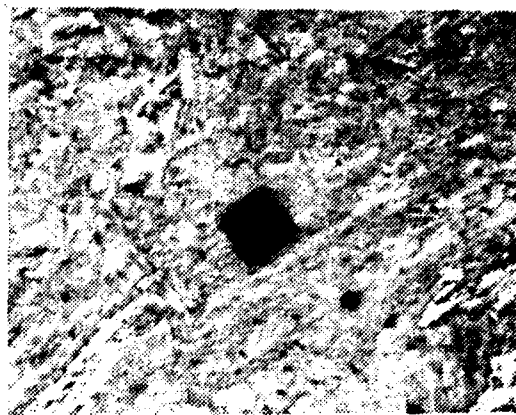
\* Note: hardness indentations were made every 0.15 mm

Figure 34. Orientation of Microhardness Traverse

a) 64X - Weld Fusion Line



b) 450X - 1.0 mm Above Fusion Line



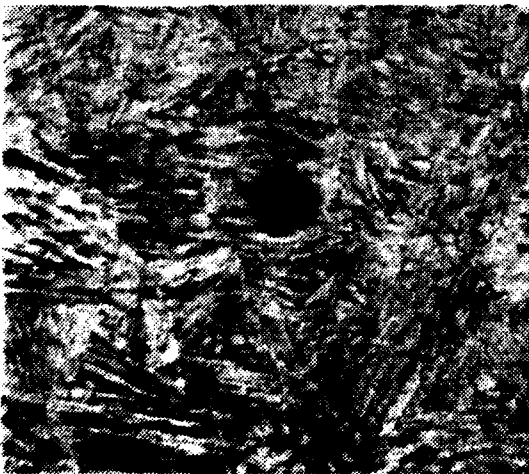
c) 450X - 0.4 mm Above Fusion Line



d) 450X - Fusion Line



e) 450X - 0.4 mm Below Fusion Line



f) 450X - 1.00 mm Below Fusion Line

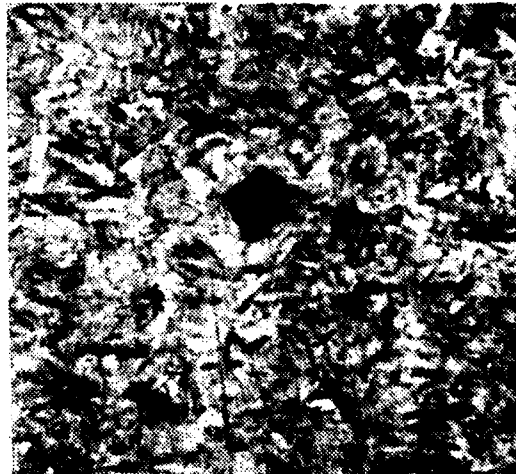


Figure 35. Microstructure of Wrought Plate Weldment  
(Plate 2)



a) 64X - Weld Fusion Line



b) 450X - 1.00 mm Above Fusion Line



c) 450X - 0.4 mm Above Fusion Line



d) 450X - Fusion Line



e) 450X - 0.4 mm Below Fusion Line



f) 450X - 1.0 mm Below Fusion Line

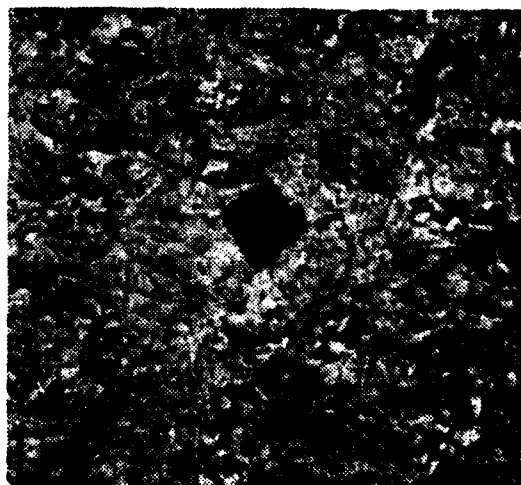


Figure 36. Microstructure of Cast Plate Weldment  
(Plate 6)



- a) 64X - Crack Initiation Site at the Root of the Helical Notch in an Unfractured Implant Specimen



- b) 250X - Crack Initiation Site at the Root of the Helical Notch, 2% Nital Etch - 30 Seconds, Crack Appears to be Intergranular in Nature.

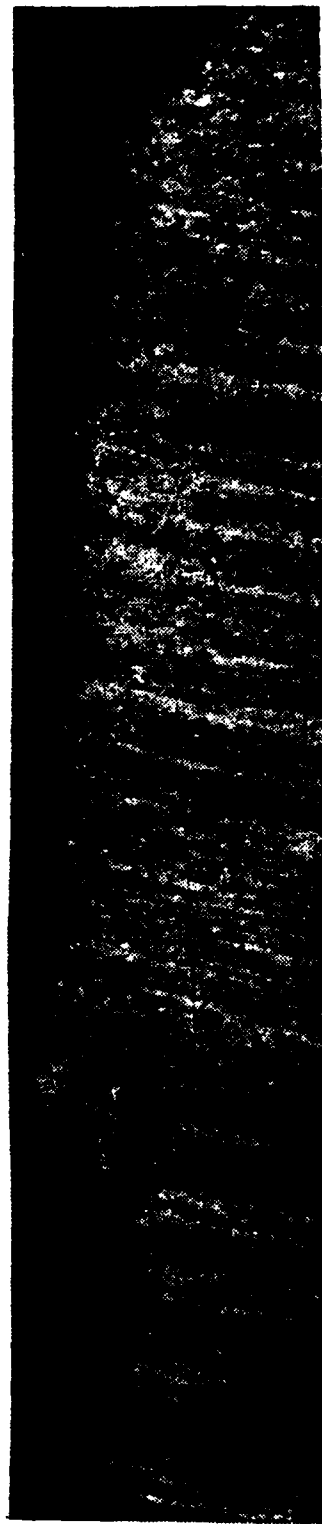


- c) 64X - Weld Penetration and Banding Visible in the Rolled HY-130 Plate, 2% Nital Etch - 30 Seconds.

Figure 37. Crack Initiation Site and Alloy Banding of Plate 2 (Wrought Plate)

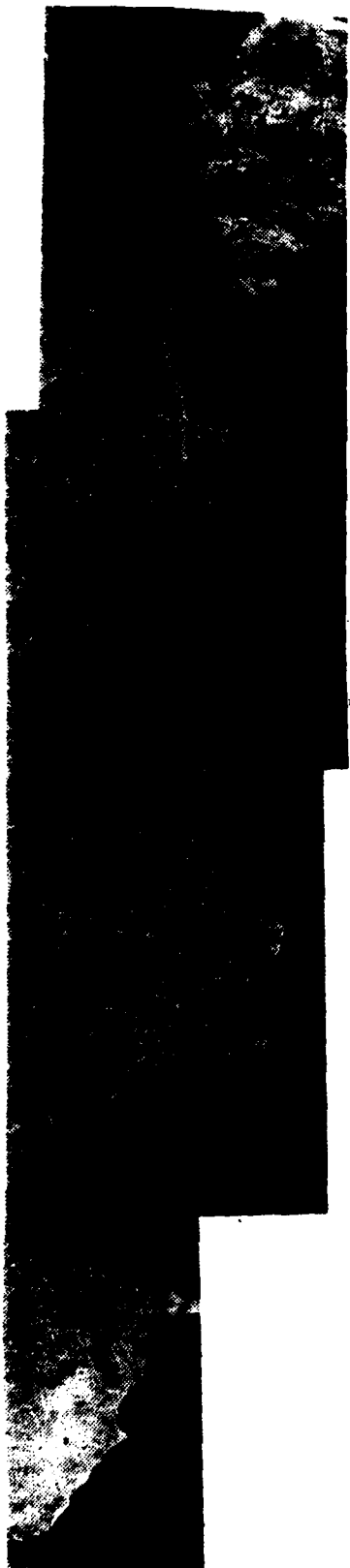


a) 64X - View of Fracture Surface, Enhanced Hydrogen Welding Conditions, 1% Nital Etch. Fracture Occurred Throughout the Weld Metal (Reduced 40%)



b) 64X - View of Fracture Surface, Normal Welding Conditions, 1% Nital Etch. Fracture Occurred Entirely in Base Metal Heat-Affected Zone (Reduced 40%)

Figure 38. Microstructure of Fractured Implant Specimens  
from Plate 2



a) 64X - View of Fracture Surface, Enhanced Hydrogen Welding Conditions, 1% Nital Etch. Fracture Occurred Primarily Through Weld Metal (Reduced 40%)



b) 64X - View of Fracture Surface, Normal Welding Conditions, 1% Nital Etch. Fracture Occurred Primarily in the Base Metal Heat-Affected Zone (Reduced 40%)

Figure 39. Microstructure of Fractured Implant Specimens  
from Plate 4



a) 64X - View of Fracture Surface, Enhanced Hydrogen Welding Conditions, 1% Nital Etch. Fracture Occurred Through Base Metal Heat-Affected Zone (Reduced 40%)



b) 64X - View of Fracture Surface, Normal Welding Conditions, 1% Nital Etch. Fracture Occurred Primarily Through the Base Metal Heat-Affected Zone (Reduced 40%)

Figure 40. Microstructure of Fractured Implant Specimens  
from Plate 6

### LIST OF REFERENCES

1. Sawhill, J. M., Jr., Dix, A. W., and Savage, W. F., "Modified Implant Testing for Studying Delayed Cracking," Welding Journal, vol. 53, no. 12, December 1974, Research Supplement, pp. 260-S to 268-S.
2. Savage, W. F., Nippes, E. F., and Sawhill, J. M., Jr., "Hydrogen Induced Cracking During Implant Testing of Alloy Steels," Welding Journal, vol. 55, no. 12, December 1976, Research Supplement, pp. 400-S to 407-S.
3. Granjon, H., "The Implants Method for Studying the Weldability of High Strength Steels," Metal Construction and British Welding Journal, vol. 1 (no. 11), November 1969, pp. 509 to 515.
4. Savage, W. F., and Nippes, E. F., "Development and Qualification of Methods for the Determination of Diffusible Hydrogen Content in Weldments," Interim Technical Report, July 1, 1977 to June 30, 1980, Office of Naval Research Contract No. N00014-75-C-0944, NR031-780 (1980).
5. Tetelman, A. S., Fracture of Solids, Wiley and Sons, New York (1962).
6. Williams, D. P., and Nelson, H. G., "Embrittlement of 4130 Steel by Low Pressure Gaseous Hydrogen," Metallurgical Transactions, vol. 1, no. 12, pp. 3451 to 3455 (1970).
7. Troiano, A. R., "The Role of Hydrogen and Other Interstitials in the Mechanical Behavior of Metals," Transactions of the American Society for Metals, vol. 52, no. 1, pp. 54 to 80 (1960).
8. Beachem, C. D., "A New Model for Hydrogen Assisted Cracking (Hydrogen Embrittlement)," Metallurgical Transactions, vol. 3, no. 2, pp. 437 to 451 (1972).
9. Conner, L. P., Rathbone, A. M., and Gross, J. H., "Development of Procedures for Welding HY-130(T) Steel," Welding Journal, vol. 46, no. 7, July 1967, Research Supplement, pp. 309-S to 321-S.
10. Savage, W. F., Nippes, E. F., and Silvia, A. J., "Prevention of Hydrogen-Induced Cracking in HY-130 Weldments," Interim Technical Report, July 1, 1976 to June 30, 1977, Office of Naval Research Contract No. N00014-75-C-0944, NR031-780 (1977).

11. Palko, W. A., Byrne, J. P., Zanis, C. A., "Processing of HY-130 Steel Castings," AFS Transactions, vol. 84, 1976, pp. 193 to 202.
12. Cincotta, P. E., The Effects of Simulated Welds on HY-130 Cast and Wrought Plate and Weld Metal Microstructure, M.S. Thesis, Naval Postgraduate School, Monterey, CA, September 1981.
13. Burcker, B. R., Fracture Properties of HY-130 Cast Plate Weldments, M.S. Thesis, Naval Postgraduate School, Monterey, CA, December 1980.
14. Sorek, M.J., A Correlation Between the Heat-Affected Zone Microstructure and the Thermal History During Welding of HY-130 Steel, M.S. Thesis, Naval Postgraduate School, Monterey, CA, September 1981.
15. Vasudevan, R., Stout, R. D., and Pense, A. W., "Hydrogen-Assisted Cracking in HSLA Pipeline Steels," Welding Journal, vol. 60, no. 9, September 1981, Research Supplement, pp. 155-S to 168-S.
16. Elger, W. M., Characterization of an HY-130 Weldment by Transmission Electron Microscopy, M.S. Thesis, Naval Postgraduate School, Monterey, CA, December 1981.
17. Boniszewski, T., Watkinson, F., Baker, R. G., and Tremlett, H. F., "Hydrogen Embrittlement and Heat-Affected Zone Cracking in Low-Carbon Alloy Steels with Acicular Microstructures," British Welding Journal, January 1965, pp. 14 to 36.
18. Speich, G. R., "Tempering of Low-Carbon Martensite," Transactions of the Metallurgical Society of AIME, vol. 245, December 1969, pp. 2553 to 2563.

INITIAL DISTRIBUTION LIST

	No. Copies
1. Defense Technical Information Center Cameron Station Alexandria, Virginia 22314	2
2. Library, Code 0142 Naval Postgraduate School Monterey, California 93940	2
3. Department Chairman, Code 69 Department of Mechanical Engineering Naval Postgraduate School Monterey, California 93940	1
4. Assistant Professor K. D. Challenger, Code 69Ch Department of Mechanical Engineering Naval Postgraduate School Monterey, California 93940	5
5. Mr. Charles Zanis, Code 2820 David Taylor Research and Development Center Annapolis, Maryland 21402	1
6. Mr. Ivo Fioritti, Code 323 Naval Sea Systems Command National Center, Building 3 2531 Jefferson Davis Highway Arlington, Virginia 20362	1
7. LT Bradley J. Mason 18773 Bernardine St. Lansing, Illinois 60438	2
8. Mr. G. Power, Code 138.3 Mare Island Naval Shipyard Vallejo, California 94950	1



FILMED  
7-8